論文 / 著書情報
Article / Book Information

題目(和文)	DNAナノ構造の基板上成長 : 設計指針, 理論解析とその実験
Title(English)	Substrate-assisted self-assembly of DNA nanostructures : design principles, theory and experiments
著者(和文)	浜田省吾
Author(English)	Shogo Hamada
出典(和文)	学位:博士(工学), 学位授与機関:東京工業大学, 報告番号:甲第8417号, 授与年月日:2011年3月26日, 学位の種別:課程博士, 審査員:山村 雅幸
Citation(English)	Degree:Doctor (Engineering), Conferring organization: Tokyo Institute of Technology, Report number:甲第8417号, Conferred date:2011/3/26, Degree Type:Course doctor, Examiner:
学位種別(和文)	博士論文
Type(English)	Doctoral Thesis

TOKYO INSTITUTE OF TECHNOLOGY

P H D T H E S I S

to obtain the title of

Ph.D. in Engineering

of Tokyo Institute of Technology

by

Shogo HAMADA

Substrate-Assisted Self-Assembly of DNA Nanostructures:

Design Principles, Theory and Experiments

Thesis Advisor: Satoshi MURATA, Masayuki YAMAMURA

prepared at Tokyo Institute of Technology and Tohoku University

February 7, 2011

Jury :

Advisor :	Masayuki YAMAMURA
	Akihiko KONAGAYA
	Daisuke KIGA
	Masamichi ISHIKAWA
	Kotaro KAJIKAWA
Advisor (External) :	Satoshi MURATA

Acknowledgments

First of all, I would like to express my gratitude to Prof. Satoshi Murata, my supervisor. My experience in this field would never started and this thesis would not have been possible without his support. Also I would like to thank Prof. Masayuki Yamamura, my advisor who gave me a generous support, especially during a year in Tohoku Univ. I sincerely thank Prof. Akihiko Konagaya, Prof. Daisuke Kiga, Prof. Masamichi Ishikawa, and Prof. Kotaro Kajikawa for various advices throughout writing this thesis.

I owe my deepest gratitude to Prof. Erik Winfree, Prof. Sung Ha Park and Dr. Rizal F. Hariadi for using and learning AFM at Caltech for the first time. I would never forget the excitement of my first observation: the moment that a vague idea took a form of existence. Great and insightful advices by Dr. Paul W. K. Rothemund and Prof. Chengde Mao encouraged me a lot. Now I'm being fascinated by a world of self-assembly.

I deeply thank Prof. Kenzo Fujimoto for discussions, advices and the generous admission of using equipments at JAIST. I would like to thank all the members of Molecular Robotics Research Group, SICE for advices at the workshop. I am indebt to Dr. Maria L. Sushko for the guidance and discussions about calculations of DLVO theory.

It is truly a pleasure to thank my colleagues of Murata lab. and wonderful neighbors of Takayasu lab in Tokyo Tech. My friends in Yamamura lab and Kiga lab gave me a new insight of Biology; especially the experience of iGEM gave me a kind of dramatic diversion in thinking. I also thank office administrators of Murata lab and Yamamura lab, Ms. Shizuka Mitoma, Ms. Rika Machida and Ms. Michiko Yoshida, for their support in office work.

Lastly and most importantly, I wish to thank my parents, Hareo and Tamami, and Hiromi, for their understanding, encouragements and tremendous support.

Contents

1 Introduction **1**
- 1.1 Introduction . . . 1
- 1.2 Questions to be answered in this thesis . . . 2
- 1.3 Structure of this thesis . . . 3

2 Motif-based DNA nanostructures **5**
- 2.1 DNA as a nanoscale building block . . . 5
- 2.2 Motifs . . . 7
  - 2.2.1 Immobilized Holliday Junction . . . 7
  - 2.2.2 DX molecules and DX Tile . . . 8
  - 2.2.3 TX tile,Cross tile, 3-point star motif and Single-stranded tile 11
- 2.3 Basic procedure for design and self-assembly of DNA motifs . . . 12
  - 2.3.1 Self-assembly . . . 15
  - 2.3.2 Observation and analysis . . . 16
- 2.4 Summary . . . 17

3 T-junction and T-motifs **19**
- 3.1 T-junction . . . 19
- 3.2 T-motif . . . 23
  - 3.2.1 Design . . . 25
  - 3.2.2 Self-assembly in free solution . . . 27
- 3.3 Summary . . . 28

4 Experiments on substrate-assisted self-assembly **29**
- 4.1 Substrate-assisted self-assembly . . . 29
  - 4.1.1 Experiments of substrate-assisted self-assembly . . . 31
- 4.2 Algorithmic self-assembly of T-motifs . . . 32
  - 4.2.1 Wang Tiles and Algorithmic Self-Assembly . . . 33
  - 4.2.2 Implementation of Cellular Automaton . . . 35
  - 4.2.3 T-motif tiles . . . 36
  - 4.2.4 Experiments . . . 39
- 4.3 Summary . . . 40

5 Theory of substrate-assisted self-assembly **43**
- 5.1 Framework of the theory of substrate-assisted self-assembly . . . 44
  - 5.1.1 Adsorption and surface-diffusion . . . 46
- 5.2 Calculation of free energy: hybridization . . . 49
- 5.3 Calculation of free energy: adsorption . . . 50
  - 5.3.1 Introduction to the DLVO theory . . . 50
  - 5.3.2 Van der Waals interactions between cylinder and surface . . . 52

5.3.3 Double-layer forces between cylinder and surface 53
5.3.4 Calculation results 58
5.4 Self-assembly model 60
5.4.1 Hybridization model of motifs 60
5.4.2 Thermodynamic equilibrium 61
5.5 Adsorption model 63
5.5.1 Thermodynamics of the Langmuir model 63
5.6 Kinetic model of self-assembly and adsorption 65
5.6.1 Self-assembly 65
5.6.2 Langmuir model for adsorption 66
5.6.3 Estimation of two-dimensional rate constant 69
5.7 Simulation 71
5.7.1 Model 71
5.7.2 Simulation in free-solution 73
5.7.3 Simulation of substrate-assisted self-assembly 75
5.8 Summary 81

6 Conclusion **83**
6.1 Answers 83
6.2 Issues for further studies 84

A Additional AFM observation and analyses of T-motifs **87**
A.1 Yield and diameter analysis example of the Ring 1.0x 87
A.2 Analyses of AFM observation 89
A.3 Additional AFM observation results 91
A.4 Tube/troidal formation of T-motif brick-wall lattice 93

B Spectrophotometer data of T-motifs **95**
B.1 Annealing/melting data of the T-motifs 95
B.2 Formation curve of self-assembly process (Ring 1.0x) 97

C Cyclic annealing of T-motif **99**

D Area analysis of monocrystal region **101**

E Calculation of monovalent/divalent ion concentration of TAE/Mg^{2+} 12.5mM buffer **105**
E.1 Monovalent ion concentration 106
E.2 Divalent ion concentration 107

F Source codes **109**
F.1 Design software 109
F.2 Simulations of self-assembly in free solution and on substrate (MATLAB) 144

Bibliography 167

Chapter 1

Introduction

Contents

1.1 Introduction 1

1.2 Questions to be answered in this thesis 2

1.3 Structure of this thesis 3

1.1 Introduction

The creation of arbitrary shapes and patterns, which precisely defined at atomic level, is one of the ultimate goal of engineering. Conventional way of making things is to cut[1] some chunk of materials, or forming them directly into arbitrary shapes[2]. However, these top-down methodologies require design information from "outwards" of the molecules; information are given to bulk materials through the process in order to define designated shapes. A precise control of process and the "mother" product[3] define the accuracy of the resultant products. This way of creation is powerful if we are able to make enough-precise references and fabrication processes, although now we are facing limitations on the basis of scale and costs. On the other hand, if we can include the information of design in molecules themselves, the cost and the scaling problem of creating shapes and patterns will be solved. This counterpart methodology is known as an idea of "bottom-up" fabrication. If we are

[1] Fabrication by removing a part of bulk materials; *e.g.* various machining and lithography.
[2] Molding, printing, pressing and rolling etc. are included in this category.
[3] The object which defines the shape of the product; *e.g.* molds and mask patterns.

able to utilize this methodology towards creating shapes and patterns large enough to combine with top-down methodology, the strength of both methods can be used for the realization of the ultimate goal.

The key of this idea is the selection of the molecule, which is able to store and use the information in itself along with a potential to transform into varieties of shapes and patterns. One of the best candidates of this "universal" molecule at this moment is DNA. DNA nanotechnology (or DNA nanoengineering, from a point of view of creating things) established a powerful methodology to design and self-assemble nanoscale shapes and patterns. This thesis seeks the possibility of the DNA molecules as a nano-scale building block. The aim of this research is to find a way to design varieties of shapes and patterns by DNA and to create meso-scale[4] structures, along with a versatile methodology which possibly bridges the gap between bottom-up and top-down methodologies.

1.2 Questions to be answered in this thesis

How can we find a way to design DNA nanostructures, and to realize self-assembly of large-scale structures by bottom-up approach? This general question can be divided into the following questions:

1. Is there any new principles to design varieties of DNA nanostructures, which have different characteristics compared to the current design?
2. What kind of shapes and patterns can be realized by the principle?
3. Can we find a versatile method to self-assemble DNA nanostructures up to meso-scale?
4. If so, how predictable and controllable is the method?

The purpose of this thesis is to provide answers to these questions.

[4]The word "meso-scale" is used to mention a size between micron to submillimeter-scales, which means as a "crossing" size of both methodologies.

1.3 Structure of this thesis

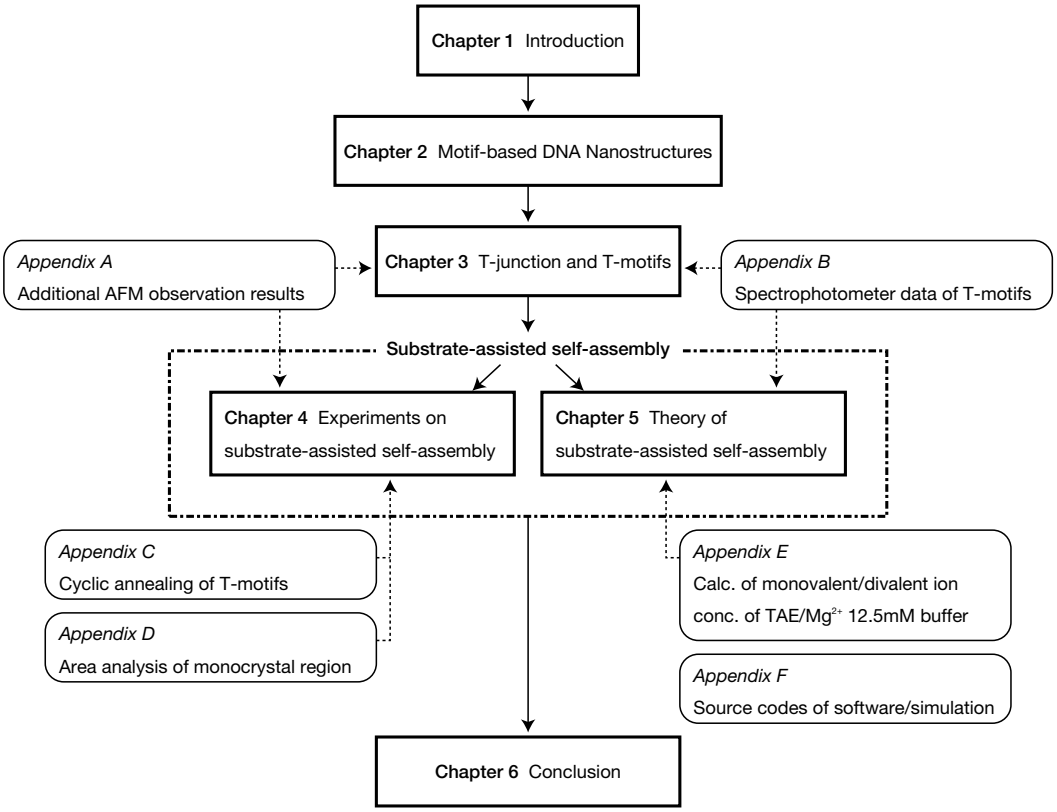

Figure 1.1: The structure of this thesis

The structure and brief description of this thesis is given as follows (Fig. 1.1),

Chapter 2 overviews a basic principle of motif-based DNA nanostructures. The fundamentals of motif and sticky ends are described, and some typical DNA motifs known as DNA tiles are reviewed. Also, the methodology of design and experimental procedures are discussed.

Chapter 3 introduces a new T-shaped junction called T-junction and T-junction based motifs, named T-motifs. The characteristics of the structure by comparison with conventional junction are discussed. Varieties of shapes and patterns can be achieved and self-assembled in free solution by this motif. The design features and experimental results of the motifs are described.

Chapter 4 explains the substrate-assisted self-assembly, a novel self-assembly method that enables us to create meso-scale nanostructures on a surface by using T-motifs. The versatility of this method and some characteristics suggested by experimental results are discussed. Moreover, an example of self-assembly of patterns using T-motif tiles is shown. A basic principle and actual designs are illustrated, and experimental results using protein binding on the patterned T-motif lattice structure are described.

Chapter 5 focuses on a fundamental theory of substrate-assisted self-assembly. The scheme of this theory can be divided into two mechanisms, such as; 1. adsorption of DNA to the surface, and 2. hybridization of DNA strands. Those binding and self-assembly processes are able to describe by thermodynamic and kinetic frameworks. The derived expressions are used for kinetic simulations of substrate-assisted self-assembly. The result shows the feasibility of the theory and illustrates some interesting phenomena discovered in experiments.

Finally, chapter 6 concludes the results and discussions in this thesis by answering the questions raised in chapter 1.

Appendix A, C and D show additional AFM data and analyses. Appendix B describes spectrophotometer data, which gives a characteristic of formation/melting process of self-assembly. Appendix E calculates monovalent/divalent ion concentrations of the buffer used in experiments. Source codes of the design software and simulations are described in Appendix F.

Chapter 2

Motif-based DNA nanostructures

Contents

2.1 DNA as a nanoscale building block 5

2.2 Motifs 7

2.2.1 Immobilized Holliday Junction 7

2.2.2 DX molecules and DX Tile 8

2.2.3 TX tile,Cross tile, 3-point star motif and Single-stranded tile 11

2.3 Basic procedure for design and self-assembly of DNA motifs 12

2.3.1 Self-assembly 15

2.3.2 Observation and analysis 16

2.4 Summary 17

2.1 DNA as a nanoscale building block

The discovery of DNA double helix by Watson and Crick[Watson 1953] widely triggered a giant leap in various scientific fields, such as molecular biology, genetics and nucleic acid chemistry etc. A driving force behind those leaps was the understanding of basic principles of duplex formation, known as Watson–Crick base-pairings of double helix. Complementarity of bases, such as Adenine (A) with Thymine (T) and Cytosine (C) with Guanine (G), gives us a "program" of DNA strands which form a double helix. Biology reads the sequence of strands and seeks meanings hidden in those codes; on the other hand, from a point of view of engineering, DNA

double helix is a molecule that structural information is implemented in terms of the sequence. Thanks to the various works in science, now we can simplify the B-form DNA as a cylinder with 2nm diameter, 10.5 base pairs for one turn and 0.34nm per base pair. This abstraction by the sequence liberates the design of DNA helix as a standardized nanoscale material with sub-nanometer precision, without digging down into the atomic-level design.

The ultimate goal of nanostructure study is to find a general methodology for creating arbitrary shapes and patterns. One of the comprehensible approaches for this goal is to create building blocks that cover mostly all variations. Recently, DNA molecule is considered to be one of the most "controllable" materials for bottom-up self-assembly (so far) because of the convenience in design. This field of research is known as structural DNA nanotechnology.

There are two basic methodologies in structural DNA nanotechnology. Each methodology has advantage and disadvantage, so we have to compare and choose the adequate way of creating nanostructures. One is called "nucleated self-assembly"[Yan 2003a], using long DNA strand as a core of the structure along with an aid of short interconnecting DNAs to self-assemble into structures. This methodology is generalized by "DNA origami"[Rothemund 2006, Douglas 2009, Dietz 2009]. DNA Origami uses long single-stranded DNA with known sequence[1] as a scaffold to fold into two and three-dimensional shapes, connected by short strands called "staple strands". The beauty of this method is that we can design arbitrary shapes as long as we follow the rules of folding. On the other hand, the size of one single structure is basically restricted by the length of the scaffold strand, so the typical upper limit of the structure is about a hundred nanometer in size. The other method is called "motif-based self-assembly". A motif is a building block for nanostructures, which uses several DNA junctions as a repeating unit. Motifs are connected each other by short single-stranded regions with complementary sequence placed at the end,

[1] Phage vector M13mp18, one of the typical vector used in biochemical experiments, is usually used as a scaffold.

known as sticky ends. This methodology has a restriction in varieties of design, because we have to consider continuity and periodicity of the helix inside/between each motif. The significance of this methodology is, however, once well-structured motif is designed and self-assembled in adequate condition, we can obtain micrometer or even up to millimeter-scaled DNA crystal structures.

This chapter focuses on the introduction of the latter motif-based DNA nanostructures. The fundamentals and important idea of motif-based self-assembly along with several milestones in history, actual designs, the procedure of assembly and observations are described.

2.2 Motifs

2.2.1 Immobilized Holliday Junction

In 1982, Nadrian Seeman proposed an idea of using "immobilized" nucleic acid junctions to form 2-dimensional and 3-dimensional lattice structures[Seeman 1982, Kallenbach 1983]. A four-way junction structure, known as Holliday junction, is an intermediate configuration found in genetic recombination. The original Holliday junction structure has a homologous sequence in the structure; therefore, a crossover point can migrate back and forth so as to exchange genetic information between two double helices by a reciprocal interchange of the strands. The idea of immobilized junction is to change this sequence into unique Watson–Crick base-pairs. This crossover conformation is then can be used as a fixed connection between helices, which extends one-dimensional geometry of double helix into higher dimensions. A design of periodical junction "networks" are originally considered to use this crossover junction in cruciform configuration, though this simple junction design often gives us a three-dimensional network rather than two-dimensional structures in free-solution[Seeman 2007, Nishimoto 2009]. This concept of connecting units in periodical manner by complementary sequence is now one of the most fundamental methodology to create two and three-dimensional objects by DNA. A periodical unit

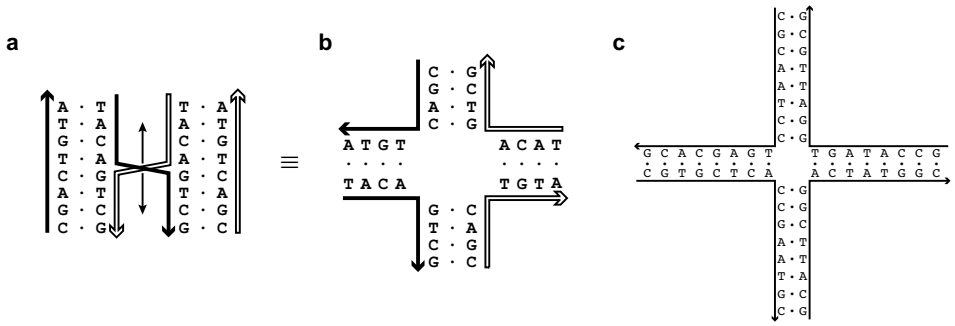

Figure 2.1: Holliday junctions. **a** Originally proposed Holliday junction structure. **b** Identical representation of Holliday junction. **c** Seeman's immobilized junction structure.

for structures is now called as a motif, and an interconnecting region placed at the edge of the motif is known as a sticky end. This concept is now known as "DNA tiles".

2.2.2 DX molecules and DX Tile

Self-assembly of periodical 2-D DNA nanostructures using the concept of motif and sticky ends is first realized by the invention of DX (Double Crossover) tile in 1998 (Fig.2.2)[Winfree 1998a]. DX tiles use DX molecules for its motif design[Fu 1993]. DX molecules have two double helices connected by two "stacked X" formation[Clegg 1994, Duckett 1988] of crossover junctions (immobilized Holliday junctions). The significance of their work was not only utilizing immobilized DNA junction, but also the definition of geometry by this junction, whose appearance is based on aligned axes. These two crossovers fix relative position of two helices in parallel. This unique geometry defined the way to utilize rigidity of DNA, thus this geometry become a fundamental to design and create DNA nanostructures. Several types of DX molecules can be designed, although DAE (Double crossover, Anti-parallel crossover junction, Even half-helical turn spacing between junctions) and DAO (Double crossover, Anti-parallel crossover junction, Odd half-helical turn spacing between junctions) molecules are widely used in actual experiments (Fig.2.3).

DNA tiles based on this DX molecule are realized by extending one of the strands at each end of the helix (Fig.2.4). A DX molecule defines the shape of the tile, and four sticky ends define the connectivity between the 'edges' of the tile. Each sticky-end assigned with specific sequence represents values and Input/Output of the system. This definition of connectivity leads us to the realization of algorithmic self-assembly of DNA tiles, described in section 4.2.

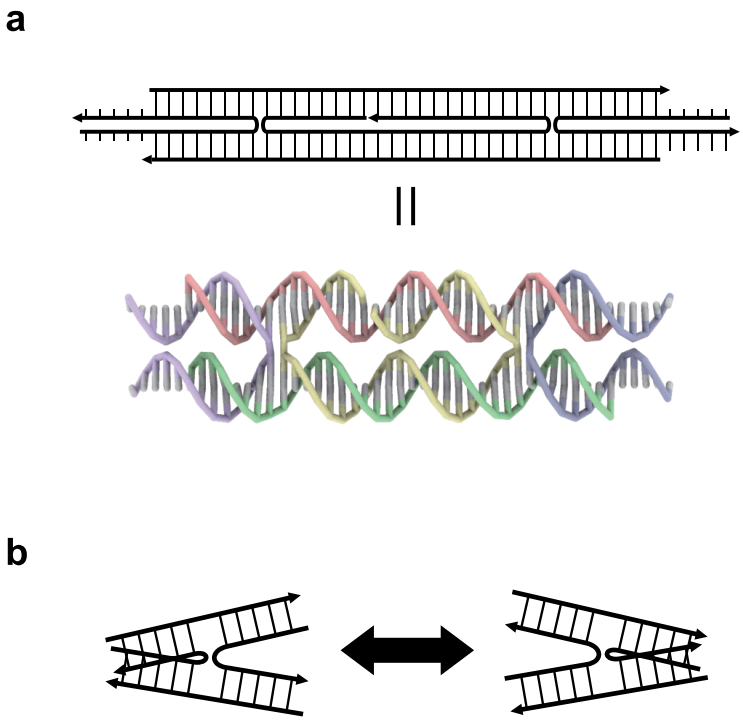

Figure 2.2: DX tile (DAE). **a** A tile consists of five DNA strands, forming two crossover junctions at the center of the motif. Sticky ends are positioned at both ends of the helices. **b** A single crossover junction cannot define an angle between helices.

One of the reasons for success of this tile concept in DNA self-assembly is a realization of "rigid" molecule design. As I mentioned before, in case of DX tiles, double crossover molecule defines the exact relation and position (topology) of helices and four sticky ends. When sticky ends are hybridized, the connected region becomes a part of the continuous double helix. Because of the both hybridization and stacking effect between helices, connected sticky ends also behave as a rigid

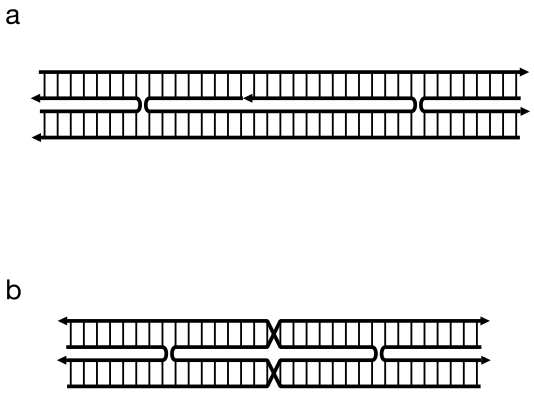

Figure 2.3: DX (Double Crossover) molecules. **a** DAE (Double crossover, Anti-parallel, Even half-helical turn spacing) molecule, **b** DAO (Double crossover, Anti-parallel, Odd half-helical turn spacing) molecule. Anti-parallel/Parallel is defined by types of crossover junction, and Even/Odd is defined by the interval width of crossover junctions inside the molecule. Arrowheads represent 3' end of the DNA strand.

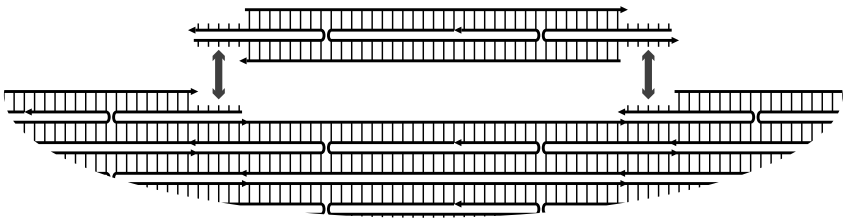

Figure 2.4: DNA tile self-assembly (DAE tile). Each DNA tile represents a "square tile". Connection between edges are interpreted as a duplex formation between sticky ends (gray arrow).

helical region comprising a part of self-assembled structure. This design of rigid motif and sticky ends enables us to design DNA nanostructures that self-assembles even in the solution (*i.e.* the degrees of freedom in all three-dimensions).

2.2.3 TX tile,Cross tile, 3-point star motif and Single-stranded tile

There are other types of motifs for two-dimensional self-assembly, which appearances are also constituted by 'bundled' parallel helices. TX (Triple crossover) tiles[LaBean 2000] are made from three helix bundles (Fig.2.5a). Each helix position is fixed by crossover junctions. Four out of six ends of the motif are used as sticky-ends as same as DX tiles.

Moreover, also there are some species of motifs which bundled helices are connected each other by flexible linkers. In these cases, the appearance of the self-assembled structure is not restricted in parallel axes; sticky ends are connected with certain degree of flexibility. One example is the cross tile (Fig.2.5b)[Yan 2003b]. Each side of the tile is made of two helices, connected by one crossover junction. Those units are connected to the neighboring helix directly on one strand and by T4 linkers (linked by a single-stranded nucleotides with a sequence of four Thymines) on the other. This cross-shaped motif forms large two-dimensional lattice structure when the adjacent tiles are self-assembled in upside down manner in order to cancel out sequence-dependent distortions caused by the motif itself. Three-point star motif[He 2005] is another example (Fig.2.5c). Each arm of this Y-shaped motif forms a pair of DNA duplex. Each pair is connected to adjacent pairs using T3 linkers, similar to the cross tile. (Notice that this motif have only three ends; we need to construct different tile system compared with four-ends when we implement algorithmic self-assembly in this case.)

Single-stranded tile[Yin 2008] is another species of motif that designed to be self-assembled into "one"-dimensional ribbon and tube structure made of bundled helices(Fig.2.5d). This motif has only sticky ends in the structure: connections

between motifs and formation of the self-assembled structure are achieved all at once. However, because of the kinetic trap during formation, the motif is difficult to self-assemble into two-dimensional lattice in free solution. This result suggests that 1. we do not always have to design a motif with complete rigidity before connected by sticky end; 2. kinetic trap has a large effect in self-assembly of motif-based DNA nanostructures in free-solution.

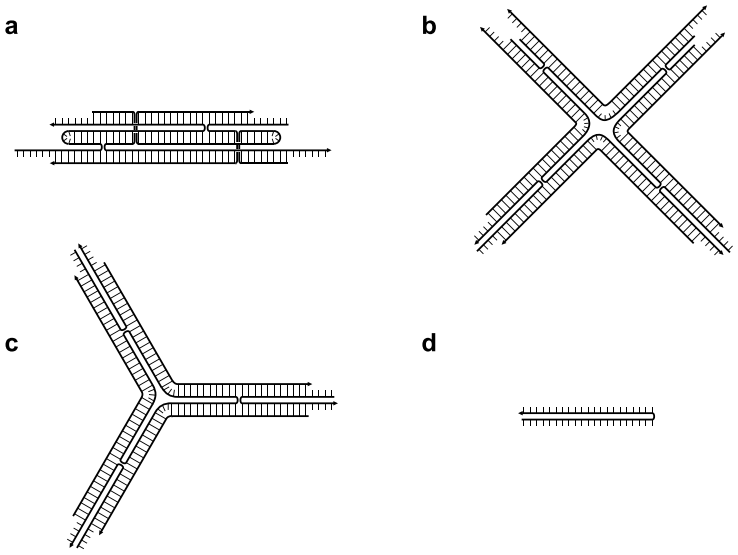

Figure 2.5: DNA tiles. **a** TX tile, **b** Cross tile, **c** Three-point star motif and **d** Single-stranded tile.

2.3 Basic procedure for design and self-assembly of DNA motifs

A design methodology of motif is a process to convert shapes into set of actual DNA sequences. This process can be divided into three stages. The first stage is to design a "shape" of motifs by combinations of several DNA junctions. The second stage is to "translate" those shapes into relations between DNA strands. The third stage is to define actual sequence that follows the relations.

Shape design

First, we design a shape of a motif by combinations of junction structures (Fig. 2.6a). We have to consider both phase and length of inter/intra-motifs at once. Adjustments are done by adding/subtraction of base pairs between junctions/motifs. The motifs have to be designed as a continuous structure excluding inconsistency of phases and lengths. Next, we divide those structures by defining sticky ends between motifs (Fig. 2.6b). Notice that the base pair length of sticky ends are usually shorter than the motif because of the process of self-assembly mentioned in section2.3.1.

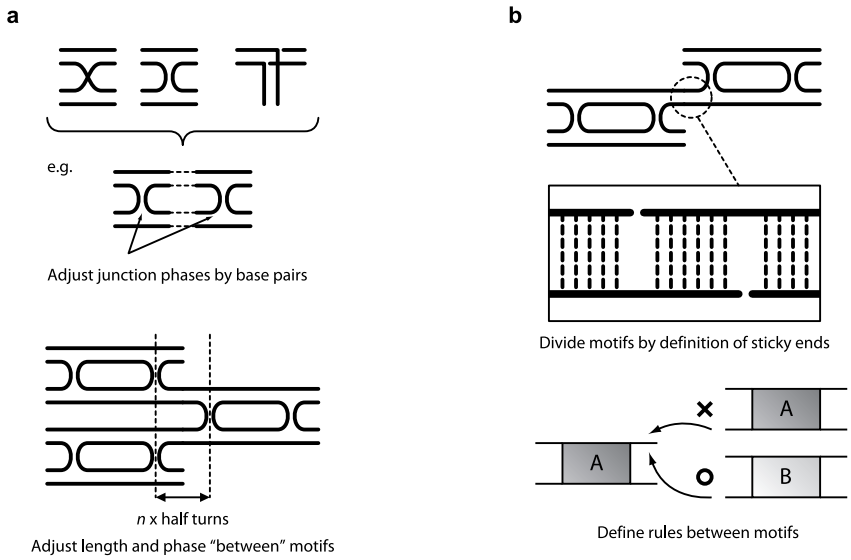

Figure 2.6: Design of shapes. **a** Design of motifs.**b** Design of sticky ends.

Translation

The next step of motif design is the translation from shapes into relations between strands (Fig. 2.7a). Current designs of DNA motifs are based on double helix formation by Watson–Crick complementarity. Because of this accurate rule, we can define regions of strands that compose a double helix with other strands (Fig. 2.7a,b). In the figure, regions that comprising double helix are segmented by different colors

(a). When we decompose the motif, the colors represent each relation between other strands at certain regions (b). Consequently, the shape design of motif is converted into colors and regions of strands.

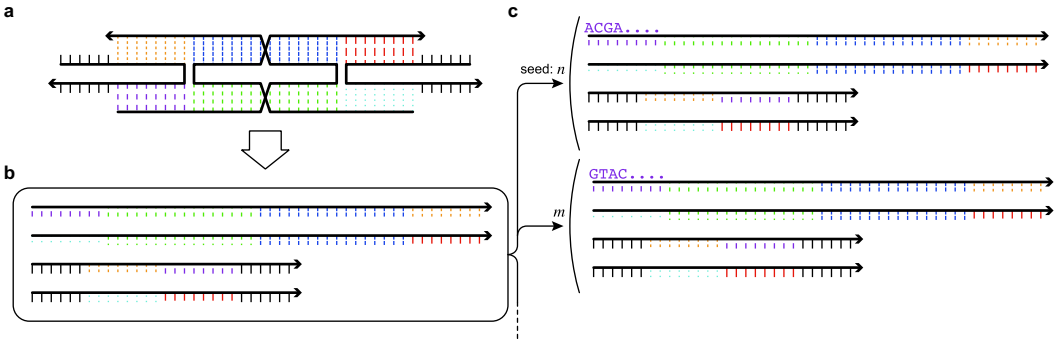

Figure 2.7: Conversion from shape into strand relations, from strand relations to actual sequences. **a** shape design, **b** strand relations defined by colors, **c** actual sequences.

Sequence Design

The last step of design is the assignment of the actual sequence based on the information between strands (Fig. 2.7c). Sequences are allocated based on the following guidelines: 1. satisfy the complementarity written down in the form of strand relations, as identified above, 2. sequences at other regions have to be orthogonal, in order to avoid unexpected hybridization or self-fold (double helix formation) between strands. This step is executed by a computer algorithm in general. The important point at this stage of design is that we have to consider only relations between strands in the sequence design; we can define actual sequence in many ways as far as they satisfy the constraints. This freedom in sequence enables us to design several types of motifs that the shape is identical but the internal sequences (and sticky end sequences) are completely different, which avoids unexpected crosstalks between motifs at the same time.

2.3.1 Self-assembly

DNA nanostructures are self-assembled by the simple process called "annealing". In general, annealing is a reformation process of complementary strands into helix by a gradual decrease in temperature. Structural DNA nanotechnology uses this process as a formation of DNA motifs and self-assembly of nanostructures in sequential order. Sample tubes are put into styrofoam box filled with hot water or thermal cycler[2], and then environmental temperature is gradually cooled down to room temperature or 4°C in about 2 days or more (Fig. 2.8). During this process, motifs are formed at high temperature because of the longer lengths of hybridization, and then structure is self-assembled using sticky ends between (already formed) motifs at lower temperature; in turn, we have to design motifs carefully so as to follow this order of assembly. This self-assembly process can be indirectly traced by UV spectrophotometer observing the absorbance of DNA hybridization at 260nm.

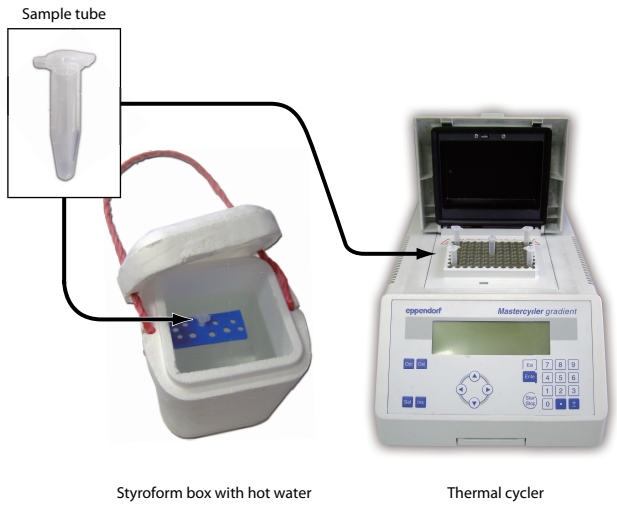

Figure 2.8: Two ways of annealing.

[2]One of the basic appliance used in biochemical experiments, which controls the temperature of the tubes inside based on a program

2.3.2 Observation and analysis

1D and 2D DNA nanostructures are often observed and analyzed by electrophoresis and AFM(Atomic Force Microscope) experiments.

Electrophoresis of DNA nanostructures

Electrophoresis is one of the common methods used in Biochemistry. When we apply external electrical field on the gel with electrolytes, charged particles/polymers are affected and electrostatic Coulomb force induces the movement. DNA has negative charge at the sugar-phosphate backbone of the strand, thus the molecule is pulled towards the anode side of the gel. Since the speed of migration is different in the length of the strands and the shapes of the structure, we can separate and classify the structures of the sample.

AFM (Atomic Force Microscope)

AFM is a type of Scanning Probe Microscope (SPM), which uses a probe placed at the tip of cantilever to observe the sample shapes fixed on a surface in high resolution. Tapping mode[3] in liquid environment is often used for observation in structural DNA nanotechnology. Tapping mode keeps an oscillating cantilever at certain constant amplitude. When the cantilever tip "touches" the surface, the oscillating amplitude is changed because of the intermolecular force between the tip and the surface: the detector perceives the difference in amplitude and converts this information to the height of the surface.

Freshly cleaved mica surface is often chosen for the surface for AFM observation of DNA nanostructures. An electrostatic interaction between mica surface and DNA via divalent (or more) cation is used for the binding of structures. This effect is known as a counter-ion effect, which weakly adsorbs DNA nanostructures on a flat surface. The details and a theoretical explanation of this phenomenon is discussed

[3]Tapping mode is a trademark of Veeco Instruments Inc.

in chapter 5.

2.4 Summary

A brief introduction of the motif-based DNA nanostructures, the methodology of design and experimental procedures are discussed in this chapter. An overview of the concept of motifs and some examples of DNA tiles are shown. Current motifs are made from several crossover junctions, mostly based on geometry of aligned helices. A certain degree of rigidity is an important factor in order to form structures in solution. Motifs are designed by three stages: design of "shapes", translation from shapes into "relations" (or constraints) between strands, and actual "sequence" design. Structures are formed by a process called annealing. Motifs have to be designed carefully so as to follow the sequential order of formation during annealing process. Self-assembled structures are observed by AFM or electrophoresis.

Chapter 3

T-junction and T-motifs

Contents

3.1 T-junction 19

3.2 T-motif 23

3.2.1 Design 25

3.2.2 Self-assembly in free solution 27

3.3 Summary 28

3.1 T-junction

A systematic methodology of structural design and assembly enabled motif-based DNA nanostructures as one of the compelling way to create nanoscale structures and patterns from molecular level. The variation of design relies on a combination of DNA junctions. Current DNA motifs are using only crossover junctions: still there are geometrical constraints and therefore limitations in design are unavoidable in some cases. In this chapter, a design of T-shaped junction named "T-junction" is described along with discussions about several characteristics that can clear some of the current limitations in design and expand further varieties of DNA nanostructures.

A T-junction (Fig.3.1b)[Hamada 2009] provides an orthogonal geometry by an interconnecting a short single-stranded interval (called a bulge loop) of a double

helix to a single-stranded end of another helix (Fig.3.1a). Both single-stranded regions meet Watson–Crick complementarity by each other, leaving no unpaired bases. When those regions are hybridized, the former duplex is perpendicularly bent and the latter is inserted into that region, resulting in an interconnection. A branch can be placed anywhere on the major groove of the trunk, using five or six nucleotides as a single-stranded region. This length is derived from the distance between backbones of complementary bases and the axial length in base pairs (Fig. 3.2). Note that a T-junction itself plays the roles of both junctions and sticky-ends, whereas junctions and sticky-ends are located at different regions in conventional crossover junction-based motifs; formation of the junction itself and connection between motifs are achieved simultaneously using T-junctions.

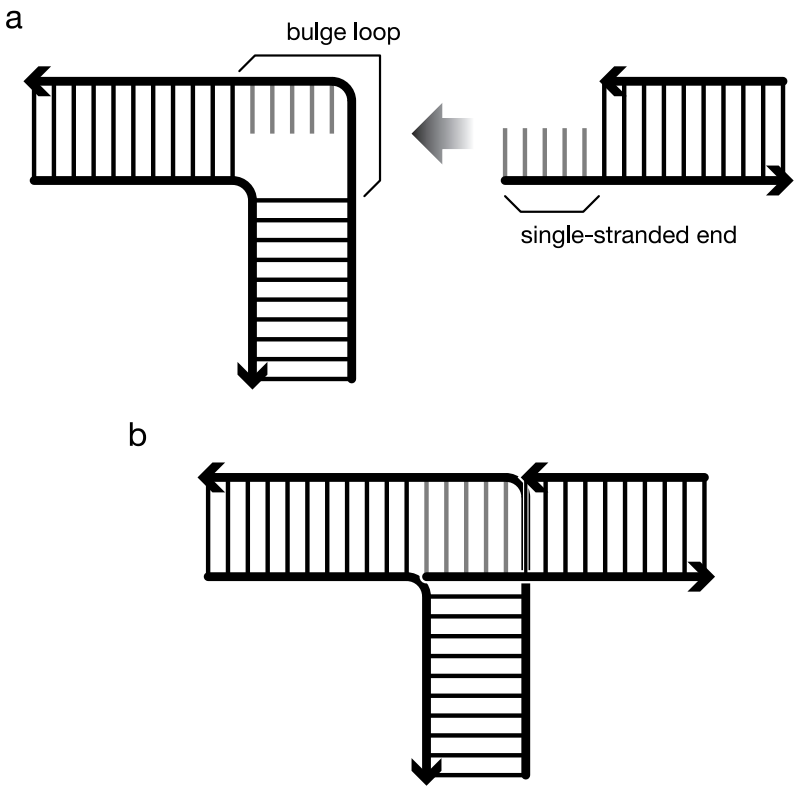

Figure 3.1: T-junction. **a** An interconnection of a bulge-loop region and a single-stranded end comprises a T-junction. **b** A schematic of formed T-junction.

This structural difference of T-junction gives us novel characteristics, such as:

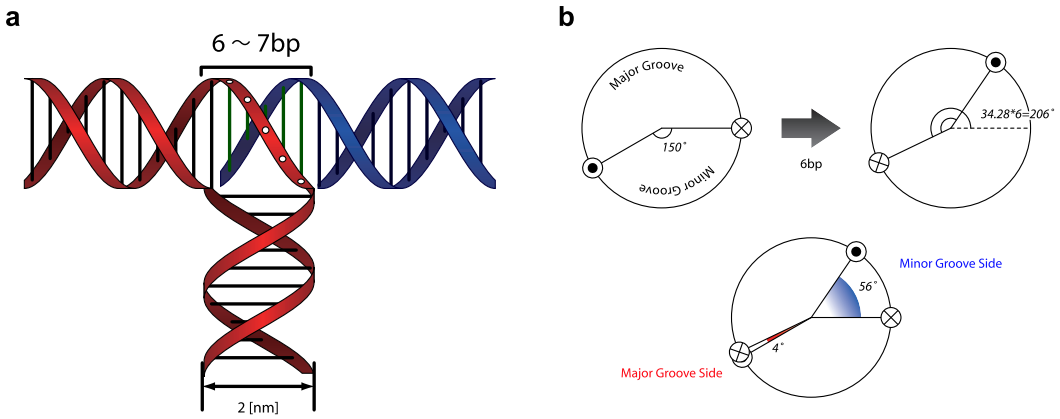

Figure 3.2: Geometrical analysis for optimal axial length and phase difference of T-junction. **a**, axial base pair length calculation. One base pair is 0.32[nm] for B-form DNA, so 6bp: 0.32 x 6 = 1.92[nm], 7bp: 0.32 x 7 = 2.24[nm]. Compared to the DNA double helix diameter (approximately 2[nm]), 6 or 7 bp is considered to be the optimal length; **b**, Phase difference in 6bp is compared with major groove side and the minor groove side. The calculation is based on that minor groove angle is 150 °and 1bp turn is 34.3 °(= 360 °/10.5). Compared with Minor groove's phase difference (56 °), Major groove side's phase difference is smaller (4 °), thus branching at this side is preferable. This result is indirectly supported by the electrophoresis experiment, comparing major groove side junction with minor groove side (data not shown).

- **Providing a new geometry**

  In the previous section, we mentioned that DX, TX, Cross and Three-point star motifs are all based on crossover junctions, and thus all motifs are using 'bundled' parallel helices as a fundamental of its design. By combining several T-junctions into a motif, we can create a broader class of shapes and patterns.

- **Improvement in structural resolution**

  The constitutional unit of one T-junction is an interconnected branch structure placed on the major groove of a double helix. This junction can define the position of the branch by itself; therefore, the spatial resolution size of a T-junction based motifs would be the length of the sticky end + 1 (6 or 7 bp (bp: number of base pairs)). On the other hand, crossover junction itself cannot define fixed formation of helices. Crossover junction based structures generally need more than two junctions to fix their conformation, and therefore they require at least one full turn (10.5 bp) for minimal fixed structure.

- **Relaxing electrostatic repulsions**

  Electrostatic repulsion among DNA backbones usually results in distortion of nanostructures. Parallel helix-bundled motifs are more likely affected by this phenomenon because adjacent helices are placed closely side-by-side to each other. T-junction can relax this effect thanks to its T-shaped formation of helices; in principle, they have clearance between helices, and the resultant nanostructure can avoid distortion observed in some parallel helix-bundled DNA motifs [Rothemund 2004a, Liu 2005].

- **Providing a balance between flexibility and geometrical accuracy**

  The key aspect whether the motif forms structure or not is mainly a matter of flexibility. Generally, single-duplex based branched motifs do not form structures due to the lack of structural integrity[Liu 1994, Yang 1998]. As a consequence, current basic strategy of DNA nanostructure design is to build

"rigid" motifs as building blocks for self-assembly in solution by combining several duplexes with crossover junctions[Sa-Ardyen 2003]. In this sense, increasing structural integrity enough to self-assemble is an important factor. On the other hand, geometrical accuracy of resulted structure regulates the maximum size and homogeneity of the structure. Although motifs are carefully designed to minimize distortion under 10.5[bp]/turn as B-DNA conformation, the helices are deviated from this standard. Solution conditions, backbone repulsion and sequence-dependent bends are some of the factors that might cause misalignment in self-assembly. Giving too much structural integrity leads to this problem, because of its strict geometrical restraint. Therefore, structural relaxation inside motif is required to avoid this issue[He 2006]; at the same time we must notice that deforming of the structure must be minimized to keep geometrical accuracy. T-motif can settle this balance with structural integrity of T-junction and structural relaxation of single duplex. T-junction's structural integrity is obtained by the absence of unpaired bases inside junction, which realizes right-angled branch and provides rigidity of the structure. Structural relaxation to keep proper geometrical accuracy is realized by torsional relaxation of single duplex.

3.2 T-motif

T-motif is the generic name for the motifs which design is based on combinations of T-junctions. Based on the design of T-junction, various T-motifs are designed and self-assembled as a demonstration to show the possibilities of this motif. In this section, the graphical abstraction for the motif design, actual examples and the AFM results of the self-assembly are discussed.

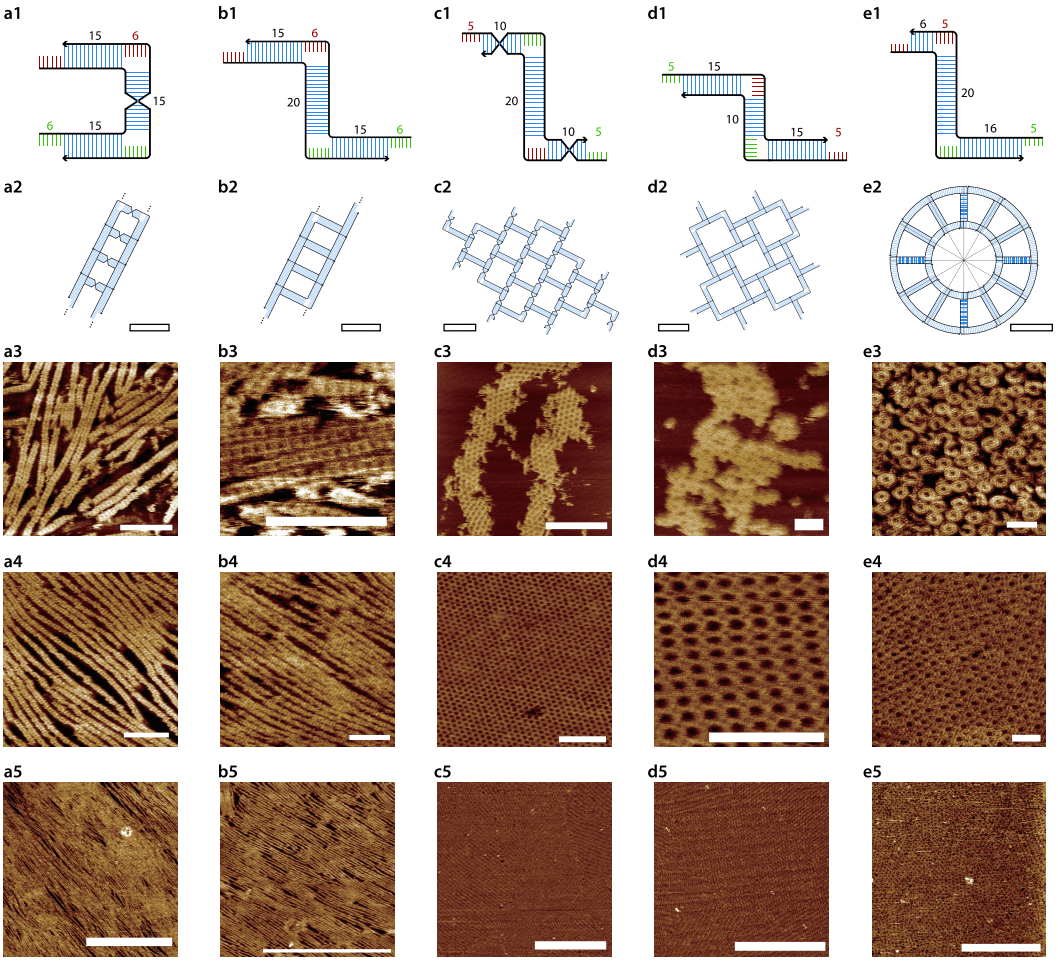

Figure 3.3: T-motifs. **a** 1-D ladder 15-15-15(7), **b** 1-D ladder 15-20-15(7), **c** 2-D brickwall lattice, **d** 2-D windmill lattice, and **e** ring1.0x. **Row 1**, schematic motif diagram. Red and green bases correspond to complementary sticky ends. Note that some crossed sequences are drawn only in order to arrange the sticky-end position properly. Length is expressed in terms of base pair (bp). **Row 2**, schematic structure diagram; **Row 3**, free-solution self-assembly results (AFM images); **rows 4 and 5**, mica-assisted self-assembly results (AFM images). Scale bars: rows 3 and 4 = 100 nm; row 5 = 1 μm.

3.2.1 Design

T-motif-based nanostructures were first designed by using 2-D graphical abstraction (Fig. 3.4). One half turn of the double helix was represented as one square, and the structure was designed with combinations of these squares. A T-junction was represented as two perpendicularly connected squares on the major groove side. This block-based abstraction aims to avoid unintended mistakes in the design process, such as reversed 5'-3' strands, major/minor grooves of helix or phase contrast arise from half turn difference. Those problems in phase difference and lengths are both considered at once. A simple computer tool is written for an aid of this design process (Appendix F). After designing by the abstraction, this information was converted into base-pair lengths (half turn=5 or 6bp of helix), and then actual sequences were determined based on the constraints between strands using different software.

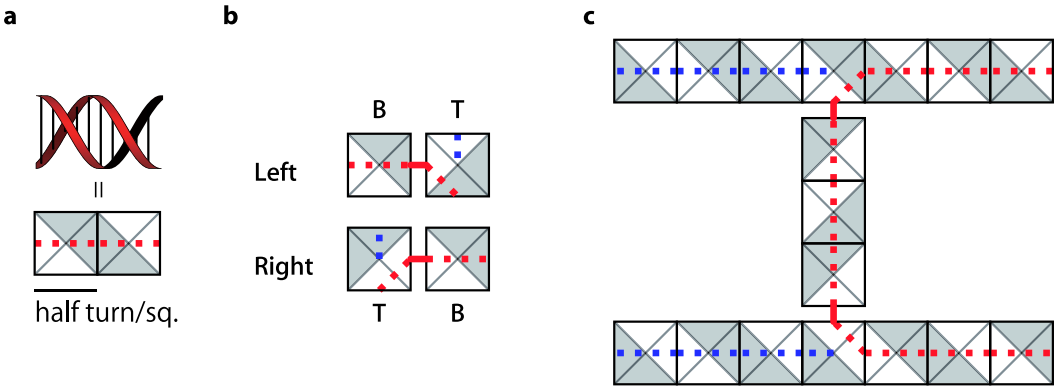

Figure 3.4: 2-D graphical abstraction. **a** Double helix. Gray area indicate minor groove, and white area indicate major groove of double helix. Colored line shows the continuity of the helix. **b** T-motif abstraction. Both 'left' and 'right' are the same structures, except those are inverted. **c** 1-D Ladder 15-15-15 as an example of this abstraction.

Two types of 'track' (ladder), two types of orthogonal coordinate porous '2-D lattice' and polar coordinate 'wheel' (or 'Ring 1.0x') structures were designed by this method. First, two types of track structures were designed to show configuration control of phases (Fig. 3.3a and 3.3b, rows 1 and 2). The connection was based

on T-shaped junctions, although the ladders' opposite 'handrail' directions were inverted in two designs. The 'rung' length of a ladder determined this inversion adjustment. Second, two types of 2-D lattice structures were designed to examine base-pair parameters (Fig. 3.3c and 3.3d, rows 1 and 2). These designs showed that even a small change in duplex length lead to drastic structural differences. The 'brick-wall' type was obtained by changing the helix length (half-turn difference) of the track structures' 'handrail'. This planar structure was designed to provide a more than three times higher resolution in square than in crossover-based porous structures[Yan 2003b]. The 'windmill' type was another pattern with two sizes of pores showing different combinations of junctions, which were connected to each other with a 90°rotation. The ring structure utilized the flexibility of the T-motif's single duplex-based structure (Fig. 3.3e, rows 1and 2). Compared with the ladder design, one side of the 'handrail' was shortened and the other was extended; thus, this length difference determined the curvature of the assembled ring structure (Fig. 3.5).

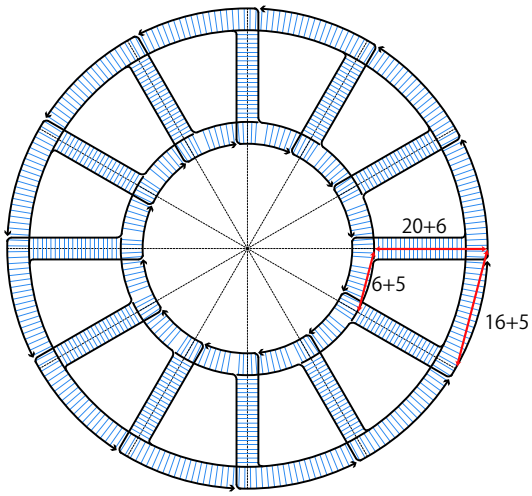

Figure 3.5: Detailed schematic of the ring 1.0x structure consists of 12 units. "Spoke" part has 20bp, however considering the hoop's duplex diameter, 6bps are added to the length of the red arrow. Inner ring's one unit is 6bp + sticky end length (5bp). Outer ring's one unit is 16bp + sticky end length (5bp). The length difference between inner and outer ring (10bp, near equals one turn of duplex) determines its curvature. The estimated diameter from this design is 37[nm].

3.2.2 Self-assembly in free solution

Each set of equimolar strands was mixed in buffer solution and slowly annealed from 95°C to room temperature or 4°C to self-assemble into structures.

UV absorbance during annealing/melting of the structure by spectrophotometer shows two-step formation of the structure (Fig.B.1). The curve shows an absorbance at the wavelength of 260nm; descents of the curve correspond to the hybridization of DNA double helix. The first descent at higher temperature indicates the formation of motifs, and the second one indicates the formation of the structure (*i.e.* motifs are connected by sticky ends). The curves of 2-D brick-wall lattice (Fig. AppendixB.1a) have a hysteresis at the second hybridization stage (lower temperature). This hysteresis has also been observed in other types of DNA tiles[Barish 2005, Schulman 2007, Yin 2008]. The result suggests that there is a kinetic barrier in the formation process, such as a nucleation barrier. Several units are needed to form stable structures, because four sticky ends of the motif are all connected with other four units. On the other hand, a hysteresis has not been found in the curve of Ring 1.0x (Fig. Appendix B.1b). This result indicates the mechanism of formation is different in 2-D lattice and "1.5"-D ring structures. Motifs of the ring are always connected with adjacent ones by two sticky ends; a nucleus is unnecessary in the formation process.

The annealed solutions were observed on the mica surface by AFM imaging. All designs formed the expected structures on free-solution annealing (Fig.3.3a to 3.3e, row 3; Fig. Appendix A.2e and f; Fig. Appendix A.3a, c, g). Both 1-D tracks were well formed, although their length was restricted for about several hundred nanometers. The 2-D brick-wall lattice was also formed with preference for the growth direction. This directed growth could have been caused by the motif's flexibility, leading to tubular structures as it grew until a particular size was reached, because the kinetic effect preferentially assumes a tube formation rather than maintaining a planar structure in solution. On the other hand, the windmill, another

type of 2-D lattice, failed to form large structures in free-solution environment. We successfully observed a closed ring structure, although its yield was not high (Fig. Appendix A.1). These phenomena of the rings are modeled and analyzed in chapter 5.

3.3 Summary

A design of T-junction and self-assemblies of T-motifs in free solution are discussed. A T-junction has several characteristics compared with crossover junction, such as; 1. a new (non-parallel) geometry, 2. an improvement in structural resolution, 3. relaxing electrostatic repulsions, 4. providing a certain degree of flexibility. Motifs designed by T-junctions are called T-motifs. Configurations of T-motifs can be controlled by the length (or phase) of helix. 2-D block-based graphical abstraction can be used for convenience. Several motifs are designed for demonstration. All designed motifs are based on two strands, forming double-elbowed shape. Large variety of shapes and patterns are designed by T-motifs: the difference in the length of helices gives a class of one to two-dimensional structures. The formation of the structures is succeeded, although yields of the complete structure (or length/size of the crystal) is not high enough, mainly because of the flexibility.

Chapter 4

Experiments on substrate-assisted self-assembly

Contents

4.1 Substrate-assisted self-assembly 29

4.1.1 Experiments of substrate-assisted self-assembly 31

4.2 Algorithmic self-assembly of T-motifs 32

4.2.1 Wang Tiles and Algorithmic Self-Assembly 33

4.2.2 Implementation of Cellular Automaton 35

4.2.3 T-motif tiles 36

4.2.4 Experiments 39

4.3 Summary 40

4.1 Substrate-assisted self-assembly

This chapter discusses the details of the experimental procedures and results of substrate-assisted self-assembly of DNA nanostructures, and the advanced examples using algorithmic self-assembly, combined with protein attachments on the lattice structures.

AFM observation results of T-motifs revealed that the formation of structures in free solution didn't grow as large as original anticipations, compared to the other

types of motifs. Especially, two-dimensional structures form tubes and troidal formations (Fig.3.3c3, AppendixA.4), or only a small fragment of planar structures (Fig.3.3d3). As mentioned in section3.2.2, this result indicates that the flexibility of motifs affects the formation of the structure itself. In case of brick-wall lattice, structural stiffness is enough to form certain kind of structures, although kinetic effect enabled to form tubes. In case of windmill lattice, the structure is assumed to be much more flexible than the brick-wall lattice, because of the discontinuity of DNA double helices at the branch of the junction in both (x and y) directions.

In order to solve these problems, here, a novel self-assembly method called "substrate-assisted self-assembly" is proposed. Substrate-assisted self-assembly uses a negative-charged surface as a substrate for DNA binding. Counter-ion effect between DNA and the surface via divalent (or multivalent) cations weakly immobilize the structure onto a surface at certain extent[1] The surface binding gives the structure a reduction of dimensionality; one and two-dimensional structure formation is accelerated because this effect works like a splint for self-assembly.

There are several advantages of substrate-assisted self-assembly, such as,

Generality of the substrate shapes/materials: By combining curved templates and DNA motifs with flexibility, we can create various DNA-based cages or membranes, whose shape is generally controlled by the templates. If the substrate has a fusibility by a certain kind of trigger, we can even remove *after* the formation of structures. Although the experiments in this chapter were carried out only using a flat planar mica substrates, note that this method can also be applied to the other types of shapes, such as spheres and even patterned templates, or even different types of substrate materials.

Wide compatibility with other types of motifs: Our experiment was performed under the same buffer conditions and annealing protocol as for crossover-based motif self-assembly; therefore, both T-junctions and crossover

[1] The details and the theory of this effect is discussed in chapter 5.

junctions are compatible and can be integrated into one design. Moreover, this method can be also applied to other motifs, potentially even to those previously thought to be impossible to self-assemble in free-solution environment.

Combination with top-down methodology: The requirement for the substrate is to have a certain binding effect assisting DNA to restrict geometrical freedom during self-assembly. This means that we can grow a DNA nanostructure on some patterned area of the substrate with appropriate binding effect.

4.1.1 Experiments of substrate-assisted self-assembly

Annealing protocol of substrate-assisted assembly is basically the same as usual free-solution self-assembly method except for an insertion of mica substrate in 0.6ml tube before annealing by thermal cycler (Fig.4.1).

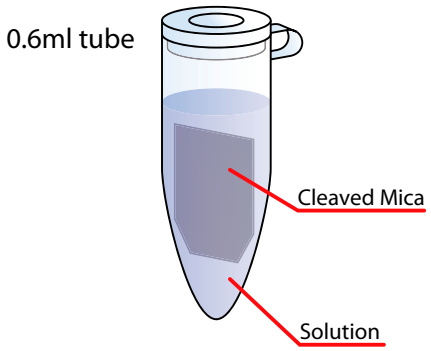

Figure 4.1: Experimental tube for mica-assisted self-assembly.

Substrate-assisted self-assembly provided qualitatively different results in comparison with the free-solution environment (Fig.3.3a to Fig.3.3e, rows 4 and 5; Fig. Appendix A.3b, d, e, f, h). The track ladders were much longer (up to micrometer scale); in addition, the ladder structures were aligned in a particular direction on the mica surface. Furthermore, although some gaps were found, almost the entire substrate surface was covered by the structure. Two types of 2-D lattices were also successfully formed (Fig. Appendix A.2a to d). A flat planar structure consisting of numbers of a few micron-sized monocrystals connected to each other was ob-

tained in both cases (Appendix Fig.D.1). In addition, the monocrystal size was enlarged by a cyclic annealing protocol (Appendix Fig.C.1). The structures were also observed without any gaps over the entire mica surface. Our estimation is that these monocrystals grow independently on the surface until they meet each other, following which part of the growth fronts are connected and form a patchwork-like appearance. Although some of the wheels had defects, most of them were successfully assembled by mica-assisted self-assembly. In addition, the wheels on the surface were aligned in hexagonal close-packed formation. These results imply that substrate assistance stabilizes a T-motif self-assembly and leads the structure to align in packed formation.

The experimental results suggest several effects of the substrate-assisted self-assembly,

- The structures are well-formed as we designed: a flexibility of structures heavily affects the formation, because of the kinetic effect and degrees of freedom in solution.
- The yield of structure is dramatically enhanced, especially in flexible structures. This result suggests that a restriction of structures on a two-dimensional surface gives us an enhancement of formation rate.
- Positional alignments/self-organization of the structures are observed in ladders and rings. This result suggests a movement of the structures on a surface.

In chapter 5, the yield and the formation rate of structures are discussed from an aspect of kinetics.

4.2 Algorithmic self-assembly of T-motifs

Substrate-assisted self-assembly enabled to self-assemble micron-scale monocrystals covering the whole surface. This qualitative difference gives T-motifs a possibility to

form complex two-dimensional algorithmic patterns on a surface. However, complex self-assemblies (by several types of motifs) on a substrate surface have not yet been investigated. This chapter discusses about the principles of algorithmic self-assembly of DNA tiles, and the actual implementation using T-motifs.

4.2.1 Wang Tiles and Algorithmic Self-Assembly

Before explaining actual implementation of DNA tiles, first we describe an abstract definition of algorithmic self-assembly[Rothemund 2004b]. The key idea of algorithmic self-assembly is a 'connection' among several types (but the same shape) of tiles using a set of local rules between adjacent tiles. In short, tiles with correct connection are successfully attached to the structure, but the tiles with incorrect connection are denied. Idealized tiles are usually square-shaped, and are connected each other by sides. Assume that we define the connection only by colors of the tile we are focusing on and four neighboring ones. For example, when white tiles are only permitted to connect with black ones, the assembled structure becomes Fig.4.2a. If we introduce a different rule such as "tiles at the opposite sides must be in the same color, but the adjacent sides must be in different colors", then one might think that the resultant structure will be like Fig.4.2b. In this case, however, rules defined only by colors of adjacent tiles are not sufficient enough to designate the unique self-assembly (Fig.4.3a). Even the attached tile itself follows the rules, although sometimes that attachment breaks the consistency of the previously assembled tiles. For example, in Fig.4.3b, black tile with question mark is induced to be an 'incorrect' assembly, because the rule between the neighboring tiles is violated because of the attachment of black tile with x-mark (three of four neighbors of the tile with question mark are black ones; *i.e.* some of the adjacent tiles become the same color). This inconsistency comes from imperfect rule definitions: more conditions between adjacent edges to restrict undesired attachments are needed. Also note that the assembly process is asynchronous: we cannot define the starting point

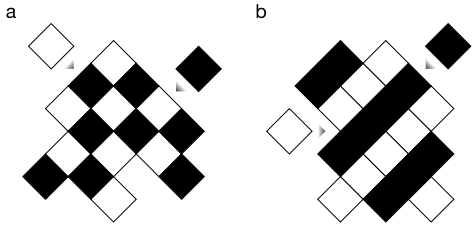

Figure 4.2: Examples of square-shaped tile assembly. **a** Checkerboard rule assembly, **b** Stripe rule assembly.

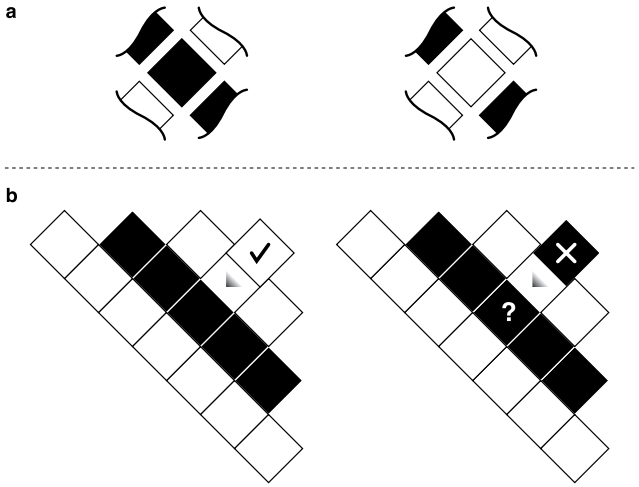

Figure 4.3: **a** Two types of tiles (Stripe rule), which is indistinguishable only by the adjacent tiles' color. **b** Examples of 'correct' attachment (left) and globally incorrect attachment (black tile with cross mark) (right).

and the order of attachments.

A 'sufficient' representation of the tile system is known as Wang tiles[Wang 1961], which uses colors on the *edge* to define connectivity between adjacent tiles (Fig.4.4a). Edges with the same color are able to connect with each other, but edges with different colors are denied. Original Wang tiles have several colors. Also note that the original Wang tiles cannot be rotated or flipped. In case of DNA algorithmic self-assembly, this idea of differently-colored edges is translated as different 'DNA sequences' at the each edge of the tile (Fig.4.4b). Only the edges with complementary sequences are connected, while the edges with non-complementary

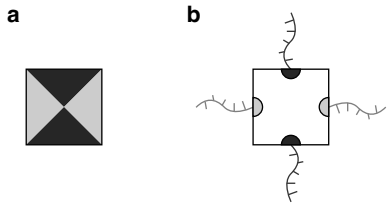

Figure 4.4: **a** Wang tile and **b** a conceptual representation of DNA tile.

sequences are denied for assembly. Because of this complementarity, the same color does not mean the same sequence: we have to think 'genders' of the edge in case of DNA algorithmic self-assembly. Various patterns of DNA tiles can be defined by some adequate, sufficient number of rules describing local connectivity at each types of tiles. The rule of self-assembly is now implemented in tile themselves as a 'tile set'. Rotation and flip of the tiles can also be avoided (or intentionally enabled) by setting those rules properly.

4.2.2 Implementation of Cellular Automaton

Definitions of inputs and outputs of the tile are one of the conceptual representations for edge distinction (Fig.4.5a). Logic gates can be described by using this representation; for example, exclusive OR (XOR) rule is translated into four types of tiles that each one has two inputs and two (same) outputs (Fig.4.5b). In this figure, we regarded the sequence at the edge of the tiles as 'digital' values; white half-circle as "0" and gray half-circle as "1". Again note that only the edges with half circles filled with the same color can be connected. We also colored tiles according to the value of outputs (0 as white, and 1 as black). An implementation of 'computation' by this algorithmic self-assembly requires another important condition; definitions of the starting point and the direction of self-assembly. A pre-formed structure with initial value is required for the boundary condition, as shown in Fig.4.6. Based on these definitions of input/outputs and initial condition, the tile system (Fig.4.7a) is now regarded as a realization of one-dimensional cellular automaton. Compared

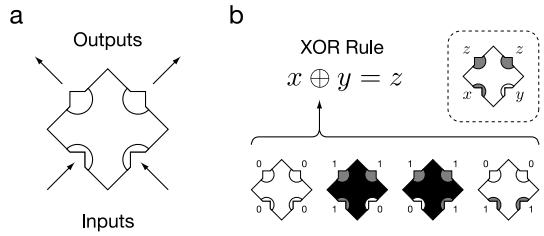

Figure 4.5: Abstraction of tile edges and representation of digital logics based on the abstraction. **a** A tile with two inputs and two outputs, **b** XOR logic gate made of four types of tiles.

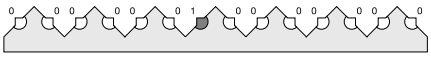

Figure 4.6: Pre-formed border with an initial value.

with the ideal one-dimensional cellular automaton (Fig.4.7b), we can notice that the space-time history of the automaton is represented in the rows of self-assembled tile structure. In the case of XOR rule tile sets and the border, a Sierpinski triangle pattern is shown as a result of self-assembly. Since 1-D cellular automata with finite symbols can simulate Turing Machine operation, this system is computationally universal in theory[Winfree 1996]. However, although the ideal Turing Machines have infinite tape size, we must deal with finite tape size (*i.e.* finite boundaries) in case of actual implementation of one-dimensional cellular automata. Also we must consider possible errors in the physical environment, such as growth errors, facet errors and nucleation errors occurring during the assembly process[Fujibayashi 2009].

4.2.3 T-motif tiles

An increase of rigidity by substrate-assisted self-assembly enabled T-motifs such as a "T-motif tile", to form complex nanoscale patterns on a surface. For algorithmic self-assembly of T-motif tiles, we picked a brick-wall motif (Fig.4.8a) for tile design. A tile comprises two T-junctions, which forms 'double-elbowed' appearance; each end of the duplex has sticky end region and is interconnected into the 'elbowed' loop region. Each tile is connected with adjacent four tiles when self-assembled

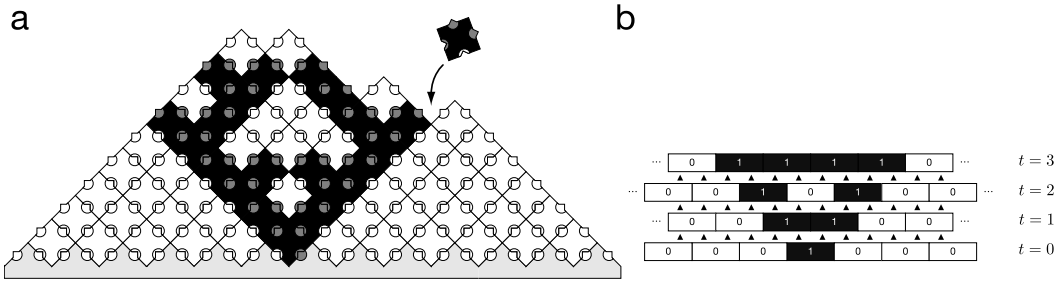

Figure 4.7: Implementation of XOR rule one-dimensional cellular automaton. **a** Self-assembly of tiles, **b** Space-time history of one-dimensional cellular automaton.

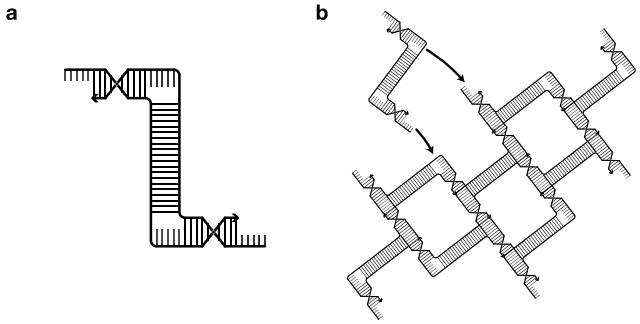

Figure 4.8: T-motif (brick-wall tile). **a** motif design, **b** self-assembly of tiles.

(Fig.4.8b), sharing each T-junction by sticky-end/loop regions. A self-assembled structure provides a two-dimensional periodical appearance made by combinations of single duplex DNAs in right-angled manner, *i.e.*, duplex DNAs are arranged in non-parallel geometry. Although tiles are connected upside down alternately in a flip-glide manner, this tile system itself is compatible with DX, TX and cross tiles because number of connections (four-ends) per one tile is the same.

The system has several advantages in design and experimental procedures in comparison with other tiles. Thanks to its single-duplex based design, the tile can avoid distortions inside the self-assembled structure. Moreover, a brick-wall motif has smaller footprints than other motifs used for DNA tiles (about 50 bp at minimum) so that denser tessellation can be achieved.

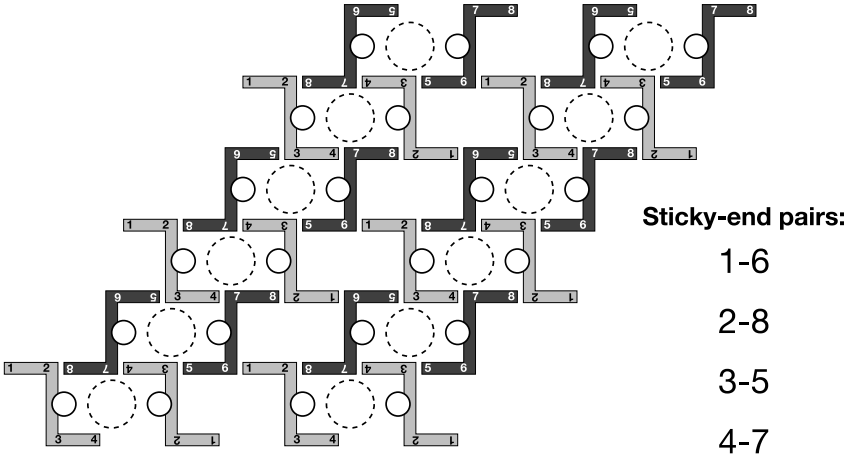

Figure 4.9: Sticky-end design and Streptavidin protein binding sites.

4.2.3.1 Design

The aim of this experiment is to demonstrate that T-motif tiles with several tile types can successfully self-assemble into two-dimensional nanostructures using several rules between sticky ends, thereby to show a capability and extensibility for algorithmic self-assembly.

Our system is made of two types of tiles. Light gray tile has sticky ends no.1 to 4, and dark gray tile has no.5 to 8. We designed sticky end connection pairs as 1-6, 2-8, 3-5 and 4-7: a resultant self-assembled structure is shown in Fig.4.9. (Note that input-output relation depends on the growth direction. In this case, we didn't use boundary structures, so either can be defined as an input.) In order to show one of the advantages of porous structures, we designed using Biotin–Streptavidin binding interaction for a visualization of pattern. A white circle at each motif indicates modified internal biotin site in DNA strands. Each Streptavidin protein fits in the 'hole' between DNA helices by two biotin sites (shown in dot circle). Patterns of the structure are recognized as B/W stripes after Streptavidin binding.

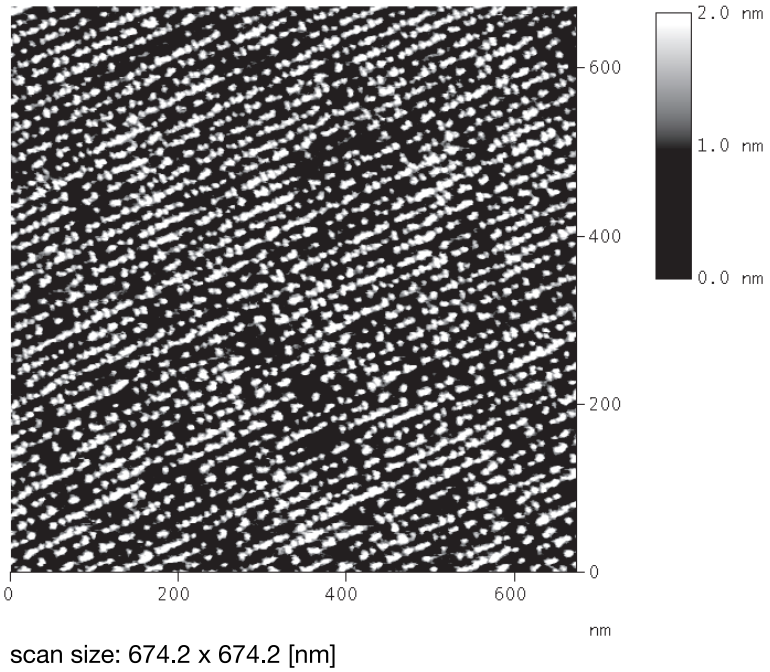

Figure 4.10: AFM observation of T-motif tiles. Height scale: 2.0nm, Scan size: 674.2×674.2nm.

4.2.4 Experiments

4.2.4.1 Procedure

A self-assembly procedure of the experiment was same as the usual experiments in free-solution, except an insertion of a cleaved mica fragment (5mm × 7mm) to the test tube. An annealing process took two days from 95°C to 20°C . After the annealing, the mica fragment was picked up from the test tube by a tweezer and then dipped into a Streptavidin solution (in a different test tube, 0.5μM) for 40 seconds for binding. After the binding, the mica is picked up again from the tube, washed 1min. by TAE/Mg^{2+} buffer and directly observed by the AFM.

4.2.4.2 Results

Fig.4.10 shows the result of self-assembly of T-motif tiles with protein binding[Hamada]. White dots in Fig.4.10a represent Streptavidin proteins, which

formed stripe patterns as we designed. Missing Streptavidins were mainly scratched off by AFM cantilever. The whole mica surface was covered by the lattice structures, although each monocrystal regions are about micron order, due to the rate of nucleation. A two-dimensional Fourier transform of the image with an iteration period of 16.5nm revealed well-distinguished peaks, proving a pattern measuring 17.6nm was formed as designed. In addition, the rate of ripping off Streptavidins indicated that the protein is properly bound by 'two' biotin sites, not only by one site (data not shown).

4.3 Summary

A novel self-assembly method called "substrate-assisted self-assembly" is introduced, and some examples including algorithmic self-assembly of T-motifs with protein bindings are shown as demonstration. Substrate-assisted self-assembly enables T-motifs to grow on a surface. This simple method has versatility in substrate shapes, motifs and even types of materials. The method enables us to create large-scale two-dimensional nanostructures in convenient way; if we can be able to use this method with top-down lithography, the way to create nanoscale patterns along with the application field of DNA nanotechnology will be greatly expanded. Moreover, substrate-assisted growth has several effects, such as an increase of flexibility, improvements of the structure yields, and alignments/self-organization of structures on a surface.

An increase of rigidity enabled algorithmic self-assembly of T-motifs. A-B tile system of brick-wall lattice is chosen for the simplest example of self-assembly using several types of tiles. Tiles are designed to hold Streptavidins between helices by two biotin sites. This tile design can be recognized as a black and white stripes after protein binding. The simple design and protein binding methodology show the reproducibility and stability of the structure. This nano-protein array mignt can be used as a "breadboard" for molecular robotics, or nano-bio applications, such as

"nanoreactors" for biochemical reactions using various types of proteins aligned via Streptavidins.

Chapter 5

Theory of substrate-assisted self-assembly

Contents

5.1 Framework of the theory of substrate-assisted self-assembly 44

5.1.1 Adsorption and surface-diffusion 46

5.2 Calculation of free energy: hybridization 49

5.3 Calculation of free energy: adsorption 50

5.3.1 Introduction to the DLVO theory 50

5.3.2 Van der Waals interactions between cylinder and surface . . . 52

5.3.3 Double-layer forces between cylinder and surface 53

5.3.4 Calculation results 58

5.4 Self-assembly model 60

5.4.1 Hybridization model of motifs 60

5.4.2 Thermodynamic equilibrium 61

5.5 Adsorption model 63

5.5.1 Thermodynamics of the Langmuir model 63

5.6 Kinetic model of self-assembly and adsorption 65

5.6.1 Self-assembly 65

5.6.2 Langmuir model for adsorption 66

5.6.3 Estimation of two-dimensional rate constant 69

5.7 Simulation 71

5.7.1 Model 71
5.7.2 Simulation in free-solution 73
5.7.3 Simulation of substrate-assisted self-assembly 75
5.8 Summary 81

5.1 Framework of the theory of substrate-assisted self-assembly

A mechanism of substrate-assisted self-assembly has not been well-understood, due to the lack of a systematic comprehension about the binding of DNA nanostructures on a substrate surface. A space-time history of the species and the states of DNA nanostructures on a surface are currently difficult to trace in real time[1]. The details and a quantitative explanation is needed in order to design substrate-assisted self-assembly in arbitrary conditions, therefore we have to develop a theoretical explanation of this phenomenon. In section 4.1, a qualitative description of the DNA binding on a surface by a counter-ion effect between DNA and the substrate is explained; however, the details of this binding, such as binding strength and the rate of bindings are not discussed. A systematic framework that comprehensively and sufficiently describe those factors, including binding process and self-assembly on a surface, is needed.

This chapter describes the theory of substrate-assisted self-assembly, and discusses the validity from the aspect of computer simulation based on a parameter calculated from actual experiments. Proposed theory of substrate-assisted self-assembly is divided into three steps (Fig. 5.1). The first step is the calculation of energies of the reactions. The reactions are mainly subdivided into two categories (Fig.5.2). One is the adsorption/desorption of the DNA species to/from the surface,

[1] Mainly because of the constraints of AFM observations, difficulties such as a long-term observation during annealing, an interference by the probe, etc.

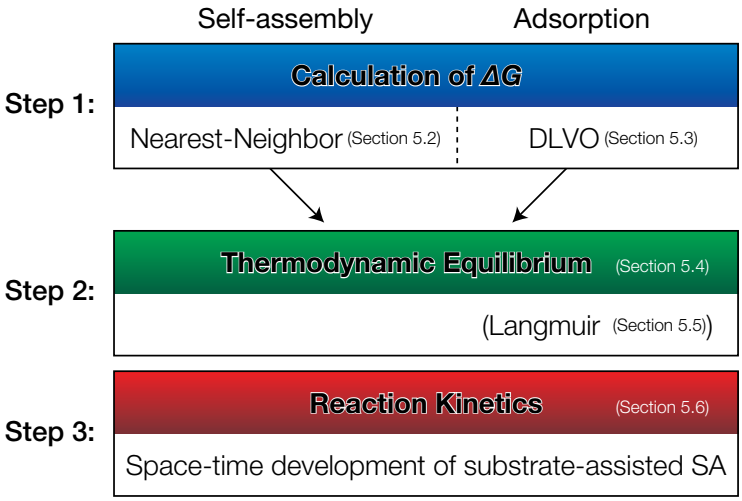

Figure 5.1: Three steps in the theory.

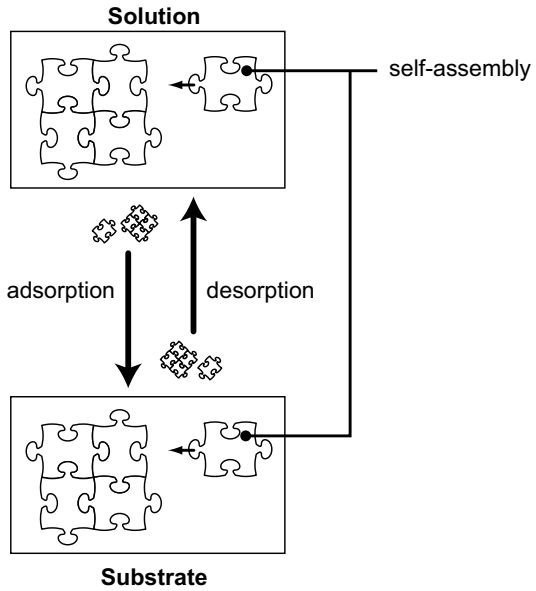

Figure 5.2: Framework of substrate-assisted self-assembly. A jigsaw-puzzle piece represents a unit of DNA nanostructure; *i.e.* a motif.

and the other is the self-assembly process in solution and on the substrate surface. The former phenomenon is described by thermodynamic equilibria of DNAs between "in" solution and "on" solid surface using binding energy calculation, and the latter phenomenon is described by calculating hybridization energy between sticky ends (Fig. 5.1, step 1). Note that this theory itself is not limited to T-motifs. Then these calculated free-energies are used in thermodynamic equilibrium constants, which define the balance of concentrations and relate each phase and state (Fig. 5.1, step 2). Finally, using these thermodynamic equilibria, the flow of species between each phase and state are converted to kinetic forms (Fig. 5.1, step 3) in order to demonstrate a time development of substrate-assisted self-assembly in section 5.7. This theory focuses on the adsorption/desorption and self-assembly reactions from aspects of the number of the species; the spatial behavior happening on the surface, such as alignments are not discussed.

5.1.1 Adsorption and surface-diffusion

It has been suggested for years that the receptor-ligand interaction on a cell surface can be speeded up because of the effect of non-specific adsorption of the ligand on a surface[Adam 1968]. This mechanism is known as a "reduction-of-dimensionality" (RD) rate enhancement, and modeled as a reaction-limited reaction by Axelrod and Wang[Axelrod 1994]. The model has been modified and extended to represent heterogeneous DNA-DNA hybridization on a solid surface using a combined reaction-diffusion limited model[Chan 1995, Erickson 2003]. It describes that the hybridization to the immobilized DNA strand can occur either directly via 3-dimensional diffusion or nonspecific reversible adsorption, followed by 2-dimensional diffusion on a surface. From the viewpoint of adsorption/diffusion, there are some similarities between this hybridization of DNA probes on a surface and substrate-assisted self-assembly. We partially adopted and modified the model to represent the phenomenon on a substrate surface of substrate-assisted self-assembly as well. The

model considers a process of single strands in free solution to the *immobilized* single-stranded DNA probes on a surface (Fig. 5.3). There are two pathways of hybridization; one is direct 3D diffusion+irreversible hybridization process, and the other is 2D diffusion+irreversible hybridization process, along with an adsorption to the surface.

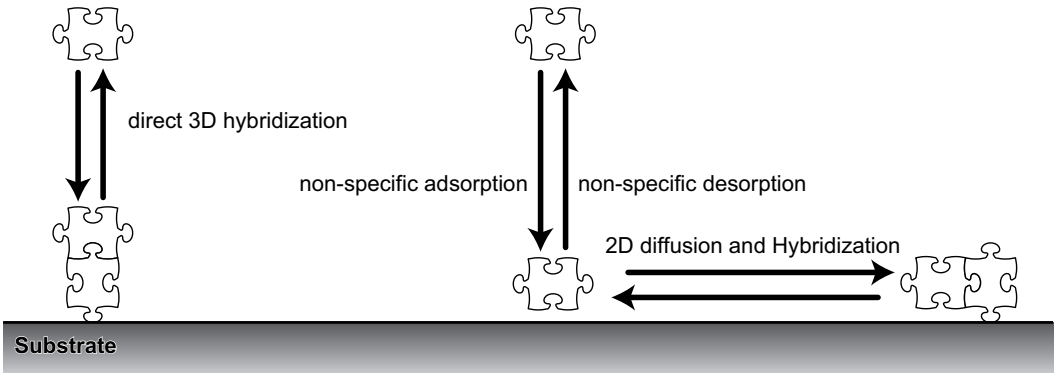

Figure 5.3: Adsorption/diffusion-limited reaction model.

The model of substrate-assisted self-assembly (Fig. 5.4) applies the idea of adsorption and 2D-diffusion-based self-assembly from the DNA probe model. The model abbreviates direct 3D self-assembly, because DNA motifs have to be on a surface before they self-assemble (*i.e.* it is assumed that the adsorption process occur first and then the motifs occupy a certain area on the substrate). Also note that the substrate-assisted assembly has reversibility in all processes, including hybridization between DNAs. Self-assembly process may occur in both free-solution and substrate surface. Multiple pathways can be conceivable in the process; two types, such as n-mer + monomer and partial n+m mer reactions are included in the model. Adsorption/desorption processes also take place in all species. (Although this scheme seems rather complicated, again notice that the reaction is only based on combinations of two elements, such as adsorption/desorption and self-assembly; therefore the framework proposed in Fig.5.2 can be applied.)

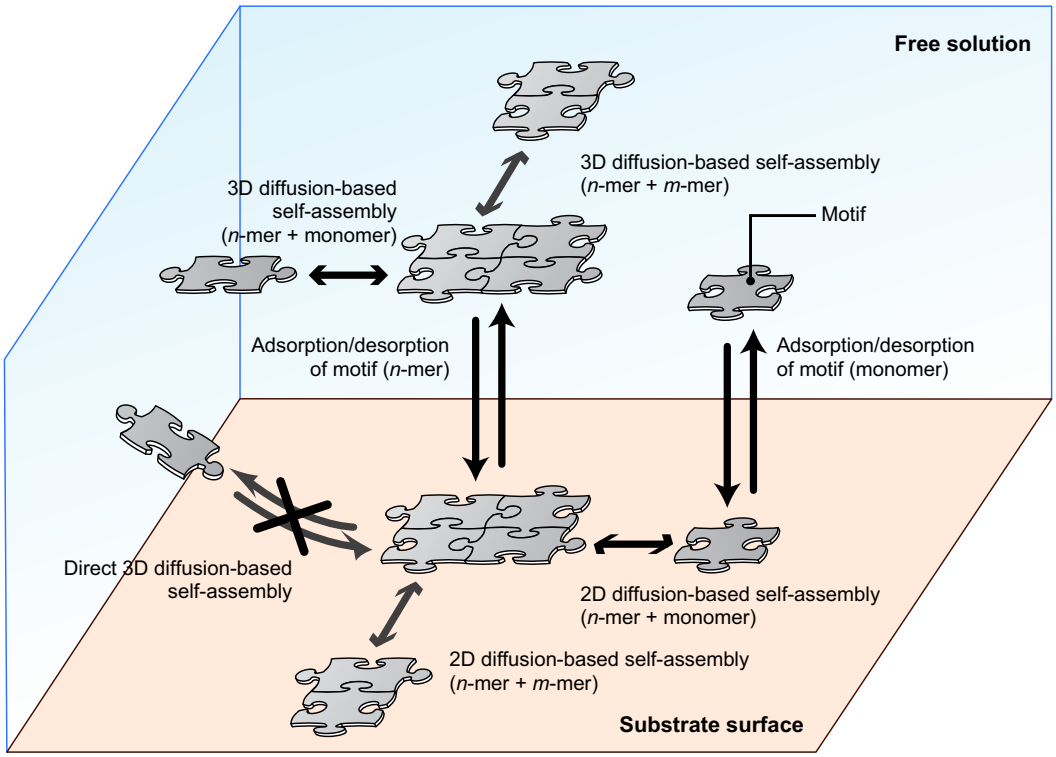

Figure 5.4: A schematic of the substrate-assisted self-assembly.

5.2 Calculation of free energy: hybridization

Gibbs free energy of hybridization is calculated by Nearest-Neighbor model. Nearest-Neighbor model for DNA duplex formation uses the sum of parameters which gives ΔH and ΔS of each pair of hybridized nucleotides.

ΔG at arbitrary temperature T[K] is given as follows,

$$\Delta G = \Delta H - T\Delta S \tag{5.1}$$

Thermodynamic parameters of each segment, initiation and symmetry corrections are given in Table 5.1. See [SantaLucia 1996] for details of the model. Note that these parameters are for the hybridization of two single strands: hybridizations under restricted flexibility, such as ring structure's open/close state transition, would be different. However, in order to simplify the calculation, the simulation mentioned in chapter 5.7 uses the same parameters in all hybridizations.

Sequence	ΔH° (kcal/mol)	ΔH° (eu (cal/K mol))	$\Delta G^\circ{}_{37}$ (kcal/mol)
AA/TT	-8.4 ± 0.7	-23.6 ± 1.8	-1.02 ± 0.04
AT/TA	-6.5 ± 0.8	-18.8 ± 2.3	-0.73 ± 0.05
TA/AT	-6.3 ± 1.0	-18.5 ± 2.6	-0.60 ± 0.05
CA/GT	-7.4 ± 1.1	-19.3 ± 2.9	-1.38 ± 0.06
GT/CA	-8.6 ± 0.7	-23.0 ± 2.0	-1.43 ± 0.05
CT/GA	-6.1 ± 1.2	-16.1 ± 3.3	-1.16 ± 0.07
GA/CT	-7.7 ± 0.7	-20.3 ± 1.9	-1.46 ± 0.05
CG/GC	-10.1 ± 0.9	-25.5 ± 2.3	-2.09 ± 0.07
GC/CG	-11.1 ± 1.0	-28.4 ± 2.6	-2.28 ± 0.08
GG/CC	-6.7 ± 0.6	-15.6 ± 1.5	-1.77 ± 0.06
initiation at G·C	(0)	(-5.9 ± 0.8)	$+1.82 \pm 0.24$
initiation at A·T	(0)	(-9.0 ± 3.2)	$(+2.8 \pm 1)$
symmetry correction	0	-1.4	$+0.4$
5'-terminal 5'-T·A-3' bp	$+0.4$	0	$+0.4$

Table 5.1: Thermodynamic parameters for DNA hybridization. [SantaLucia 1996]

5.3 Calculation of free energy: adsorption

5.3.1 Introduction to the DLVO theory

Interaction energy between DNA and the surface gives an important information to describe the phenomena of adsorption and desorption. Although there are other theoretical and experimental study for an interaction between DNA and mica surface mediated by monovalent and multivalent cations using the counterion correlation model[Pastré 2006, Pastré 2003], in this section, Sushko et al.'s method[Sushko 2006, Sushko 2007] is used to calculate energy curve between DNA and mica surface. The interaction energy curve is derived using DLVO (Derjaguin and Landau[Derjaguin 1941], Verwey and Overbeek[Verwey 1948]) theory. DLVO theory describes an interaction between two charged surfaces through liquid medium. The theory assumes that the interaction mainly comes from two types of forces: one is *van der Waals force*, and the other is *double-layer force*. Van der waals force is the sum of non-covalent and non-electrostatic interaction forces (London dispersion force, Debye force, etc.), even occur with neutral molecules. On the other hand, double layer force is occurred by a charged surface in a liquid. Surface charge is induced by dissociation of charged groups, or by adsorption of charged ions (or molecules) in solution. In case of mica-DNA, both surface is negatively like-charged, so the monovalent/divalent ion in solution (*i.e.* oppositely charged counterions) balances the surface charge. This counterion distribution gives the electric potential between two surfaces. Note that a "repulsive" force (not an attracting force) occurs between likely charged surfaces in counterion solution. This phenomenon is given by a osmotic pressure between counterions; an entropic effect surpasses a force rooted in electrostatic interactions[Israelachvili 1992]. Configurational entropy loss forces back the surfaces when both are approaching each other.

DLVO theory can be applied to any kind of shapes not only between two spheres or planar surfaces, but also between two different types of surfaces. In this section, we consider an interaction between a cylinder and a flat planar surface. Hereafter,

a cylinder is considered as a model for DNA double helix and a planar surface is for mica surface.

Generic parameters and signs are given as follows (Fig. 5.5):

Distance between a cylinder and a planar surface d

Cylinder radius (DNA) $r_0 = 1$[nm]

Unit cylinder length $L = 0.34$[nm] (Note that the calculation is based on the length of base pair.)

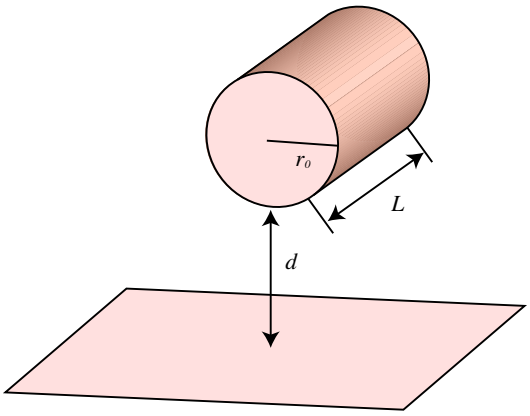

Figure 5.5: Signs used in DLVO model.

DLVO force curve can be written as a sum of van der Waals force ($vdW(d)$) and double layer force ($E_{dl}(d)$) as a function of distance d,

$$DLVO(d) = vdW(d) + E_{dl}(d) \tag{5.2}$$

5.3.1.1 Calculation of Debye length

Van der Waals force and double-layer force between a cylinder and a plane both require the Debye length for its calculation. Debye length ($1/\kappa$) characterizes a screening/shielding distance of electric fields by ions in the solution[Dill 2003]. The distance is affected by the concentrations and valence of ions; in case of buffer

solution with several types of cations, we have to consider overall ionic strength of a solution.

Ionic strength I of a solution is defined as,

$$I = \frac{1}{2}\sum_{n=i}^{n} c_i z_i^2 \tag{5.3}$$

where c_i is the molar concentration of ion i, z_i is the charge number of the ion. Concentration of each ion in case of TAE/Mg^{2+} 12.5mM buffer is calculated at Appendix E.

Inverse square of the Debye length (κ^2) is defined as follows from a derivation of linearized Poisson–Boltzmann (Debye–Hückel) equation,

$$\kappa^2 = \frac{2e^2 I N_A}{D\varepsilon_0 RT} \tag{5.4}$$

D is the dielectric constant of the solution. D is approximately equal to the dielectric constant of the solvent (in this case, water(≈ 78)), due to the small contribution of the ions themselves to the solution. N_A is Avogadro's number, e is elementary electric charge, ε_0 is permittivity of vacuum, R is gas constant, and T is temperature.

5.3.2 Van der Waals interactions between cylinder and surface

The calculation of non-retarded van der Waals force between a cylinder and a plane has been first investigated by Richmond[Richmond 1974]. A simple form of van der Waals force contribution at short distance ($\kappa d < 1$) is derived by Sushko[Sushko 2010],

$$vdW(d) = -\frac{\pi r_0^2 L \kappa_m^2}{4d}(\Delta_{cm}^{\parallel} + \Delta_{cm}^{\perp} \cdot \Delta_{sm}^{\perp}) \tag{5.5}$$

The notations used in equation (5.5) are:

$$\Delta^{\parallel}_{cm} = \frac{\varepsilon^{\parallel}_c - \varepsilon_m}{2\varepsilon_m} \tag{5.6}$$

$$\Delta^{\perp}_{cm} = \frac{\varepsilon^{\perp}_c - \varepsilon_m}{\varepsilon^{\perp}_c + \varepsilon_m} \tag{5.7}$$

$$\Delta^{\perp}_{sm} = \frac{\varepsilon^{\perp}_s - \varepsilon_m}{\varepsilon^{\perp}_s + \varepsilon_m} \tag{5.8}$$

where $\varepsilon^{\parallel}_c$, $\varepsilon^{\perp}_c$ are the dielectric permittivities of the cylinder in the parallel/perpendicular directions to the cylinder axis respectively, $\varepsilon^{\perp}_s$ is the dielectric permittivity of the substrate, and ε_m is the dielectric permittivity of the medium. In case of DNA-Mica in aqueous solution, parameters are: $\varepsilon^{\parallel}_c = \varepsilon^{\perp}_c \approx 2.5$, $\varepsilon^{\perp}_s \approx 5$ and $\varepsilon_m \approx 78$.

κ^{-1}_m is a normalized Debye length [Sushko 2007],

$$\kappa^2_m = (\varepsilon_0 k_B T)\kappa^2 \tag{5.9}$$

5.3.3 Double-layer forces between cylinder and surface

5.3.3.1 Outline of the calculation

Several steps are required to calculate double-layer forces between a cylinder and a surface (Fig. 5.6). Here we follow the steps proposed by Sushko [Sushko 2007]. First we calculate surface potential of both cylinder (DNA) and flat planar surface (Mica) using surface charge density of the materials. Second, the mid-plane potential (potential at the midpoint distance($d/2$) between DNA and mica) is derived by surface potential via Poisson–Boltzmann equation. Then the mid-plane pressure is calculated by summation of effect, arise from contributing ions in the solution. Finally, the pressure is integrated and the energy at the distance d is computed.

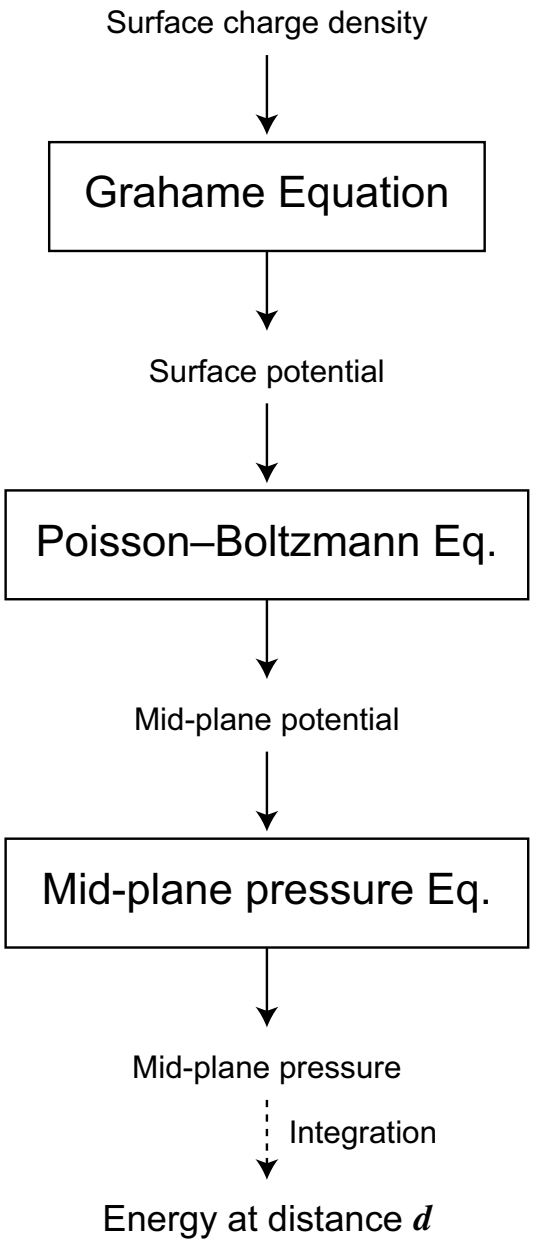

Figure 5.6: Outline of the double-layer force calculation.

5.3.3.2 Grahame equation

Grahame equation gives a surface charge density of arbitrary material from surface potential of the material, monovalent/divalent cation concentration of solution, temperature etc. In this case, we inversely solve this equation in order to calculate the surface potential of cylinder (DNA) or plane (Mica) from surface charge densities.

Surface charge densities of DNA and mica can be calculated by physical properties and chemical formula of each material.

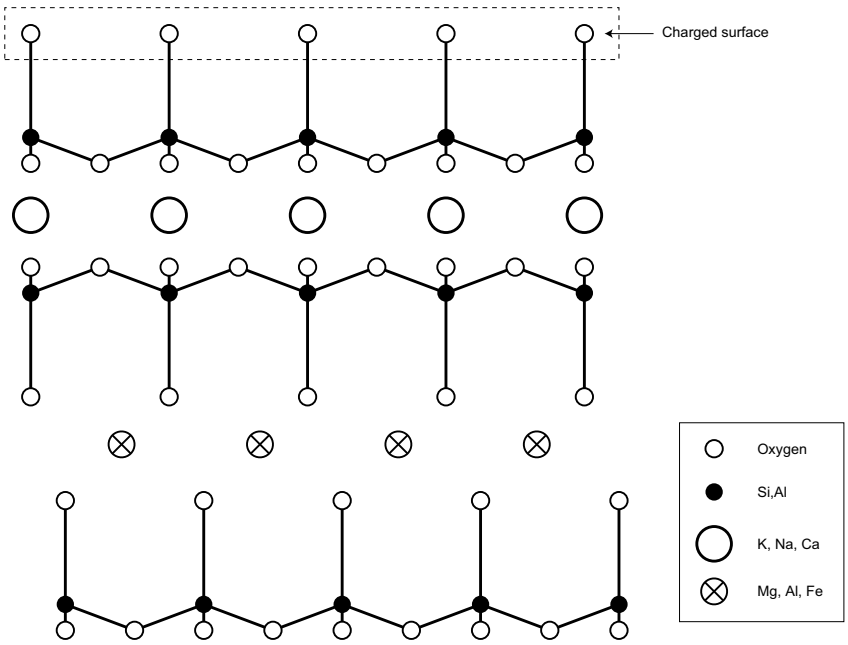

Figure 5.7: Cross section of the mica structure. Composite layers are linked by potassium ions. The surface of the mica is covered by hexagonally coordinated oxygens. The structure may regarded as a having a central layer $Mg_3(OH_6)$ (in phlogopite); *i.e.* each Oxygen exposed on a surface can be regarded as O^-.

Mica A mica is a composite sheet in which a layer of octahedrally coordinated cations is sandwiched between two identical layers of linked $(Si, Al)O_4$ tetrahedra (Fig.5.7)[Deer 1966]. Calculated from the physical distance between oxygens exposed on a surface, a surface of mica has negative charges of $\sigma_{mica} = 2.1 \times 10^{18}\text{sites/m}^2 \approx -0.3\text{C/m}^2$ [Rojas 2002, Carlsson 2004].

DNA Consider DNA double helix as a cylinder. Each phosphate group in DNA backbone has one negative charged site, per strand. Therefore, surface charge density of the molecule is approximated as

$$\sigma_{DNA} = \frac{1}{(2\pi \cdot 0.34 \cdot 1/2) \times 10^{-18}} = 0.93 \times 10^{18}\text{sites/m}^2 \quad (5.10)$$

$$= -0.15[\text{C/m}^2] \quad (5.11)$$

Grahame equation is written down as follows,

$$\begin{aligned}\sigma^2 = 2\varepsilon_m\varepsilon_0 k_B T\big\{&[\text{Na}^+]_\infty(\text{e}^{-e\psi_0^{pl,c}/k_BT} + \text{e}^{e\psi_0^{pl,c}/k_BT} - 2) \\ &+[\text{Mg}^{2+}]_\infty(\text{e}^{-2e\psi_0^{pl,c}/k_BT} + 2\text{e}^{e\psi_0^{pl,c}/k_BT} - 3)\big\}\end{aligned} \quad (5.12)$$

Note that the equation can be used in any types of material if we can calculate surface charge density of the material. We do not have to restrict the counterpart of DNA adsorption to mica: we can also calculate other types of materials, such as silicon dioxide ($\sigma = -0.8\text{C/m}^2$)[Dong 1998], and can seek optimal ion concentration etc. for DNA binding.

Surface potential of DNA, mica and SiO_2 is calculated as an example (Fig. 5.8). Note that surface potential also depends on temperature T.

5.3.3.3 Poisson-Boltzmann equation

Mid-plane potential between two charged surfaces (ψ_m) are derived by a linear superposition approximation. This method calculates a potential at the mid-plane (distance $d/2$) between the cylinder and the flat plane surface using a sum of non-linear Poisson–Boltzmann equation[Tuinier 2003].

$$\begin{aligned}\psi_{\text{m},d/2} =&\frac{2k_BT}{e}\left\{\left(\ln\left[\frac{1+\gamma_{pl}}{1-\gamma_{pl}}\right]\right)\right. \\ &\left.+\left(\frac{K_0(\kappa(d/2+r_0))}{K_0(\kappa r_0)\exp(-\kappa d/2)}\ln\left[\frac{1+\gamma_c\text{e}^{-\kappa d/2}}{1-\gamma_c\text{e}^{-\kappa d/2}}\right]\right)\right\}\end{aligned} \quad (5.13)$$

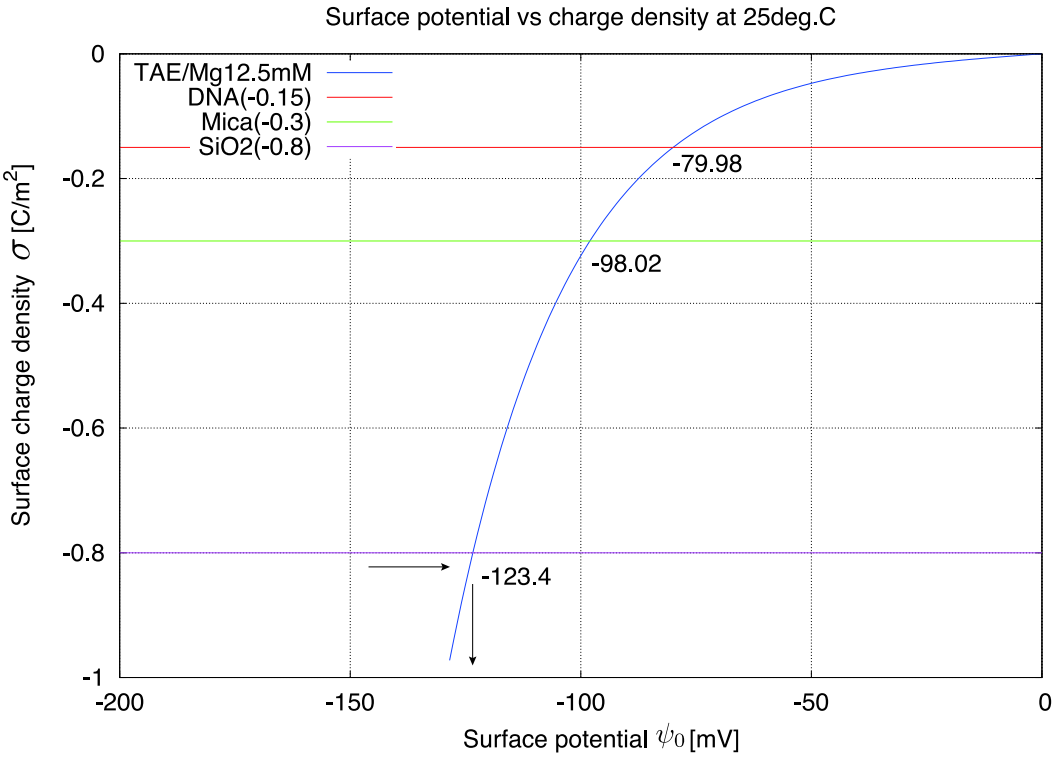

Figure 5.8: Results of Grahame equation of TAE/Mg^{2+} 12.5mM buffer at 25°C .

γ_{pl} and γ_c are defined as

$$\gamma_{pl,c} = \tanh\left(\frac{e\psi_0^{pl,c}}{4k_BT}\right) \tag{5.14}$$

where K_0 is the zeroth-order modified Bessel function of a second kind,

$$K_0(x) = \int_0^\infty \frac{\cos(xt)}{\sqrt{t^2+1}}dt \tag{5.15}$$

5.3.3.4 Pressure between cylinder and surface

Using mid-plane potential (equation 5.13), the pressure between cylinder and planar surface is calculated as

$$\begin{aligned} P_x(d) =& k_BT\rho_\infty(\mathrm{NaCl})[(e^{-e\psi_m/k_BT}-1)+(e^{+e\psi_m/k_BT}-1)] \\ &+k_BT\rho_\infty(\mathrm{MgCl_2})[(e^{-2e\psi_m/k_BT}-1)+2(e^{+e\psi_m/k_BT}-1)] \end{aligned} \tag{5.16}$$

where ρ_∞(NaCl) and ρ_∞($MgCl_2$) are the bulk concentration of salts, respectively. (The first term is the pressure contributed by Na^+, the third term is contributed by Mg^{2+}, and the second and the forth terms are contributed by Cl^- ions.)

Finally, the energy between cylinder and plane at distance d can be calculated as an integration of the pressure,

$$E_{dl}(d) = 2\pi r_0 L\int_d^\infty P_x(x)dx \tag{5.17}$$

5.3.4 Calculation results

Fig.5.9 is the result of the calculation of energy between DNA and mica at 300K, using TAE/Mg^{2+}12.5mM buffer. The calculation for the actual concentration of monovalent and divalent cations are discussed in Appendix E.

The obtained DLVO energy curve result has only one shallow minimum at 3.5[nm], -0.02[eV/bp]. Note that the interaction energy is given in unit of eV. The

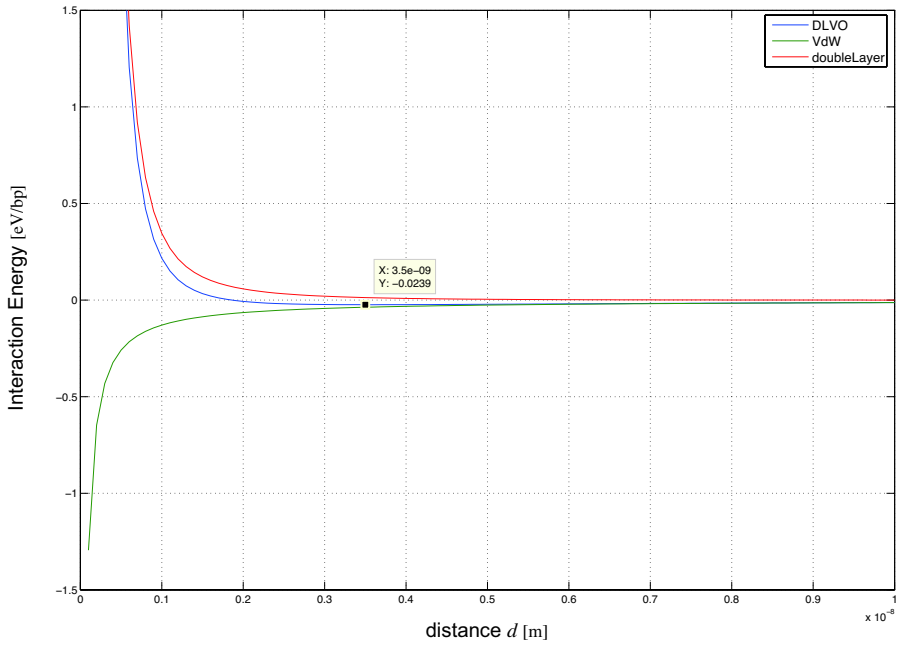

Figure 5.9: DVLO curve of DNA-Mica interaction at 300K (TAE/Mg^{2+}12.5mM). Green line indicates van der Waals energy curve, Red line indicates double layer energy curve, and Blue line is the DLVO interaction energy curve (calculated as a sum of van der Waals and double layer).

value is $\approx -0.92 k_B T$ per base pair, when converted. This minimum value represents the energy of binding, and the distance is the preferable clearance between mica and DNA. Note that this distance is calculated by using only two types of forces; other interactions, such as counterion correlated binding and various short-range effects are not considered, so the actual distance between mica and DNA might be different. However, when the DNA approaches far away from the surface (until around the debye length scale(≈ 1.69[nm])), this theory can be applied.

Another interesting result is that the scale of binding energy per base pair is about the same as $k_B T$. This suggests that, in TAE/Mg^{2+} buffer, binding of a single motif (assume ≤ 50 bp) still can be (weakly) fluctuated by a thermal motion.

5.4 Self-assembly model

5.4.1 Hybridization model of motifs

Self-assembly process of the substrate-assisted self-assembly is modeled by a reaction between motifs. When we simplify this process, the hybridization of sticky ends gives the difference in free energy, and the rate of reaction due to the size and reaction site of the motif can be adjusted by a "effective" concentration of each species (see section 5.4.2).

The reaction of hybridization is modeled as a two-state first-order system[Wetmur 1991, Winfree 1998b],

$$\mathrm{ssDNA}_1 + \mathrm{ssDNA}_2 \rightleftarrows \mathrm{dsDNA} \tag{5.18}$$

Hereafter the mark of each species are simplified as follows,

$$X + Y \rightleftarrows Z \tag{5.19}$$

In case of motif-based self-assembly, we regard X, Y and Z as species of the structure (motif or motifs).

5.4.2 Thermodynamic equilibrium

Thermodynamic equilibrium constant of reaction (5.19) is defined as a balance of activity of each species (in our case, a motif or self-assembled motifs),

$$K(T) \equiv \frac{a_z}{a_x a_y} \tag{5.20}$$

where activity a_k is expressed by a molar fraction of each species x_k and activity coefficient γ_k,

$$a_k = \gamma_k x_k \tag{5.21}$$

$$x_k = \frac{[\mathrm{m}_k]}{[\mathrm{ALL}]} \tag{5.22}$$

Note that $[\mathrm{m_k}]$ is a concentration of each species (k).

Assume activity coefficient is same at all species ($\gamma_k = \gamma(\mathrm{const.})$), because the size of the molecule and number of reaction sites are supposed to be a main determining factor of this coefficient. In case of DNA motifs, we can approximate the size of molecules and the numbers of reaction site (*i.e.* sticky ends) are mostly the same, at least in magnitude.

$$K(T) = \frac{[\mathrm{Z}][\mathrm{ALL}]}{[\mathrm{X}][\mathrm{Y}]\gamma} \tag{5.23}$$

Thermodynamic equilibrium constant can be expressed as a function of Gibbs free energy of reaction via definition of chemical potential $\mu_k^0(T)$,

$$K(T) \equiv \exp\left[\frac{\mu_x^0(T) + \mu_y^0(T) - \mu_z^0(T)}{RT}\right] \tag{5.24}$$

$$= \exp\left[\frac{-\Delta G_{rxn}^0}{RT}\right] \tag{5.25}$$

Thus, the thermodynamic equilibrium constant is expressed in two ways by equation (5.23) and (5.24),

$$(K(T) =)\frac{[\mathrm{Z}][\mathrm{ALL}]}{[\mathrm{X}][\mathrm{Y}]\gamma} = \exp\left[\frac{-\Delta G^0_{rxn}}{RT}\right] \tag{5.26}$$

Commonly used equilibrium is expressed by a balance of concentrations[2],

$$K_c(T) = \frac{[\mathrm{Z}]}{[\mathrm{X}][\mathrm{Y}]} \tag{5.27}$$

Equation (5.26) is rewritten by an expression using $K_c(T)$,

$$\begin{aligned} K_c(T) &\equiv \frac{[\mathrm{Z}]}{[\mathrm{X}][\mathrm{Y}]} && (5.28)\\ &= \frac{\gamma}{[\mathrm{ALL}]}\exp\left[\frac{-\Delta G^0_{rxn}}{RT}\right] && (5.29)\\ &= q\exp\left[\frac{-\Delta G^0_{rxn}}{RT}\right] && (5.30) \end{aligned}$$

where q is defined as an activity parameter,

$$q \equiv \frac{\gamma}{[\mathrm{ALL}]} \tag{5.31}$$

and q can be approximated as a constant if the total number of molecules can be considered as a fixed number. (This approximation is valid in case of low concentration.)

Using the same way of derivation, the relation between the equilibrium constant of concentrations and Gibbs free energy of the reaction $X \rightleftarrows Z$ can be defined and written as,

[2]We often simplify that the equilibrium defined by activities and concentrations are the same, however, such approximation is applicable only in case of low concentrations.

$$K_c(T) \equiv \frac{[\mathrm{Z}]}{[\mathrm{X}]} \tag{5.32}$$

$$= \exp\left[\frac{-\Delta G^0_{rxn}}{RT}\right] \tag{5.33}$$

Note that the parameter q does not appear in this case.

5.5 Adsorption model

5.5.1 Thermodynamics of the Langmuir model

The adsorption model of substrate-assisted self-assembly is considered to be a Langmuir model. The reason of using this model is that some experimental results of non-specific adsorptions of DNAs on the glass surface and many other cases of polymer adsorptions are well-explained by this model[Chan 1995]. Glass surface is negatively charged[Behrens 2001] as same as mica surface, so the mechanism of the adsorption/desorption itself is supposed to be identical. Moreover, experimental results of T-motifs grown on a mica surface suggests that the surface is always covered by monolayer of DNA nanostructures; the adsorption model for multilayers, such as BET model[Brunauer 1938], should be inappropriate for the phenomenon.

The adsorption isotherm of Langmuir model is written as follows:

$$\theta = \frac{aC}{1 + aC} \tag{5.34}$$

where θ is the fractional coverage of the surface, a is the constant related with the equilibrium constant of adsorption, and C is the concentration of molecules.

The isotherm can be derived by the reaction of adsorption/desorption. First, define the reaction of adsorption as,

$$S^* + P \rightleftarrows SP \tag{5.35}$$

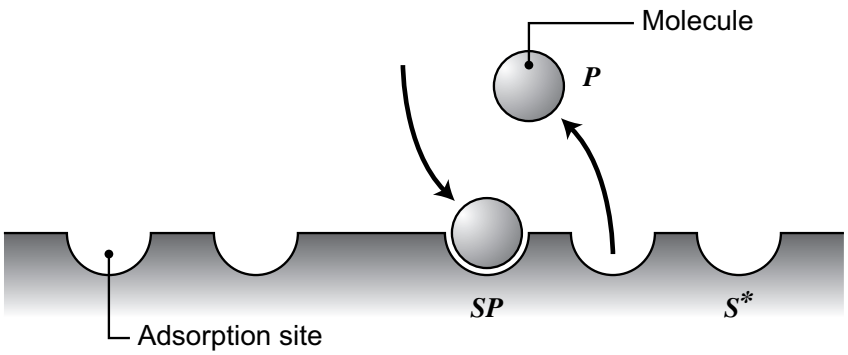

Figure 5.10: Langmuir model.

which S^* is the empty adsorption site, P is the molecule and SP is the occupied adsorption site by the molecule (Fig.5.10).

Equation suggests that the equilibrium of concentrations of the Langmuir model and relations with free energy would be,

$$K_{c,ad}(T) = \frac{[\mathrm{SP}]}{[\mathrm{S}^*][\mathrm{P}]} \tag{5.36}$$

$$\left(= \frac{\gamma_{ad}}{[\mathrm{ALL}]} \exp\left[\frac{-\Delta G^0_{ad}}{RT}\right]\right) \tag{5.37}$$

(Note that activity coefficient γ_{ad} is same in this case. $\gamma_{ad} = \gamma$ is used in simulations, because if we assume γ_{ad} of [SP] and [S*] are the same (both are related with adsorption sites), those two factors are reduced; therefore leftover γ_{ad} is related with [P].)

Define θ as,

$$\theta = \frac{[\mathrm{SP}]}{[\mathrm{S}^*] + [\mathrm{SP}]} \tag{5.38}$$

Then, equation (5.36) can be written as,

$$K_{c,ad}(T) = \frac{\theta}{(1-\theta)[\mathrm{P}]} \tag{5.39}$$

[P] = C, $K_{c,ad}(T) = a$, so the equation can be rearranged as follows,

$$a = \frac{\theta}{(1-\theta)C} \tag{5.40}$$

Or, equivalently,

$$\theta = \frac{aC}{1+aC} \tag{5.41}$$

Therefore, the isotherm of Langmuir model is derived.

5.6 Kinetic model of self-assembly and adsorption

5.6.1 Self-assembly

This section describes a kinetic model of self-assembly and adsorption in quasi-static process.

The velocities of the reaction 5.18 are defined as,

$$-[\dot{\text{dsDNA}}] = [\dot{\text{ssDNA}}_{1\text{or}2}] = k_r[\text{dsDNA}] - k_f[\text{ssDNA}_1][\text{ssDNA}_2] \tag{5.42}$$

where k_f is a forward reaction rate, and k_r is a reverse reaction rate.

Using simplified expression of motifs,

$X + Y \rightleftarrows Z$

$$-[\dot{\text{Z}}] = [\dot{\text{X or Y}}] = k_r[\text{Z}] - k_f[\text{X}][\text{Y}] \tag{5.43}$$

$X \rightleftarrows Z$

$$-[\dot{\text{Z}}] = [\dot{\text{X}}] = k_r[\text{Z}] - k_f[\text{X}] \tag{5.44}$$

The velocities are 0 at the equilibrium state, thus

$$K_c(T) = \frac{k_f}{k_r} \tag{5.45}$$

Forward reaction can be considered as a diffusion-based reaction but rate-limited step in both in free solution and on a surface, approximately independent of oligo length and sequence[Quartin 1989]. Experimental results supports this speculation[Chan 1995]; a rate constant for oligonucleotide association in solution to be about 4×10^6[/M/sec], which was two to three orders of magnitude smaller than the diffusion-limited rate[Bloomfield 1974]. Another FRET experiment gave a rate constant of 5.7×10^5[/M/sec], despite of the estimated diffusion-limited rate of 8.9×10^9[/M/sec][Parkhurst 1995].

In this thesis, the rate defined by Winfree[Winfree 1998b] for the theory of self-assembly of DNA tiles is used,

$$k_f \approx 6 \times 10^5 \text{ [/M/sec]} \tag{5.46}$$

Thus, using this notation the reverse reaction rate is defined as,

$X + Y \rightleftarrows Z$

$$k_r \equiv k_f / K_c(T) = k_f \cdot (1/q) \exp\left[\frac{\Delta G^0_{rxn}}{RT}\right] \tag{5.47}$$

$X \rightleftarrows Z$

$$k_r \equiv k_f / K_c(T) = k_f \cdot \exp\left[\frac{\Delta G^0_{rxn}}{RT}\right] \tag{5.48}$$

Note that these thermodynamic and kinetic equations for the reaction disregard the effect of energy of activation.

5.6.2 Langmuir model for adsorption

Define the reaction rate of adsorption v_a as,

$$v_a = \mu_3 P_p P_a P_r \tag{5.49}$$

in which μ_3 is the number of molecules that collides to the surface from gas/solution phase, P_p is the probability of that the collision location is the adsorption site, P_a the probability of that the site is available for adsorption, and P_r is the probability of the success of adsorption.

Note that this definition and the theory are originally used for direct hybridization kinetics of oligonucleotide to the surface with probe DNAs[Erickson 2003]; however, we can follow the same or similar formula because of the generality of kinetics colliding to two-dimensional surface from the bulk solution remains.

The rate of collisions μ_3 between a bulk solution of concentration c_3 and a solid wall of *unit surface area* of Brownian particles is derived below[Reif 1965, Erickson 2003].

$$\mu_3 = \frac{\langle v \rangle_3 c_3}{4} \tag{5.50}$$

where $\langle v \rangle_3$ is the instantaneous speed of the Brownian molecule (averaged over the Maxwellian distribution of speeds).

For Brownian motion the velocity is finite, defined as[Axelrod 1994],

$$\langle v \rangle_n = \zeta_n \sigma_n \tag{5.51}$$

in which σ_n is the frequency of collision, multiplied by the run between the collisions ζ_n (or the Brownian persistence distance[Chan 1995]).

The frequency of collisions can be related to the diffusion coefficient D_n,

$$D_n = \frac{\zeta_n \sigma_n^2}{2n} \tag{5.52}$$

Thus, from equations (5.50), (5.51) and (5.52),

$$\mu_3 = \frac{3D_3c_3}{2\sigma_3} \tag{5.53}$$

P_p is defined as a fraction of adsorption site area A_{site} and an average area of the surface per adsorption site area $A_{surface}$,

$$P_p = \frac{A_{site}}{A_{surface}} \tag{5.54}$$

$$= \frac{A_{site}}{\frac{1}{([\mathrm{S}^*]+[\mathrm{SP}])N_A}} \tag{5.55}$$

where N_A is Avogadro's number.

P_a is considered as the "vacancy" of the site, so the parameter is defined as,

$$P_a = \frac{[\mathrm{S}^*]}{[\mathrm{S}^*] + [\mathrm{SP}]} \tag{5.56}$$

P_r is the probability of the adsorption that depends on the reaction. The probability is unknown and arbitrary assigned as χ_n.

As a result, the adsorption rate of colloidal particles from the bulk solution to the surface per unit area is written as,

$$v_{ad} = \frac{3D_3A_{site}N_AP_r}{2\sigma_3}[\mathrm{S}^*][\mathrm{P}] \tag{5.57}$$

$$= k_{ad}[\mathrm{S}^*][\mathrm{P}] \tag{5.58}$$

Note that $c_3 = [P]$, and the rate is defined by per unit area. The result corresponds to the reaction of Langmuir model in equation (5.35).

The adsorption rates represented in terms of [mol/l] are defined as,

$$-[\dot{\mathrm{SP}}]\cdot\frac{A_{substrate}}{V} = [\dot{\mathrm{S}^*}]\cdot\frac{A_{substrate}}{V} = [\dot{\mathrm{P}}] = (k_{de}[\mathrm{SP}] - k_{ad}[\mathrm{S}^*][\mathrm{P}])\cdot\frac{A_{substrate}}{V} \tag{5.59}$$

where $A_{substrate}$ is a area of the substrate, and V is the volume of the reaction chamber. We have to notice that [SP] and [S*] is defined as a concentration on a surface [mol/m^2].

Using thermodynamic equilibrium of adsorption (eq. 5.36), the desorption rate constant (k_{de}) can be defined as,

$$k_{de} \equiv k_{ad}/K_{c,ad}(T) \tag{5.60}$$

$$= k_{ad} \cdot \frac{[\mathrm{ALL}]}{\gamma_{ad}} \exp\left[\frac{\Delta G^0_{ad}}{RT}\right] \tag{5.61}$$

The theoretical forward adsorption rate constant k_{ad} can be calculated by solving the values in equation (5.57), using a method by Chan[Chan 1995]. However, the actual adsorption rate is considered to be highly dependent on the conditions; the theoretical calculation generally defines only an upper limit of the constant. The equation (5.57) suggests that the forward reaction is three-dimensional diffusion-based, therefore, in the simulation below, we use the same value introduced in equation (5.46) as a realistic value for the forward adsorption rate constant. Also notice that $\chi_3 \leq 0.001$, used in receptor-ligand model on cell surface by Axelrod[Axelrod 1994] and also used in hybridization model by Chan[Chan 1995], qualitatively agrees that the decrease of value is given in order of magnitudes.

5.6.3 Estimation of two-dimensional rate constant

In this section, a rough estimation for the calculation of the rate constant of particle that reacts under a confinement in two-dimensional surface is discussed. Discussions about equation (5.46) explained that the actual rate constant is much smaller than the calculated results, so the direct calculation of 2-D rate constant is rather meaningless in actual use. In this theory, a fraction of 2-D/3-D reaction rate constant is calculated, which supposedly be the same value even in the real condition. (Remember the discussion about χ_3 of the adsorption rate constant in previous section:

we can assume this approximation is valid if the probability of success is mostly the same in 2-D and 3-D, and is multiplied to the theoretical calculation.)

In theory[v Smoluchowski 1917], the rate constant of two types of particles (A, B) in 3-dimensional bulk solution can be expressed as,

$$k_{3D} = 4\pi D_3 R \tag{5.62}$$

which R is the sum of the particle radius ($r_A + r_B$, known as the encounter radius) and D_3 is the sum of diffusion coefficients ($D_A + D_B$).

On the other hand, the two-dimensional rate constant of reaction is modeled by circular disks[Adam 1968, Berg 1977, Keizer 1985],

$$k_{2D} = \frac{2\pi D}{\ln(b/R) - c} \tag{5.63}$$

in which b is the half of the mean distance between two "targets", in this case motifs. c is the constant that is different depends on the model and assumptions. In this theory, we use $c = 0.231$[Keizer 1985].

Therefore, the fraction of the rate constant between dimensions is,

$$\frac{k_{2D}}{k_{3D}} = \frac{1}{2R(\ln(b/R) - c)}\left(\frac{D_2}{D_3}\right) \tag{5.64}$$

We used $D_2 = 5 \times 10^{-13}$, $D_3 = 1.3 \times 10^{-10}$[Erickson 2003], $R = 10^{-8}$m, $b = 2R$ for an extreme case of the reaction. The value can be calculated as,

$$\frac{k_{2D}}{k_{3D}} \approx 4 \times 10^5 \tag{5.65}$$

Thus, the forward reaction rate constant at two-dimensional surface would be,

$$k_{f,2D} = k_f \cdot \frac{k_{2D}}{k_{3D}} \approx 2.4 \times 10^{11} \tag{5.66}$$

The estimated result gives significantly larger forward reaction rate constant in

2D in comparison with the value in 3D. This value is used in the simulations in the following section.

5.7 Simulation

5.7.1 Model

The theory of DNA self-assembly in free solution and on substrate are applied to the kinetic-based computer simulation (source codes in Appendix F). The aim of this simulation is to demonstrate that some peculiar phenomena related with substrate-assisted self-assembly can be explained by this theory. 1.0x Ring structure (Fig.3.5) is chosen for the simulation model because of the following reasons:

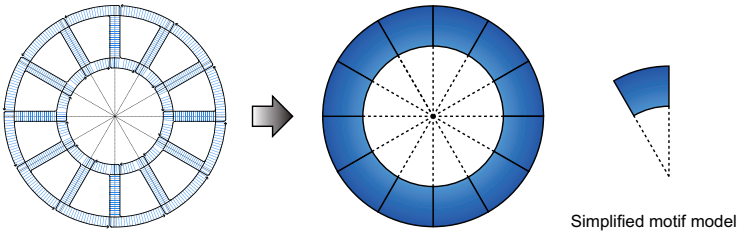

Figure 5.11: Design of ring1.0x and simplified representation (simulation model).

- Simple (only from one type of motif), closed structure
- Size-controllable (by design)
- Simple formation mechanism: we do not have to think about the nucleation process of the structure (*e.g.* two-dimensional DNA tiles), so more accurate simulation can be made.
- Reaction tracing by spectrophotometer (in free solution experiment) is available
- Some interesting phenomena related with substrate-assisted assembly, such as: 1. increase of the yield, 2. self-organization of structures (solid-liquid phase

transition), 3. shape transition (spiral-ring transition by kinetic effect)

This simplified motif model is used for simulations (Fig. 5.11). Although the "real" structure has a certain degree of flexibility (because of this reason, distributions are observed in the diameter of closed structure), assume that the model is always rigid, forming closed "dodecagon" structure as designed. The motif behaves as a molecule, or species for the reaction. According to the theory, the motif is approximated as a homogeneous sphere or disk.

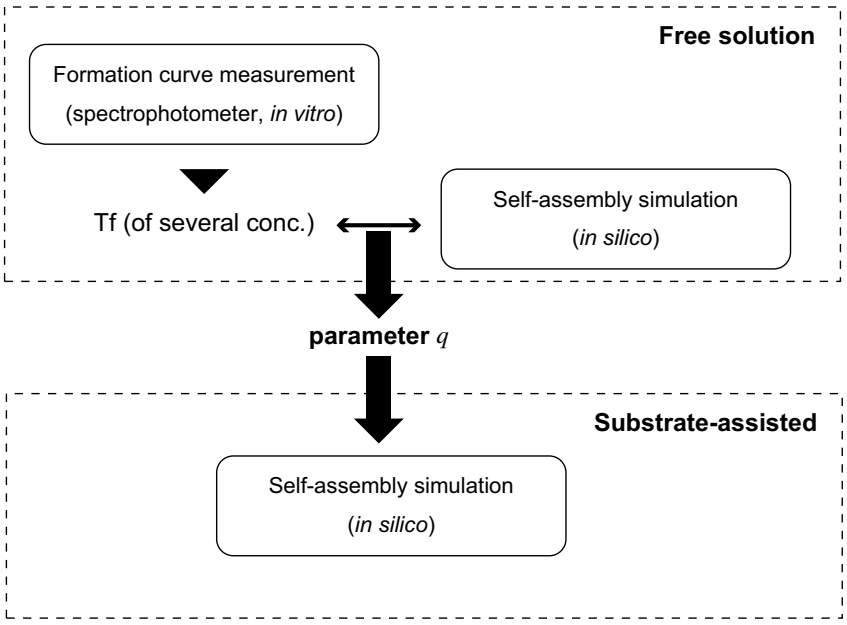

Figure 5.12: Simulation framework.

Simulations consist of two stages (Fig. 5.12). First, a comparison between simulation results and the melting curve data obtained from spectrophotometer is made. The simulation results give us the time record of concentrations of each species, where the one arbitrary parameter q (equation5.31) needs to be adjusted. (Roughly speaking, parameter q shifts the temperature of formation rate curve in the simulation.) Note that both experiments and simulations are executed under low DNA concentrations, thus the parameter q can be treated as a constant value. Then, the estimated q is introduced to the model for substrate-assisted self-assembly.

The model of substrate-assisted self-assembly is designed as an extension of the free-solution self-assembly model, so the same parameter value can be applied.

5.7.2 Simulation in free-solution

Simulation of self-assembly in free-solution is modeled as follows:

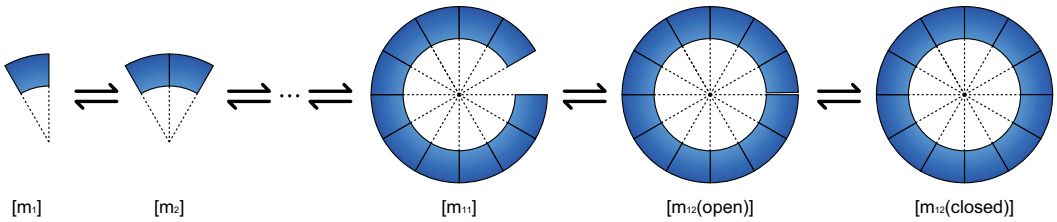

Figure 5.13: Simulation model of self-assembly in free solution.

$[\mathrm{m_n}]$ consists of $n \times [\mathrm{m_1}]$ molecules. The connection between molecules are made by hybridization of two sticky ends. Two sticky ends are considered to be connected at the same time. $[\mathrm{m_{12}}]$ has two states, such as "open" and "closed"; the difference between those states are the hybridization of the last two sticky ends.

To simplify the reaction, we consider only two types of pathways, such as,

$$[\mathrm{m_n}] + [\mathrm{m_1}] \rightleftarrows [\mathrm{m_{n+1}}] \tag{5.67}$$

$$[\mathrm{m_n}] + [\mathrm{m_{12-n}}] \rightleftarrows [\mathrm{m_{12}(open)}] \tag{5.68}$$

Same equations and parameters mentioned in the theory section are used for thermodynamic equilibrium constants and kinetic reaction rates. Although the pathways are limited, the reaction mainly relies on $[\mathrm{m_1}]$, so the qualitative behavior of this model is still conserved.

First, the simulation is compared to the spectrophotometer experiments. The initial adjustment is done by comparing the T_f of 0.66μM, -0.3° C /min. (Appendix B.1b). The experimental result showed $T_f = 312.48$[K]. Parameter q is obtained as

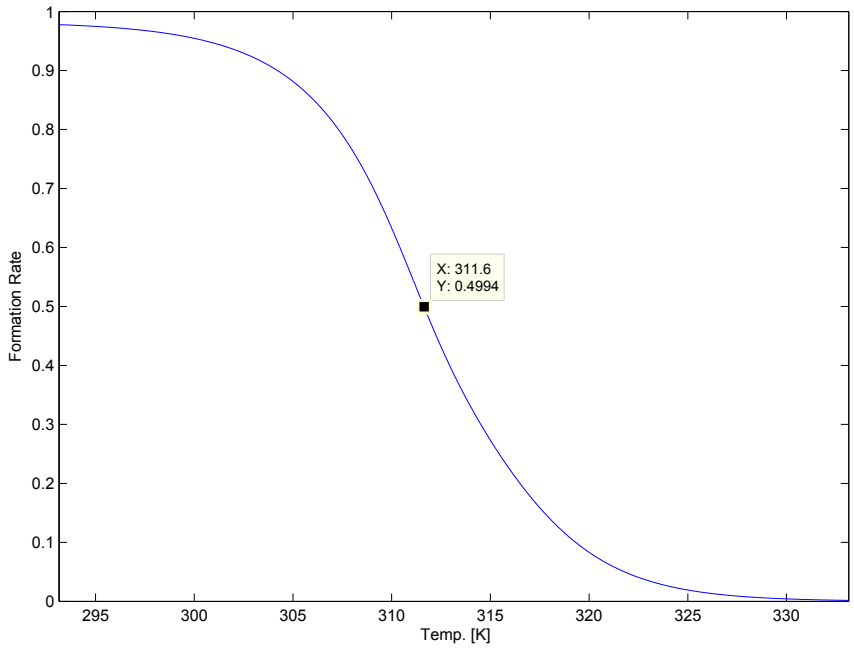

(a) Formation rate in solution

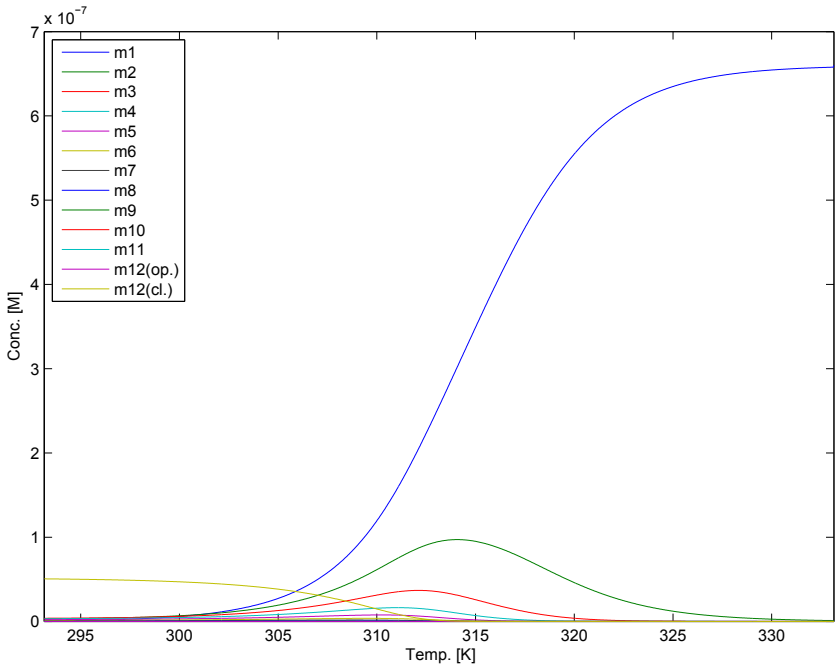

(b) Conc. of species

Figure 5.14: Simulation result of 0.66 μM, $1/q = 6 \times 10^4$. **a** Formation rate (the ratio of hybridized sticky ends) versus temperature [K]. A temperature at formation rate= 0.5 is the T_f (formation temperature) of self-assembly. In this case, $T_f \approx$ 311.6[K]. **b** Concentration of the species. Note that [m_{12}] increases and mostly dominates in the solution at the end of annealing.

$1/q = 6 \times 10^4$ from the result (Fig.5.14). Calculated T_f from the simulation was 311.6[K]. Note that the larger $1/q$ gives the lower T_f.

In order to verify the accuracy of this parameter q and the model, a comparison of the additional results at different temperature and annealing rates is made (Appendix B.2). Measurements of 10, 1 and 0.5 μM at annealing rate of 0.5°C /min. are compared. T_f (formation temperature, [K]) of respective samples were: 317.15 [10μM], 311.52 [1μM], 311.42 [0.5μM]. On the the other hand, the simulation results were: 320.2 [10μM], 312.8 [1μM], 310.5 [0.5μM]. Thus, these results were well agreed between orders of $10^{-1} \sim 10^1 \mu$M.

5.7.3 Simulation of substrate-assisted self-assembly

The simulation of substrate-assisted self-assembly has been executed by using an extended model of the previous section. Here, species on a surface and the adsorption/desorption reactions are added (Fig. 5.15).

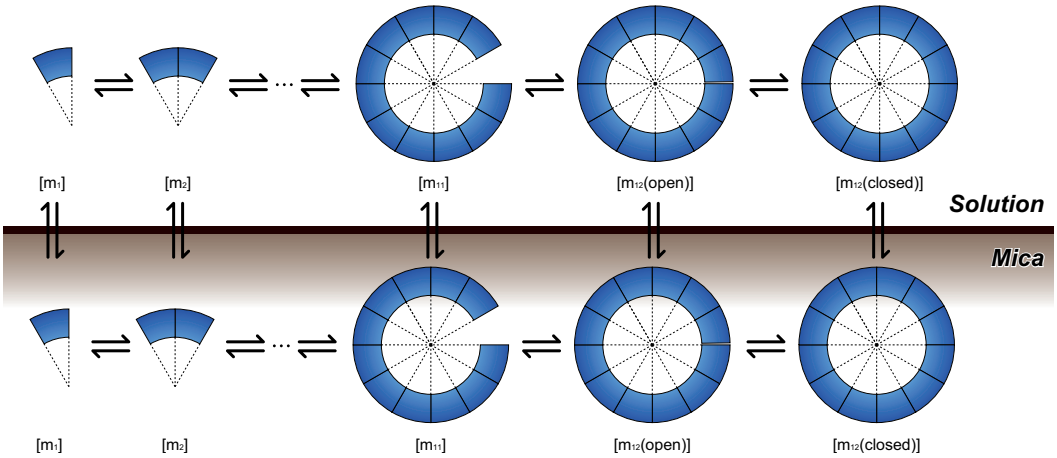

Figure 5.15: Simulation model of substrate-assisted self-assembly.

Again, the pathways used in this simulation are as same as which used in free-solution (equations 5.67,5.68).

The adsorption/desorption process is modeled as follows:

Langmuir adsorption model uses a concept of "adsorption sites", which are considered as exclusive binding sites of molecule. In case of substrate-assisted self-assembly on a substrate surface, this concept can be interpreted as a hypothetical "lattice" of a substrate surface; each area represents one exclusive binding site for one motif (Fig.5.16). (Each [m_n] occupies n sites.) A motif (or motifs) can move on the surface, so the number of empty binding sites can be regarded as an unoccupied area on the surface divided by an area of one site = an area of single motif.

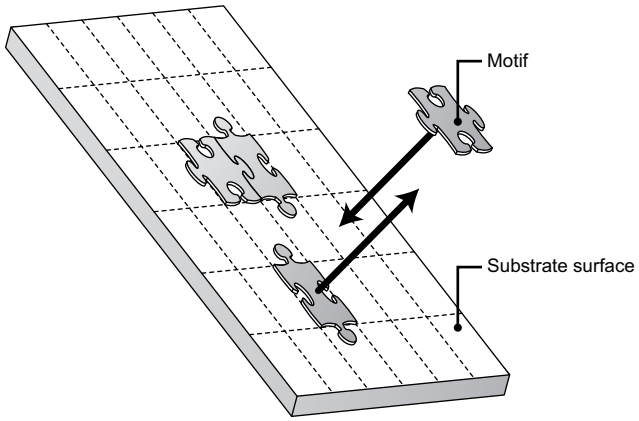

Figure 5.16: Lattice model of a substrate surface.

Thus, the total number of adsorption sites can be calculated as,

$$n_{site} = \frac{A_{substrate}}{A_{surface}} \tag{5.69}$$

where $A_{substrate}$ is the total area of the mica surface, and $A_{surface}$ is the area of one motif occupies on a surface. (Note that this approximation assumes $A_{surface} = A_{site}$ of equation (5.54)).

In order to be accurate with the experimental conditions, the volume of reaction chamber is set to 200[μl], the area of the substrate surface(mica) is set to $5 \times 7(\times 2)$[mm^2], and initial concentration [m_1(sol)] is set to 0.1[μM]. Annealing rate is -0.05°C /min.

Obtained simulation results revealed some qualitative characteristics of

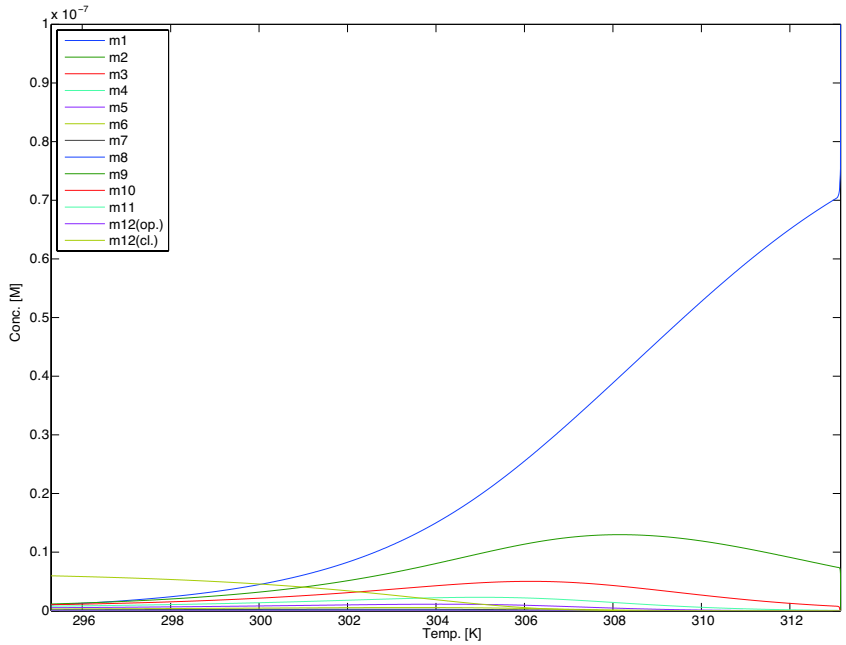

(a) Free solution

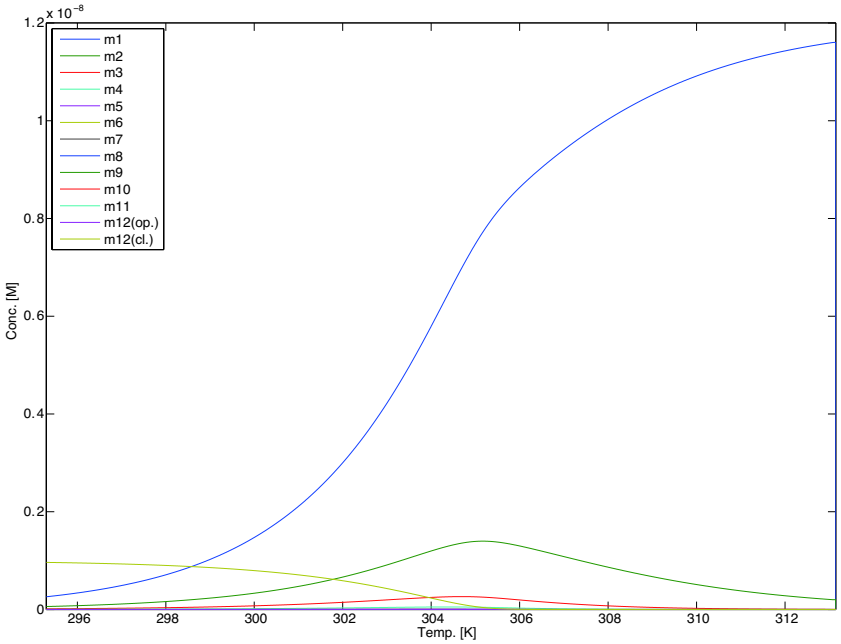

(b) Substrate surface

Figure 5.17: Simulation results of substrate-assisted self-assembly. Horizontal axes represent temperature. 0.1 μM, $1/q = 6 \times 10^4$. **a** Concentrations of the species in solution. **b** Concentrations of the species on the substrate surface. Note that the order of concentrations are different in a and b.

substrate-assisted self-assembly. Time developments of the species (Fig. 5.17) show the effect of substrate adsorption. The difference of the rate constant in 3D and 2D gives different proportions of each species in solution and on surface.

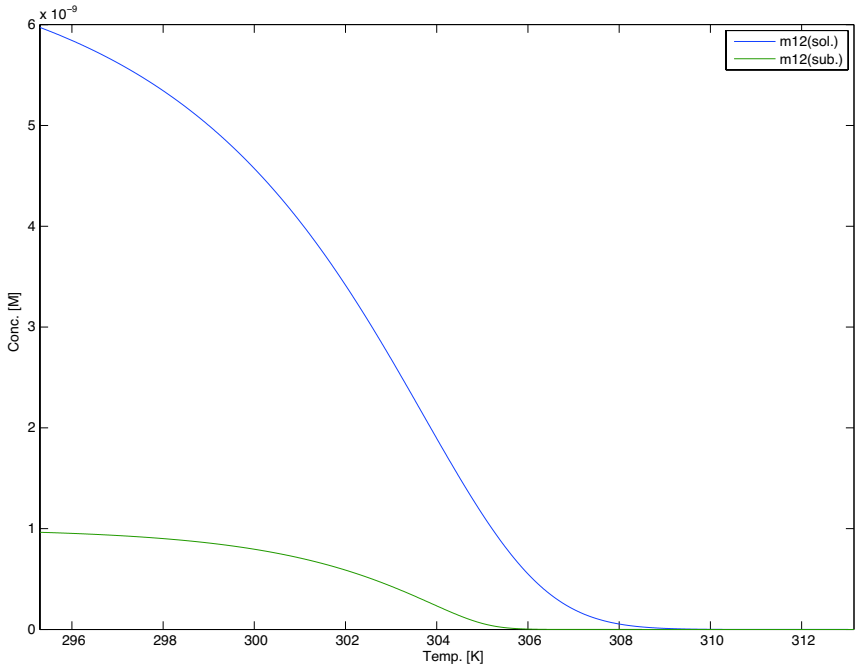

Figure 5.18: Concentration of rings ($[m_{12}(\text{open} + \text{close})]$) in free solution and on the substrate

A comparison of ring formation in solution and on the surface (Fig. 5.18) suggests the difference of starting point and the speed of the formation. According to the result, the formation of the rings on a surface starts at lower temperature, compared to the rings in free solution. It also suggests that the enhancement in rates on the surface also affects the rate in free solution. The difference in formation velocities is caused by a higher value of kinetic rate constant of formation on the surface. The formation of rings on a surface via self-assembly and adsorption are compared by a calculation of a percentage of formation rates (Fig. 5.19). This shows that the most of the rings on a surface are supplied by self-assembly process;

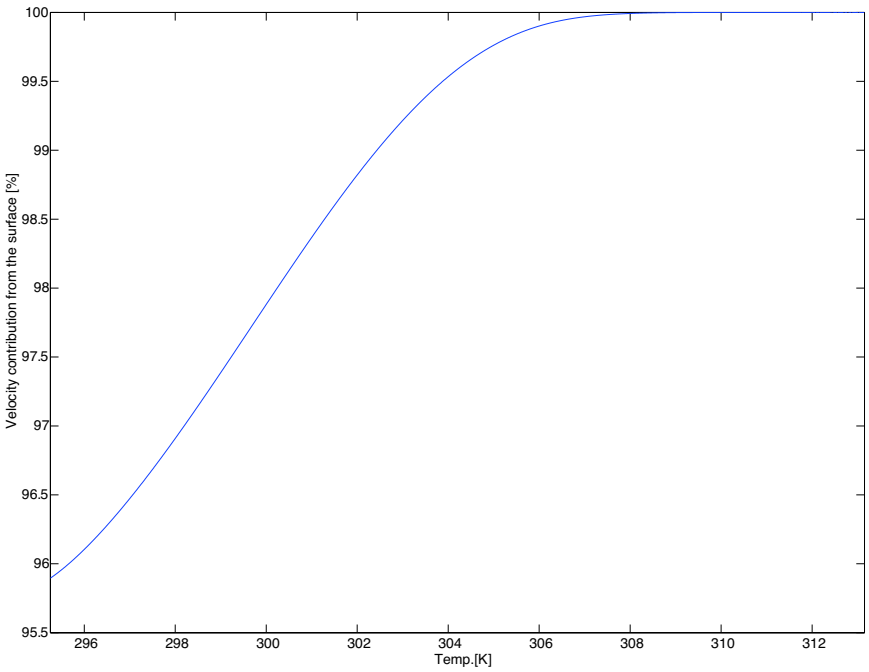

Figure 5.19: Percentage of formation rates of m12(close+open) contributed from self-assembly process.

the difference of starting temperature of formation between in solution and on the surface can be explained by this result. (*i.e.* The contribution from the solution is small, so the formation of the rings on the surface is less affected by the adsorption process and the starting temperature will become different.)

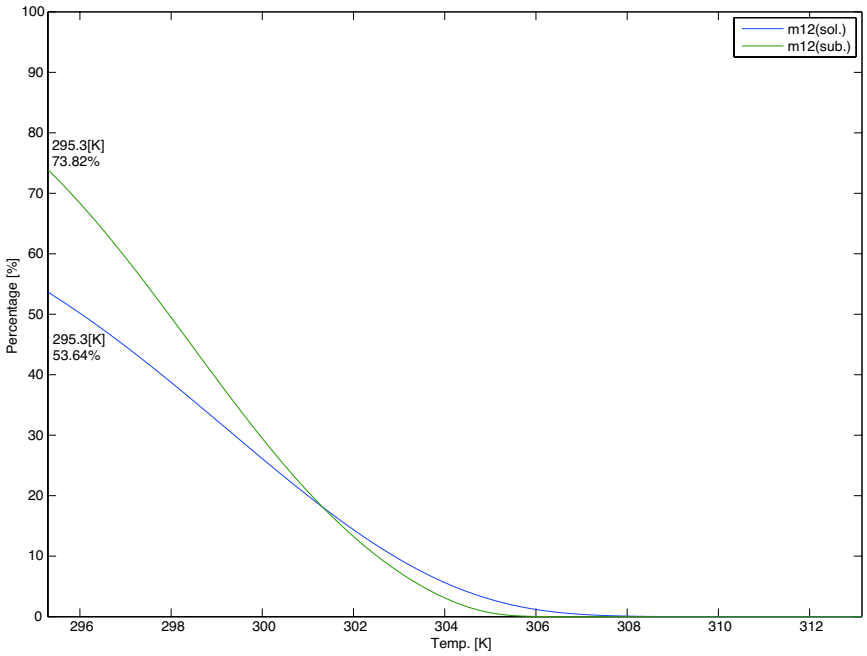

Figure 5.20: Yields of rings (%) in free solution and on the substrate

The difference in yields (Fig. 5.20) proves that the substrate-assisted self-assembly has an effect of providing higher yields in self-assembly process. In this annealing protocol (-0.05°C /min.), the difference is obvious; about ≈74% of formation yield on the substrate, on the other hand, about ≈54% in free solution (295.3[K]). AFM analysis (Appendix A) suggested the same tendency in the yields.

5.8 Summary

The theory of substrate-assisted self-assembly and kinetic simulations of the process are described. Although the simulations are verified only in case of mica substrate, the theory of substrate-assisted self-assembly itself has generality and can be applied to any kind of DNA structures or substrate materials. This versatility of the theory gives us not only the information of optimum conditions for assembly, but also provides understanding of the precise phenomena during the assembly process.

The process of substrate-assisted self-assembly can be divided into two elements, such as adsorption/desorption and hybridization. The former energy calculation can be described by a DLVO theory between cylinder and surface. The latter calculation is done by nearest-neighbor method of DNA hybridization. Both energies are used as values of thermodynamic equilibrium of reactions. Rigorous derivations of the equilibrium revealed that the activity coefficient of species becomes an important parameter q for the reaction. This parameter can be determined by a measurement of T_f(formation temperature) of self-assembly. Kinetic rates are derived from this parameter, thermodynamic equilibrium of the reaction, and the forward rate constant. The forward rate constant is given in 3-D; however, the 2-D rate constant was unknown. We adopted the fraction of ideal rate constant in 2-D/3-D for the estimation. Kinetic simulations of substrate-assisted self-assembly is executed using the ring structures. The results successfully explains some characteristic phenomena of substrate-assisted self-assembly, such as differences in a formation speed and yields.

Chapter 6

Conclusion

6.1 Answers

This thesis aims to answer the questions raised in section 1.2. Namely,

1. Is there any new principles to design varieties of DNA nanostructures, which have different characteristics compared to the current design?
2. What kind of shapes and patterns can be realized by the principle?
3. Can we find a versatile method to self-assemble DNA nanostructures up to meso-scale?
4. If so, how predictable and controllable is the method?

Chapter 2 and 3 answers the first question. A summary of DNA nanostructures in chapter 2 showed that the current motifs are only using crossover junction for the design. This analysis suggested that an invention of alternative junction could lead to novel geometries, which widely expands the variety of nanostructures. The novel T-junction structure is my solution for this suggestion. As a demonstration, five types of motifs called T-motifs are designed from only two strands of DNA. The experimental result suggests that wide varieties of 1 to 2-D (or maybe even 3-D) structures can be realized by this principle. In comparison with crossover-based motifs, T-motifs have several characteristics not only providing a new geometry, but also in terms of improving structural resolution and flexibility etc. The pro-

posed design of T-junction and T-motifs are the new principle for design of DNA nanostructures, which gives us new characteristics in DNA nanostructures.

The second question is answered in chapters 3 and 4. T-motifs themselves can create varieties of shapes and porous patterns, such as ladder structures to ring structures, brickwall and windmill lattice patterns. In addition, if we use advanced way of self-assembly called algorithmic self-assembly, we can even create complex patterns on the lattice structures using protein attachments.

The third question is answered in chapter 4. Substrate-assisted self-assembly can grow DNA nanostructures dramatically larger on substrate surface. This methodology is not restricted in certain motifs or substrates; we may even use conventional motifs or different substrates. Substrate-assisted self-assembly makes the structure covering on the whole surface up to meso-scale (or potentially even larger). Moreover, several interesting phenomena were found, including improvements of the assembly yield. These effects are also one of the advantages of the substrate-assisted self-assembly.

The last question is answered in chapter 5. The theory of substrate-assisted self-assembly gives us an insight of the mechanism of this methodology. We can reproduce and predict the phenomena under various concentrations, surface area, substrate materials, etc. Kinetic simulations using this theory revealed the time development of the process along with some phenomena observed by the actual experiments.

6.2 Issues for further studies

Several important issues can be conceived for further studies. The first issue is about the varieties of surface-growth motifs. Although T-motifs are found to be one of the suitable motifs for surface growth, other possibilities of design still remains. Is there any fundamental condition for substrate-assisted self-assembly in terms of the structural design? If we can use varieties of motifs including crossover-based

DNA nanostructures such as DX tiles and DNA origamis on a substrate surface, the range of design will be dramatically broaden. The second issue is about further understanding the phenomena on the surface. Although we succeeded in describing adsorption and assembly process of substrate-assisted self-assembly, it only describes from the aspect of concentrations and species/states. If we want to describe further details of the phenomena such as movements and alignments of the motifs on the surface, we need to consider the forces between DNAs on a surface. This requires precise modeling of DNA-DNA interaction along with a consideration about the mobility on a surface and consideration of other effects, such as excluded volume effects and depletion forces. This research leads to a design and control of phase transition and self-organization of DNA nanostructures on a surface, using both specific and non-specific interactions between molecules. The third issue is about an usage of DNA nanostructures in applications. Although substrate-assisted self-assembly on a mica surface is achieved, we have to seek for the optimal conditions of different materials, especially SiO_2, for practical applications of this methodology. The theory will be a strong tool for this.

Substrate-assisted self-assembly has a large possibility to become a bridge between top-down methodologies, such as lithography, and bottom-up DNA nanoengineering. I believe the investigations mentioned above lead us to the new era of creating things, bringing the best of both worlds.

Appendix A

Additional AFM observation and analyses of T-motifs

A.1 Yield and diameter analysis example of the Ring 1.0x

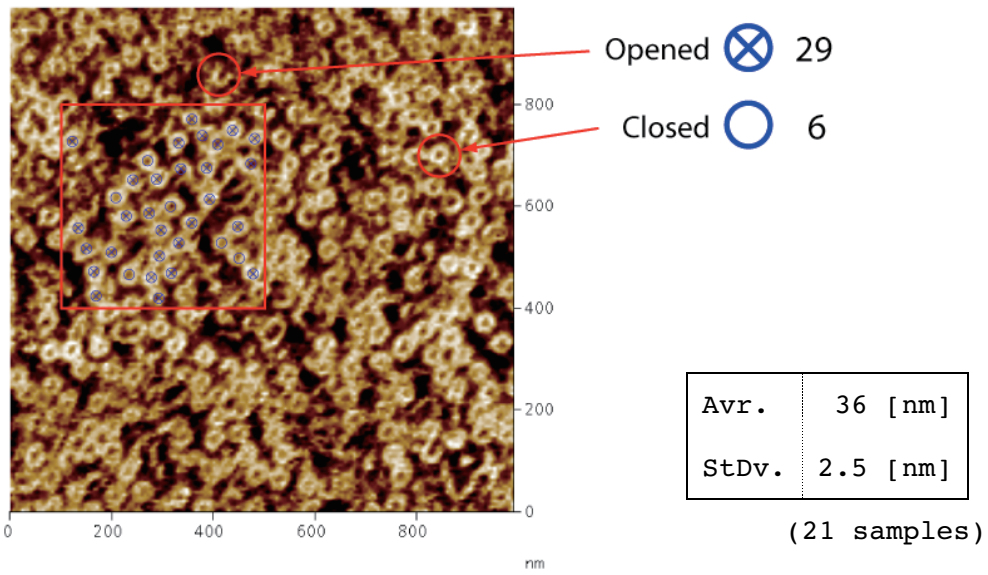

Figure A.1: Yield and diameter analysis example of the Ring (in free-solution environment)

A yield of the structure is approximately 17%, counting the percentage of observed closed ring in the whole ring-like structures inside 400[nm] × 400[nm] square including opened (uncompleted) structures. (Closed ring: 6, Opened ring: 29; some of the defects are supposedly damaged by AFM cantilever tip.) This analysis has difficulties in reproducibility because of annealing conditions and intervention by AFM. The average and standard deviation (36 ± 2.5 [nm]) of the diameter from randomly taken 21 samples from this image suggest most of the closed Wheel is consistent with the design in Fig.3.5 (estimated diameter 37 [nm]).

A.2 Analyses of AFM observation

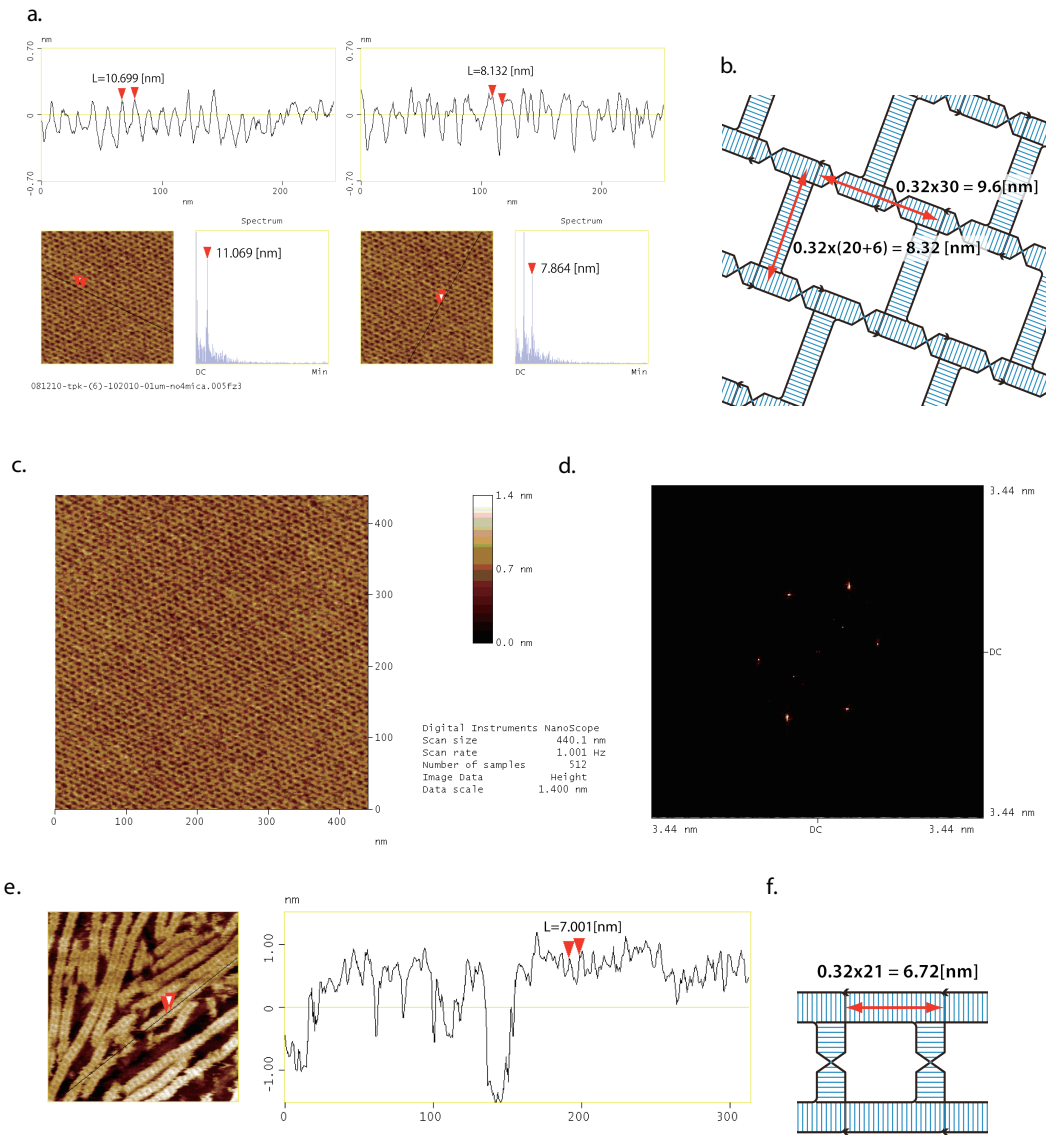

Figure A.2: Analyses of AFM observation

a,b section height of brick-wall lattice; **a** longitudinal and latitudinal section results. Sharp peak of spectrum denotes highly uniform structural periodicity; **b** designed length of lattice; **c,d** 2D-fourier transformation image of brick-wall lattice. The result implies homogeneity of the structure; **e-f** section analysis of ladder 15-

15-15(7); **e** rung interval section analysis; **f** designed length of ladder. All results (a-e) are consistent with the design.

A.3 Additional AFM observation results

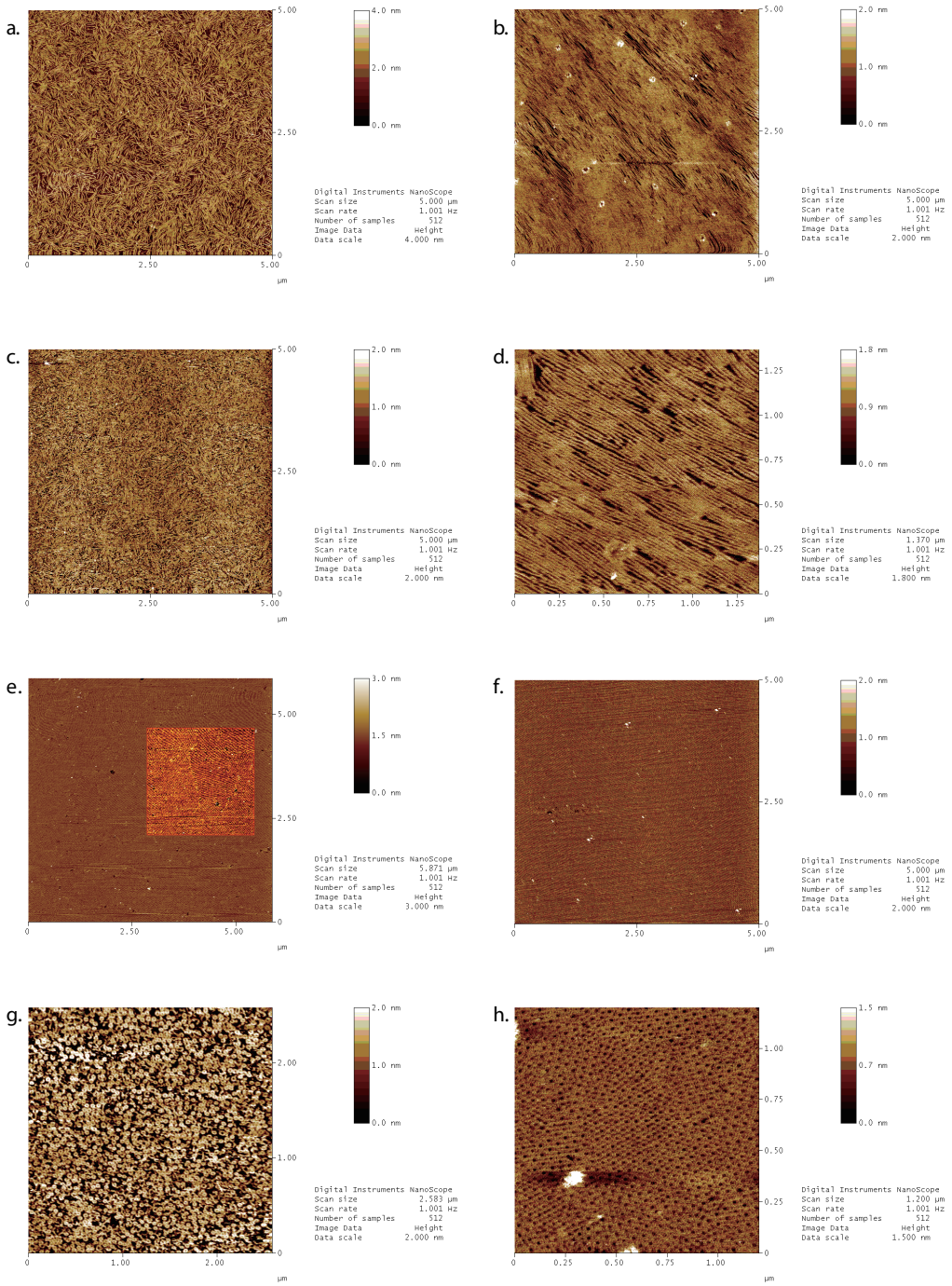

Figure A.3: Additional AFM observation results

a Ladder 15-15-15(7) (free-solution); **b** ladder 15-15-15(7) (substrate-assisted); **c** ladder 15-20-15(7) (free-solution); **d** ladder 15-20-15(7) (substrate-assisted); **e** brick-wall lattice (substrate-assisted) [Contrast enhanced in the red box area by Adobe Photoshop]; **f** windmill lattice (substrate assisted); **g** wheel (free-solution); **h** wheel (substrate-assisted). Note that length and alignment are qualitatively changed in a,c and b,d. In e,f, almost the entire substrate surface is covered by the structure. Patchwork-like monocrystalic region can be recognized from moiré pattern[Koyfman 2009, Hexemer 2005]. (Continuous moiré pattern indicates the monocrystal area.) This moiré pattern occurs because of the interference between structures' lattice pitch and the AFM's grating pitch (i.e. sampling resolution). Our estimation is that these monocrystals grow independently on the surface until they meet each other, following which part of the growth fronts are connected and form a patchwork-like appearance. This means that the size of a monocrystal depends on the number of nuclei on the substrate surface; thus, we could create large-scale crystals with nucleus density control. Plates g,h indicate the difference between free-solution and mica-assisted self-assembly of wheel structure. Compared to the free-solution, mica-assisted assembly yield is increased (up to almost 100%), and also most of the structures are aligned in hexagonal close-packed formation. This 2-D movement of the structures on the substrate during or after self-assembly can be explained by the minimization of surface exposure to solutions.

A.4 Tube/troidal formation of T-motif brick-wall lattice

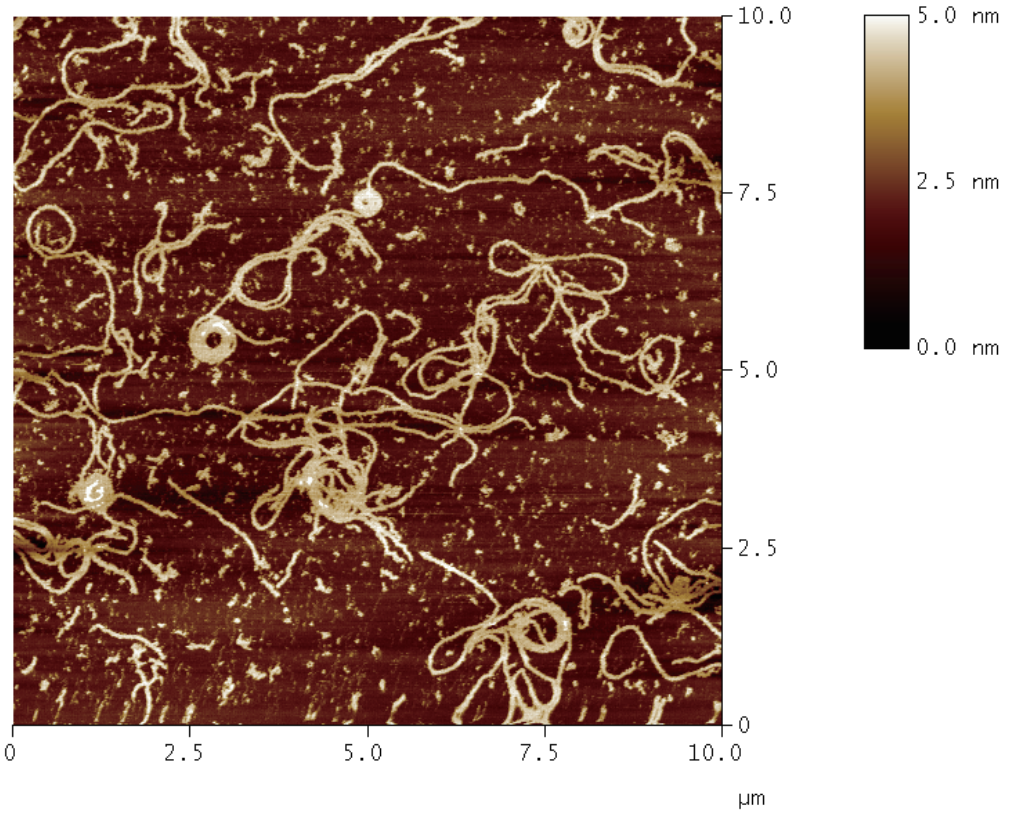

Figure A.4: Tube/troidal formation of T-motif brick-wall lattice

Appendix B

Spectrophotometer data of T-motifs

B.1 Annealing/melting data of the T-motifs

a Melting/annealing measurement of brick-wall lattice. **b** Melting/annealing measurement of Wheel (Ring1.0x). Both experiments were done in free-solution environment. Conditions: 0.66μM (Final concentration); 3000μl (TAE/Mg^{2+} buffer); cooling-heating rate at 0.3°C /min (85°C $\rightarrow$ 20°C $\rightarrow$ 85°C); UV wavelength is 260nm. V-630BIO (JASCO, Inc.) is used for measurement. Temperature values in the graph indicate points of inflection. The melting and annealing curve indicate a two-step formation process (formation of the motif/self-assembly of the motif).

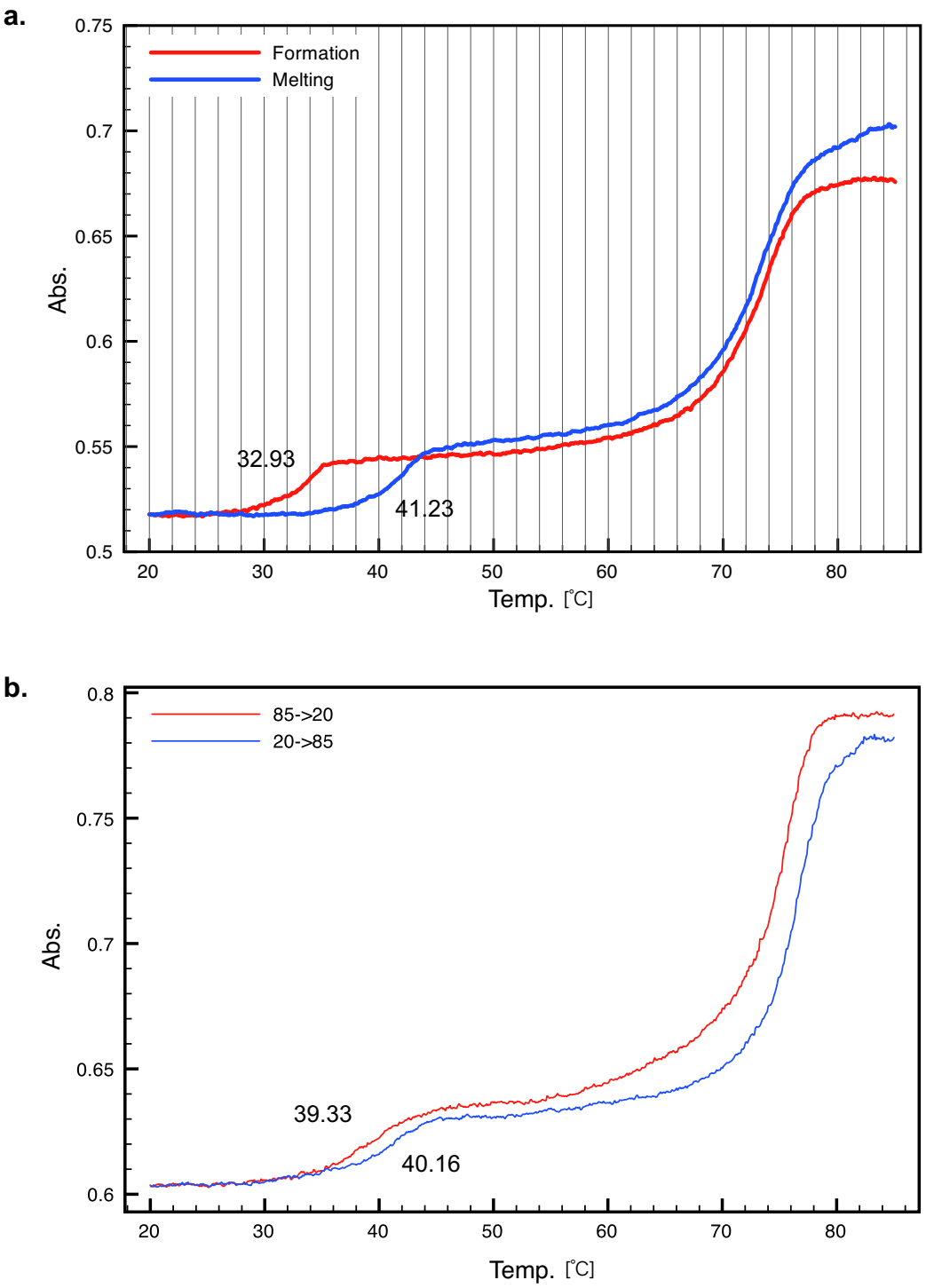

Figure B.1: UV absorbance at 260nm during annealing/melting of the T-motifs. Numbers in the graph indicates temperature of the formation/melts.

B.2 Formation curve of self-assembly process (Ring 1.0x)

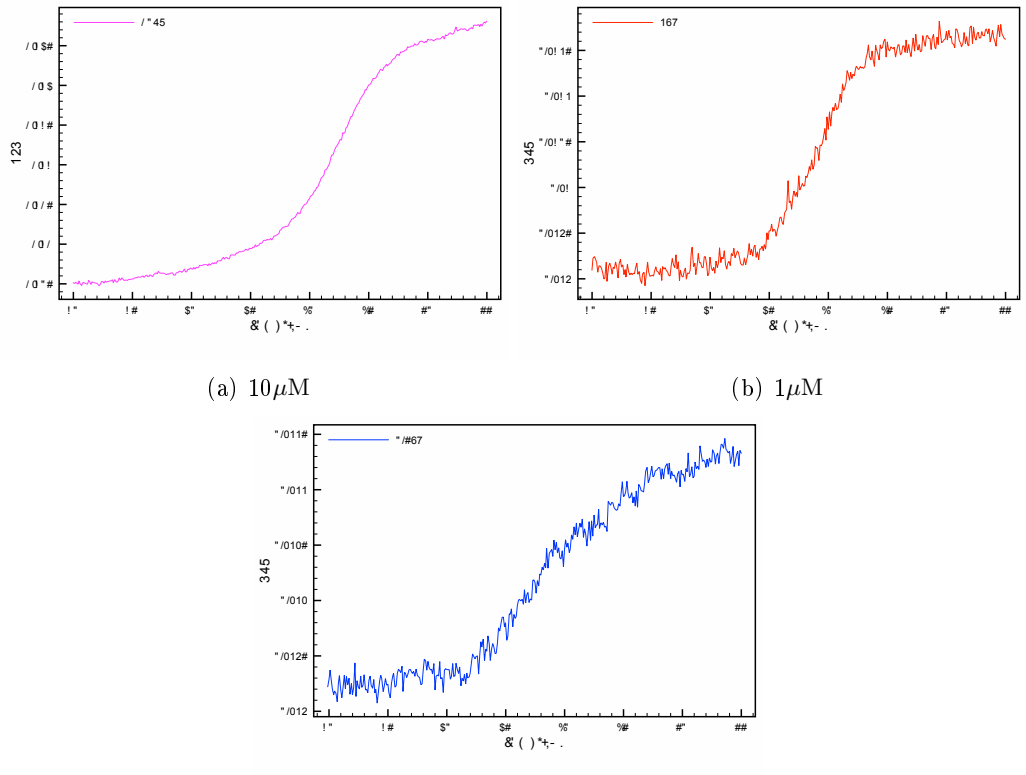

(a) 10μM (b) 1μM

(c) 0.5μM

Figure B.2: Formation curves of Ring 1.0x.

All experiments are carried out in free-solution environment. Samples are prepared at 10μM (motif conc.) in TAE/Mg^{2+} buffer. The sample is first annealed by hot water from 90°C to room temperature, and then diluted to the respective concentrations for measurements (10, 1, 0.5μM). Measurements are done by heating up to 55°C , then cooling down to 20°C by the rate of 0.5°C /min. (Note that this measurement is focusing on the second process of formation curve (*i.e.* self-assembly of motifs).) UV wavelength is 260nm. V-630BIO (JASCO, Inc.) is used for measurement. Capillary jacket for melting temperature measurement is used for the experiment, so the exact volume of the sample is unknown. Calculated T_f (for-

mation temperature) of respective samples are: 44.10°C [10μM], 38.37°C [1μM], 38.27°C [0.5μM]. 0.1μM was unable to measure because of the low concentration. In comparison with Fig. B.1, certain range of errors in formation temperature are recognized in the result. These are mainly due to: 1. difference in apparatus, 2. sample preparation, 3. calculation algorithm of T_f.

Appendix C

Cyclic annealing of T-motif

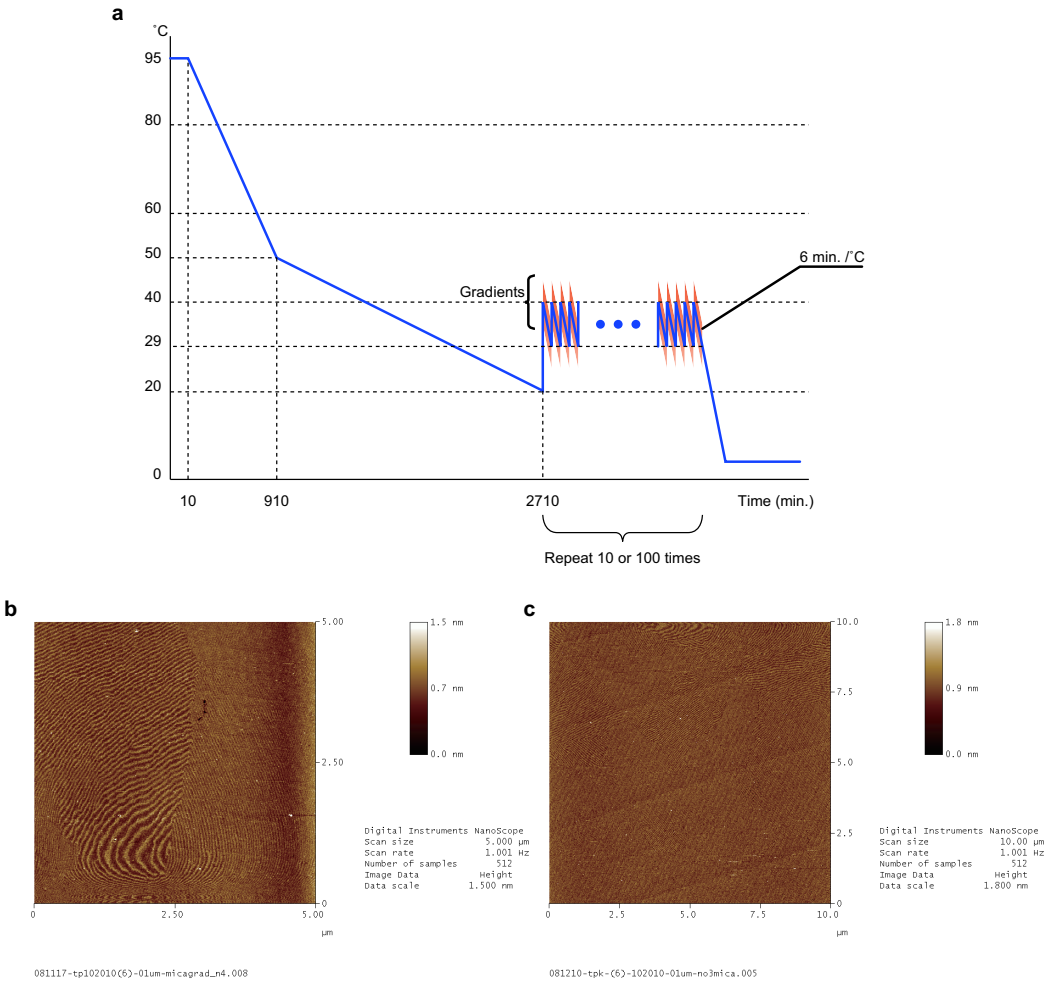

Figure C.1: Cyclic annealing protocol of T-motif (Brick-wall lattice)

Optimized annealing protocol for larger growth and its observation results of brick-wall lattice. **a** Annealing protocol derived from Appendix Fig. B.1. **b-c**,

AFM observation results; **b** 10 times repeat, Grad. 34.1°C to 23.0°C ; **c** 100 times repeat, Grad. 32.1°C to 21.0°C . Compared with the results in Appendix Fig. A.3, the size of monocrystal (continuous moiré pattern) are enlarged, however we need further study to determine the exact enlarged ratio of the monocrystal.

Appendix D

Area analysis of monocrystal region

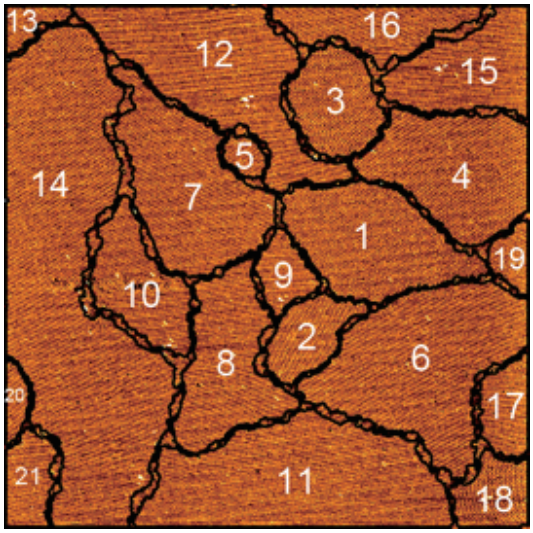

Figure D.1: Area analysis of T-motif windmill lattice

No.	area [px^2]
1	16100
2	5597
3	8338
4	16311
5	1589
6	24905
7	18659
8	13769
9	3591
10	9222
11	27083
12	22082
13	2119
14	51431
15	11049
16	8023
17	4414
18	4831
19	2312
20	1711
21	4368

Area analysis of windmill lattice monocrystals self-assembled by mica-assisted method. Scan area: 5 [μm] (512 [px]) $\times$ 5 [μm] (512[px]). Average of all areas: 1.169 [μm^2]. Monocrystal area identifications (black borders) based on moiré patterns are operated semi-automatically by Adobe Photoshop (Quick Selection Tool), and pixel counts are analyzed by ImageJ. The largest area of the windmill lattice observed in case of free-solution assembly is 0.1289 [μm^2] (Fig. 3.3 d3); therefore we can roughly

estimate the ratio of the monocrystal area between free-solution and mica-assisted methods at least nine (9.069) times in this example. (In case of the brick-wall lattice, we couldn't identify each monocrystal area by AFM due to the formation of tubes in a free-solution environment.)

Appendix E

Calculation of monovalent/divalent ion concentration of TAE/Mg^{2+} 12.5mM buffer

---

TAE buffer with Magnesium ion of 12.5mM concentration is one of the standard buffer we use in structural DNA nanotechnology. TAE stands for Tris base, Acetic acid and EDTA. In order to calculate adsorption energy on the mica surface, we have to solve the "actual" monovalent and divalent ion concentrations, because Tris/Tris-acetate is under equilibrium conditions.

A typical composition of TAE/Mg^{2+}12.5mM buffer is as follows:

- Monovalent ion

  Tris/Tris-acetate 40mM

- Divalent ion/ Chelating agent

  EDTA (Ethylenediaminetetraacetic acid) 1mM

  Mg^{2+} 12.5mM

- final pH: 8.3

E.1 Monovalent ion concentration

Consider Tris-acetate acts as a monovalent ion ($[TrisH^+]$):

Tris-acetate $[(HOCH_2)_3C - NH_3^{(+)} \cdot CH_3COO^{(-)}]$

Tris $[(HOCH_2)_3C - NH_2]$

Acetate $CH_3COOH \rightleftharpoons [CH_3COO^-][H^+]$

Equilibrium constants of Acetate and Tris can be defined as:

$$K_a = \frac{[CH_3COO^-][H^+]}{[CH_3COOH]} \tag{E.1}$$

$$K_b = \frac{[Tris][H^+]}{[TrisH^+]} = 10^{-8.06} \tag{E.2}$$

Note that the ionization degree of Acetate is low (mostly in $[CH_3COOH]$) in Formula E.1. pH of K_b is at 25°C .

Several equations can be derived from the conditions above:

$$[Tris] + [TrisH^+] = 0.04[M] \tag{E.3}$$

$$[H^+] = 10^{-8.3} \tag{E.4}$$

Substitute the conditions into Formula E.2,

$$\frac{[Tris] \cdot 10^{-8.3}}{[TrisH^+]} = 10^{-8.06} \tag{E.5}$$

therefore,

$$[Tris] = 10^{0.24} \cdot [TrisH^+] \tag{E.6}$$

From Equations E.3 and E.6,

$$[\mathrm{TrisH}^+] = \frac{0.04}{1 + 10^{0.24}} = 0.0146[\mathrm{M}] \tag{E.7}$$

E.2 Divalent ion concentration

Because of the excess concentration of Mg^{2+} in the buffer, we can neglect the chelating effect of EDTA to the divalent metal ions in this case. Consequently, the divalent ion concentration is 12.5[mM].

Appendix F

Source codes

F.1 Design software

A simple computer tool for block-based abstraction of T-motif is written by Javascript, CSS and HTML. Drag and drop function etc. are implemented using Yahoo! UI Library ver.2 (http://developer.yahoo.com/yui/).

```
<!DOCTYPE html PUBLIC "-//W3C//DTD XHTML 1.0 Transitional//EN"
"http://www.w3.org/TR/xhtml1/DTD/xhtml1-transitional.dtd">
<html xmlns="http://www.w3.org/1999/xhtml">
<head>
<meta http-equiv="Content-Type" content="text/html; charset=UTF-8" />
<meta name="viewport" content="height=420;user-scalable= no;initial-
scale=4.0;">
<title>T-motif Designer (demo)</title>
<style type="text/css">
/*margin and padding on body element
  can introduce errors in determining
  element position and are not recommended;
  we turn them off as a foundation for YUI
  CSS treatments. */
body {
margin:0;
```

```
padding:0;
background-color: #000;
}
#loadForm {
position: fixed;
top: 100px;
left: 120px;
visibility: hidden;
}
#loadButton {
left: 600px;
top: 300px;
position: fixed;
visibility: hidden;
}
#cancelButton {
left: 520px;
top: 300px;
position: fixed;
visibility: hidden;
}
</style>

<link rel="stylesheet" type="text/css" href="http://yui.yahooapis.com/2.7.0/
build/fonts/fonts-min.css" />
<script type="text/javascript" src="http://yui.yahooapis.com/2.7.0/build/
yahoo-dom-event/yahoo-dom-event.js"></script>
<script type="text/javascript" src="http://yui.yahooapis.com/2.7.0/build/
```

```
dragdrop/dragdrop-min.js"></script>
<script type="text/javascript" src="http://yui.yahooapis.com/2.7.0/build/
yahoo/yahoo-min.js"></script>
<script type="text/javascript" src="http://yui.yahooapis.com/2.7.0/build/dom/
dom-min.js"></script>
<script type="text/javascript" src="http://yui.yahooapis.com/2.7.0/build/
event/event-min.js"></script>

<style type="text/css">
<!--
#canvas {
position:absolute;
left:50px;
top:0px;
width:1550px;
height:1200px;
z-index:1;
overflow: visible;
background-image: url(img/background.png);
visibility: visible;
cursor: default;
}
body,td,th {
font-family: ヒラギノ角ゴ Pro W3, Hiragino Kaku Gothic Pro, メイリオ,
Meiryo, Osaka, ＭＳ Ｐゴシック, MS PGothic, sans-serif;
}
#block_canvas {
position:relative;
```

```
left:100px;
top:200px;
width:50px;
height:50px;
z-index:2;
overflow: hidden;
visibility: visible;
background-color: #FFF;
cursor: move;
background-image: url(img/block.png);
}
#toolBar {
position:fixed;
left:0px;
top:0px;
width:55px;
height:1200px;
z-index:999999999;
overflow: visible;
cursor: default;
background-image: url(img/bar_shadow.png);
}
#block_toolBar {
position:fixed;
left:0px;
top:15px;
width:50px;
height:50px;
```

```
z-index:1000000000;
background-image: url(img/block.png);
overflow: visible;
}
#block_T-junction-r_toolBar {
position:fixed;
left:0px;
top:85px;
width:50px;
height:100px;
z-index:1000000000;
background-image: url(img/T-junction-r.png);
overflow: visible;
}
#block_T-junction-l_toolBar {
position:fixed;
left:0px;
top:205px;
width:50px;
height:100px;
z-index:1000000000;
background-image: url(img/T-junction-l.png);
overflow: visible;
}
#evac {
width: 0px;
}
#initialDisplay {
```

```
position:absolute;
left:0px;
top:0px;
width:1600px;
height:1200px;
z-index:1000000000;
background-image: url(img/gray.png);
}
#initialDescription {
position:absolute;
left:152px;
top:52px;
width:588px;
height:319px;
z-index:1000000001;
visibility: visible;
}
#initialDescription {
font-family: Arial, Helvetica, sans-serif;
color: #FFF;
position: fixed;
}
#load {
position:fixed;
left:10px;
top:350px;
width:30px;
height:23px;
```

```
z-index:1000000000;
background-image: url(img/load.png);
}
#save {
position:fixed;
left:10px;
top:372px;
width:30px;
height:23px;
z-index:1000000000;
background-image: url(img/save.png);
}



-->
</style>


<script type="text/javascript">


    (function() {

var Dom = YAHOO.util.Dom;
var Event = YAHOO.util.Event;


//選択されたブロックの ID 表
```

```
var selectedBlock = new Array();

//settings for created blocks
function setBlock(el,x,y,z){
Dom.setStyle(el, 'left', x+'px');
Dom.setStyle(el, 'top', y+'px');
Dom.setStyle(el, 'position', 'absolute');
Dom.setStyle(el, 'overflow', 'hidden');
Dom.setStyle(el, 'zIndex', z);
Dom.setStyle(el, 'cursor', 'move');
setBlockRot(el);
return;
};

//rotation settings (default:0deg.)
function setBlockRot(el){
if(el.type=='DH'){
Dom.setStyle(el, 'width', '50px');
Dom.setStyle(el, 'height', '50px');
switch(el.ori){
case 90:  Dom.setStyle(el, 'backgroundImage',
'url(img/block_90.png)'); break;
case 180: Dom.setStyle(el, 'backgroundImage',
'url(img/block_180.png)'); break;
case 270: Dom.setStyle(el, 'backgroundImage',
'url(img/block_270.png)'); break;
default:  Dom.setStyle(el, 'backgroundImage',
'url(img/block.png)'); break;
```

```
}
} else if(el.type=='T-junction-l'){
switch(el.ori){
case 90:  Dom.setStyle(el, 'width', '100px'); Dom.setStyle(el, 'height', '50px');
Dom.setStyle(el, 'backgroundImage',
'url(img/T-junction-l_90.png)'); break;
case 180: Dom.setStyle(el, 'width', '50px'); Dom.setStyle(el, 'height', '100px');
Dom.setStyle(el, 'backgroundImage',
'url(img/T-junction-l_180.png)'); break;
case 270: Dom.setStyle(el, 'width', '100px'); Dom.setStyle(el, 'height', '50px');
Dom.setStyle(el, 'backgroundImage',
'url(img/T-junction-l_270.png)'); break;
default:  Dom.setStyle(el, 'width', '50px'); Dom.setStyle(el, 'height', '100px');
Dom.setStyle(el, 'backgroundImage',
'url(img/T-junction-l.png)'); break;
}
//Dom.setStyle(el, 'width', '50px');
//Dom.setStyle(el, 'height', '100px');
//Dom.setStyle(el, 'backgroundImage',
'url(img/T-junction-l.png)');
} else if(el.type=='T-junction-r'){
switch(el.ori){
case 90:  Dom.setStyle(el, 'width', '100px'); Dom.setStyle(el, 'height', '50px');
Dom.setStyle(el, 'backgroundImage',
'url(img/T-junction-r_90.png)'); break;
case 180: Dom.setStyle(el, 'width', '50px'); Dom.setStyle(el, 'height', '100px');
Dom.setStyle(el, 'backgroundImage',
'url(img/T-junction-r_180.png)'); break;
```

```
case 270: Dom.setStyle(el, 'width', '100px'); Dom.setStyle(el, 'height', '50px');
Dom.setStyle(el, 'backgroundImage',
'url(img/T-junction-r_270.png)'); break;
default:  Dom.setStyle(el, 'width', '50px'); Dom.setStyle(el, 'height', '100px');
Dom.setStyle(el, 'backgroundImage',
'url(img/T-junction-r.png)'); break;
}
//Dom.setStyle(el, 'width', '50px');
//Dom.setStyle(el, 'height', '100px');
//Dom.setStyle(el, 'backgroundImage',
'url(img/T-junction-r.png)');
}
};



//DDRegion from DD
//
// DDRegion 作成の準備
DDRegion = function(id, sGroup, config) {
this.cont = config.cont;
DDRegion.superclass.constructor.apply(this, arguments);
};

//YAHOO.util.DD を継承して、DDRegion を作る。
//ref: http://d.hatena.ne.jp/tetsuya_odaka/20081025/1224961927
YAHOO.extend(DDRegion, YAHOO.util.DD, {
// cont は呼び出し時に上書きされる。
cont: null,
```

```
init: function() {
// スーパークラスの init を呼ぶ。
DDRegion.superclass.init.apply(this, arguments);

this.initConstraints();

// window が resize されたら initConstraints をよぶ Event を仕掛ける。
Event.on(window, 'resize', function() {
this.initConstraints();
}, this, true);
},

initConstraints: function() {
// cont（canvas）の領域（top,right,bottom,left）を求める。
var region = Dom.getRegion(this.cont);

//この（DDRegion）インスタンスの要素オブジェクトの取り出し。
var el = this.getEl();

//座標（x=right、top を取り出す）
var xy = Dom.getXY(el);

//DD インスタンスの幅、高さを 10 進整数としてパースする。
var width = parseInt(Dom.getStyle(el, 'width'), 10);
var height = parseInt(Dom.getStyle(el, 'height'), 10);

//DD インスタンスの X(left)-canvas の left 値（left として動ける pix）
var left = xy[0] - region.left;
```

```
//canvas の right 値-(DD インスタンスの left 値＋インスタンスの幅)
//DD インスタンスが right へ動ける距離
var right = region.right - xy[0] - width;

//Set top to y minus top
//DD インスタンスの Y(top)-canvas の top 値（top として動ける pix）
var top = xy[1] - region.top;

//Set bottom to bottom minus y minus height
//canvas の bottom 値-(DD インスタンスの top 値＋インスタンスの高さ)
//DD インスタンスが bottom へ動ける距離
var bottom = region.bottom - xy[1] - height;

//DD.setXConstraint(),DD.setYConstraint() を使って動きに
//制約（Constraint）を与える
//X 軸に沿っては（上で求めた left と right の間を動ける）
this.setXConstraint(left, right, 50);
//Y 軸に沿っては（上で求めた top と bottom の間を動ける）
this.setYConstraint(top, bottom, 50);
}
});
//DDRegion End



//Id list of all Blocks
var block_ids = new Array(0);
```

```
//DomReady
        YAHOO.util.Event.onDOMReady(function() {



//toolbar block element
     var blockToolBar_dd = new YAHOO.util.DD("block_toolBar");
var blockTjunction_r_ToolBar_dd = new YAHOO.util.DD("block_T-junction-r_toolBar");
var blockTjunction_l_ToolBar_dd = new YAHOO.util.DD("block_T-junction-l_toolBar");
var blockCoordinateX = 0;
var blockCoordinateY = 0;

//Drag drop target
var tar = new YAHOO.util.DDTarget("canvas");

//zindex for all blocks
var zindex = 100;



//
//behaviors at Dropped on canvas/events
//

//blockToolBar_dd
     blockToolBar_dd.onDragDrop = function() {
createNewBlock('DH', 0);
   };
```

```
blockToolBar_dd.onInvalidDrop = function() {
Dom.setStyle("block_toolBar", 'top', '');
Dom.setStyle("block_toolBar", 'left', '');
Dom.removeClass('canvas', 'over');
    };

     blockToolBar_dd.onDragOver = function() {
         Dom.addClass('canvas', 'over');
     };

     blockToolBar_dd.onDragOut = function() {
         Dom.removeClass('canvas', 'over');
     };

blockToolBar_dd.onDrag = function(){
var position_blockToolBar_dd = YAHOO.util.Dom.getXY("block_toolBar");
blockCoordinateX = position_blockToolBar_dd[0];
blockCoordinateY = position_blockToolBar_dd[1];
};
//blockToolBar_dd End

     //blockTjunction_r_ToolBar_dd
     blockTjunction_r_ToolBar_dd.onDragDrop = function() {
createNewBlock('T-junction-r', 0);
   };

blockTjunction_r_ToolBar_dd.onInvalidDrop = function() {
```

```
Dom.setStyle("block_T-junction-r_toolBar", 'top', '');
Dom.setStyle("block_T-junction-r_toolBar", 'left', '');
Dom.removeClass('canvas', 'over');
    };

     blockTjunction_r_ToolBar_dd.onDragOver = function() {
         Dom.addClass('canvas', 'over');
     };

     blockTjunction_r_ToolBar_dd.onDragOut = function() {
         Dom.removeClass('canvas', 'over');
     };

blockTjunction_r_ToolBar_dd.onDrag = function(){
var position_blockToolBar_dd = YAHOO.util.Dom.getXY("block_T-junction-r_toolBar");
blockCoordinateX = position_blockToolBar_dd[0];
blockCoordinateY = position_blockToolBar_dd[1];
};
//blockTjunction_r_ToolBar_dd End

//blockTjunction_l_ToolBar_dd
     blockTjunction_l_ToolBar_dd.onDragDrop = function() {
createNewBlock('T-junction-l', 0);
   };

blockTjunction_l_ToolBar_dd.onInvalidDrop = function() {
Dom.setStyle("block_T-junction-l_toolBar", 'top', '');
Dom.setStyle("block_T-junction-l_toolBar", 'left', '');
```

```
Dom.removeClass('canvas', 'over');
    };

     blockTjunction_l_ToolBar_dd.onDragOver = function() {
         Dom.addClass('canvas', 'over');
     };

     blockTjunction_l_ToolBar_dd.onDragOut = function() {
         Dom.removeClass('canvas', 'over');
     };

blockTjunction_l_ToolBar_dd.onDrag = function(){
var position_blockToolBar_dd = YAHOO.util.Dom.getXY("block_T-junction-l_toolBar");
blockCoordinateX = position_blockToolBar_dd[0];
blockCoordinateY = position_blockToolBar_dd[1];
};
//blockTjunction_l_ToolBar_dd End
//behavior at Dropped on canvas end

function createNewBlock(blocktype, blockori) {
var newBlock = document.createElement('DIV');
newBlock.id = Dom.generateId();
//window.alert(blocktype);
//add new id to the list
block_ids.push(newBlock.id);

//add type and orientation to newBlock
Dom.addClass(newBlock,'type');
```

```
newBlock.type = blocktype;

Dom.addClass(newBlock,'ori');
newBlock.ori = blockori;



//set properties for the new block
var arrayNewBoxCoordinate = new Array(2);
arrayNewBoxCoordinate[0] = blockCoordinateX-(blockCoordinateX%50);
arrayNewBoxCoordinate[1] = blockCoordinateY-(blockCoordinateY%50);

//set configuration
setBlock(newBlock, arrayNewBoxCoordinate[0],
arrayNewBoxCoordinate[1], zindex);
zindex += 1;

//add new block to the canvas
document.body.appendChild(newBlock);

var block_dd = new DDRegion(newBlock, '', { cont: 'canvas' });

//newBlockをあらかじめ選択する
fn_block_onclick(newBlock);

//move back toolbar block
switch(blocktype){
case 'DH': Dom.setStyle('block_toolBar', 'top', '');
Dom.setStyle('block_toolBar', 'left', ''); break;
```

```
case 'T-junction-r': Dom.setStyle('block_T-junction-r_toolBar', 'top', '');
Dom.setStyle('block_T-junction-r_toolBar', 'left', ''); break;
case 'T-junction-l': Dom.setStyle('block_T-junction-l_toolBar', 'top', '');
Dom.setStyle('block_T-junction-l_toolBar', 'left', ''); break;
default: break;
}
        Dom.removeClass('canvas', 'over');

//debug_use
//document.getElementById("canvas").innerHTML = '
newBlock.id:'+newBlock.id;
//newBlock.innerHTML = block_dd;


block_dd.onMouseDown = function(){fn_block_onclick(newBlock)};

return;
}



//Data loading functions
loaddata = function(e){
load_data();
hide_load_forms();
};

//load data
```

```
function load_data(){
var contents = Dom.get("loadForm").value;
var contents_row = new Array(0);
contents_row = contents.split("\n");

//行ごとに読み込み
for(var i in contents_row)
{
if ((contents_row[i].charAt(0) == "#")||(contents_row[i].charAt(0) == "")){
//コメント, 空行は無視する
} else {
//行ごとの要素を読み込み
var items = new Array(0);
items = contents_row[i].split(",");

//対象となる行のデータ保持のための var
var id_of_this_block;
var ori_of_this_block;
var type_of_this_block;
var x_of_this_block;
var y_of_this_block;

//item の名前とその値をそれぞれ読み込む
for(var j in items)
{
var nameandvalue = new Array(0);
nameandvalue = items[j].split(":");
//window.alert(nameandvalue[0] + '+' +nameandvalue[1]);
```

```
switch (nameandvalue[0]){
case 'id': id_of_this_block = nameandvalue[1]; break;
case 'ori': ori_of_this_block = nameandvalue[1]; break;
case 'type': type_of_this_block = nameandvalue[1]; break;
case 'X': blockCoordinateX = nameandvalue[1]; break;
case 'Y': blockCoordinateY = nameandvalue[1]; break;
default: break;
}
}

//読み込んだデータに基づきそれぞれブロックを生成する - ただし id については
すでに表示しているものに加えるため，新たに生成
//window.alert(blockCoordinateX);
createNewBlock(type_of_this_block, parseInt(ori_of_this_block));

}
}

//フォームをクリアする
Dom.get("loadForm").value = '# paste your data here';

return;
}



//Settings for usual canvas movement
            //var box1 = new YAHOO.util.DDProxy("block_canvas");
```

```
//box1.setXConstraint(0, 1550, 50);
//box1.setYConstraint(0, 1200, 50);

//key handler
//回転・削除用
var upkeyup = new YAHOO.util.KeyListener ( document , {shift:true, keys: 38} ,
{fn: upkeyup_handler}, "keyup" );
upkeyup.enable();
var downkeyup = new YAHOO.util.KeyListener ( document , {shift:true, keys: 40} ,
{fn: downkeyup_handler}, "keyup" );
downkeyup.enable();
var delkeyup = new YAHOO.util.KeyListener ( document , {keys: 8} ,
{fn: delkeyup_handler}, "keyup" );
delkeyup.enable();
var delkeyup2 = new YAHOO.util.KeyListener ( document , {keys: 46} ,
{fn: delkeyup_handler}, "keyup" );
delkeyup2.enable();

//移動用
var rkeyup = new YAHOO.util.KeyListener ( document , {keys: 37} ,
{fn: rightkeydown_handler}, "keydown" );
var lkeyup = new YAHOO.util.KeyListener ( document , {keys: 39} ,
{fn: leftkeydown_handler}, "keydown" );
var ukeyup = new YAHOO.util.KeyListener ( document , {keys: 38} ,
{fn: upkeydown_handler}, "keydown" );
var dkeyup = new YAHOO.util.KeyListener ( document , {keys: 40} ,
{fn: downkeydown_handler}, "keydown" );
rkeyup.enable();
```

```
lkeyup.enable();

ukeyup.enable();

dkeyup.enable();


//toolbar 'click' addListeners

YAHOO.util.Event.addListener("load", "mousedown", loadbutton_mousedown);

YAHOO.util.Event.addListener("load", "mouseup", loadbutton_mouseup);

YAHOO.util.Event.addListener("save", "mousedown", savebutton_mousedown);

YAHOO.util.Event.addListener("save", "mouseup", savebutton_mouseup);


//load window addlisteners

YAHOO.util.Event.addListener("loadButton", "click", loaddata);

YAHOO.util.Event.addListener("cancelButton", "click", hideforms);


        });




//toolbar click functions


loadbutton_mousedown = function(e){

Dom.get("load").innerHTML = "<img src='img/button_shadow.png'>";

};

loadbutton_mouseup = function(e){

YAHOO.util.Event.preventDefault(e);

Dom.get("load").innerHTML = "";

YAHOO.util.Event.removeListener("initialDisplay", "click");
```

```
Dom.setStyle("initialDisplay", 'visibility', 'visible');
Dom.setStyle("loadForm", 'visibility', 'visible');
Dom.setStyle("loadButton", 'visibility', 'visible');
Dom.setStyle("cancelButton", 'visibility', 'visible');
};

savebutton_mousedown = function(e){
Dom.get("save").innerHTML = "<img src='img/button_shadow.png'>";
};
savebutton_mouseup = function(e){
YAHOO.util.Event.preventDefault(e);
Dom.get("save").innerHTML = "";
download_data();
window.alert('Downloaded to your computer. Rename the extention to TXT.');
};


//save&download data

function download_data(){

var contents = '';

//delete selection frames
for (var i in block_ids)
{
contents += ('id:' + i + ',' + 'X:' + Dom.getX(Dom.get('yui-gen'+ i)) + ',' +
'Y:' + Dom.getY(Dom.get('yui-gen'+ i)) + ',' + 'type:' +
```

```
 Dom.get('yui-gen'+ i).type + ',' + 'ori:' + Dom.get('yui-gen'+ i).ori + '\n');
}

//download generated contents
var text = "data:application/octet-stream," + encodeURIComponent(contents);
location.href = text;
}



//load
//実際の load の関数は .onDOMReady 内に．ここはフォームを隠す関数だけ
hideforms = function hideforms(){
Dom.setStyle("initialDisplay", 'visibility', 'hidden');
Dom.setStyle("loadForm", 'visibility', 'hidden');
Dom.setStyle("loadButton", 'visibility', 'hidden');
Dom.setStyle("cancelButton", 'visibility', 'hidden');
}
function hide_load_forms(){
Dom.setStyle("initialDisplay", 'visibility', 'hidden');
Dom.setStyle("loadForm", 'visibility', 'hidden');
Dom.setStyle("loadButton", 'visibility', 'hidden');
Dom.setStyle("cancelButton", 'visibility', 'hidden');
}



//block onClick functions
function fn_block_onclick(block){
```

```
//focus を仮につくったテキストフィールドにあてることで，キーを押したときの誤
動作をなくす
Dom.get("evac").focus();

//delete selection frames
for (var i in block_ids)
{
//Dom.get("canvas").innerHTML += i;
Dom.get('yui-gen'+ i).innerHTML = '';
}
//release selected id list
selectedBlock = [];

//add newly selected id
selectedBlock.push(block.id);

//display selection at clicked object
block_selection(block);

//Dom.get('canvas').innerHTML = selectedBlock[0];
};



//選択されたものを縁取る
function block_selection(block){
if(block.type=='DH'){
//Dom.get('canvas').innerHTML = "DH";
```

```
block.innerHTML = "<img src='img/selected.png'>";
} else if((block.type=='T-junction-l') || (block.type=='T-junction-r')){
//Dom.get('canvas').innerHTML = "T";
if((block.ori=='0') || (block.ori=='180')){
block.innerHTML = "<img src='img/selected-T.png'>";
} else {
//90,270 rotation
block.innerHTML = "<img src='img/selected-T_90.png'>";
};
};
};

//Keyup functions

//移動用
//right key

var rightkeydown_handler = function(e){
for (var i in selectedBlock)
{
var x = Dom.getX(Dom.get(selectedBlock[i]));
if(x>50){
Dom.setX(Dom.get(selectedBlock[i]), x-50);
}
//選択されたものを縁取りする
block_selection(Dom.get(selectedBlock[i]));
}
}
```

```
//left key

var leftkeydown_handler = function(e){
for (var i in selectedBlock)
{
var x = Dom.getX(Dom.get(selectedBlock[i]));
if(x<1550){
Dom.setX(Dom.get(selectedBlock[i]), x+50);
}
//選択されたものを縁取りする
block_selection(Dom.get(selectedBlock[i]));
}
}

//up key

var upkeydown_handler = function(e){
for (var i in selectedBlock)
{
var y = Dom.getY(Dom.get(selectedBlock[i]));
if(y>0){
Dom.setY(Dom.get(selectedBlock[i]), y-50);
}
//選択されたものを縁取りする
block_selection(Dom.get(selectedBlock[i]));
}
}
```

```
//down key

var downkeydown_handler = function(e){
for (var i in selectedBlock)
{
var y = Dom.getY(Dom.get(selectedBlock[i]));
if(y<1150){
Dom.setY(Dom.get(selectedBlock[i]), y+50);
}
//選択されたものを縁取りする
block_selection(Dom.get(selectedBlock[i]));
}
}

//回転・削除用

//up key
var upkeyup_handler = function(e){

//YAHOO.util.Event.preventDefault(e);

//get selectedblock array and change ori of all items
for (var i in selectedBlock)
{
//Dom.get('canvas').innerHTML = Dom.get(selectedBlock[i]).ori;

if(Dom.get(selectedBlock[i]).ori==270){
```

```
Dom.get(selectedBlock[i]).ori = 0;
} else {
Dom.get(selectedBlock[i]).ori += 90;
}

//場所の調整．新しい ori に準じる
if( (Dom.get(selectedBlock[i]).type=='T-junction-l') &&
(Dom.get(selectedBlock[i]).ori == 90)){
var x = Dom.getX(Dom.get(selectedBlock[i]));
Dom.setX(Dom.get(selectedBlock[i]), x-50);
};
if( (Dom.get(selectedBlock[i]).type=='T-junction-l') &&
(Dom.get(selectedBlock[i]).ori == 180)){
var x = Dom.getX(Dom.get(selectedBlock[i]));
var y = Dom.getY(Dom.get(selectedBlock[i]));
Dom.setX(Dom.get(selectedBlock[i]), x+50);
Dom.setY(Dom.get(selectedBlock[i]), y-50);
};
if( (Dom.get(selectedBlock[i]).type=='T-junction-l') &&
(Dom.get(selectedBlock[i]).ori == 270)){
var y = Dom.getY(Dom.get(selectedBlock[i]));
Dom.setY(Dom.get(selectedBlock[i]), y+50);
};
if( (Dom.get(selectedBlock[i]).type=='T-junction-r') &&
(Dom.get(selectedBlock[i]).ori == 90)){
var x = Dom.getX(Dom.get(selectedBlock[i]));
Dom.setX(Dom.get(selectedBlock[i]), x-50);
};
```

```
if( (Dom.get(selectedBlock[i]).type=='T-junction-r') &&
(Dom.get(selectedBlock[i]).ori == 180)){
var x = Dom.getX(Dom.get(selectedBlock[i]));
var y = Dom.getY(Dom.get(selectedBlock[i]));
Dom.setX(Dom.get(selectedBlock[i]), x+50);
Dom.setY(Dom.get(selectedBlock[i]), y-50);
};
if( (Dom.get(selectedBlock[i]).type=='T-junction-r') &&
(Dom.get(selectedBlock[i]).ori == 270)){
var y = Dom.getY(Dom.get(selectedBlock[i]));
Dom.setY(Dom.get(selectedBlock[i]), y+50);
};

setBlockRot(Dom.get(selectedBlock[i]));
//選択されたものを縁取りする
block_selection(Dom.get(selectedBlock[i]));
}



};
var downkeyup_handler = function(e){

//YAHOO.util.Event.preventDefault(e);

//get selectedblock array and change ori of all items
for (var i in selectedBlock)
{
//Dom.get('canvas').innerHTML = Dom.get(selectedBlock[i]).ori;
```

```
if(Dom.get(selectedBlock[i]).ori==0){
Dom.get(selectedBlock[i]).ori = 270;
} else {
Dom.get(selectedBlock[i]).ori -= 90;
}

//場所の調整．新しい ori に準じる
if( (Dom.get(selectedBlock[i]).type=='T-junction-l') &&
(Dom.get(selectedBlock[i]).ori == 0)){
var x = Dom.getX(Dom.get(selectedBlock[i]));
Dom.setX(Dom.get(selectedBlock[i]), x+50);
};
if( (Dom.get(selectedBlock[i]).type=='T-junction-l') &&
(Dom.get(selectedBlock[i]).ori == 90)){
var x = Dom.getX(Dom.get(selectedBlock[i]));
var y = Dom.getY(Dom.get(selectedBlock[i]));
Dom.setX(Dom.get(selectedBlock[i]), x-50);
Dom.setY(Dom.get(selectedBlock[i]), y+50);
};
if( (Dom.get(selectedBlock[i]).type=='T-junction-l') &&
(Dom.get(selectedBlock[i]).ori == 180)){
var y = Dom.getY(Dom.get(selectedBlock[i]));
Dom.setY(Dom.get(selectedBlock[i]), y-50);
};
if( (Dom.get(selectedBlock[i]).type=='T-junction-r') &&
(Dom.get(selectedBlock[i]).ori == 0)){
var x = Dom.getX(Dom.get(selectedBlock[i]));
```

```
Dom.setX(Dom.get(selectedBlock[i]), x+50);
};
if( (Dom.get(selectedBlock[i]).type=='T-junction-r') &&
(Dom.get(selectedBlock[i]).ori == 90)){
var x = Dom.getX(Dom.get(selectedBlock[i]));
var y = Dom.getY(Dom.get(selectedBlock[i]));
Dom.setX(Dom.get(selectedBlock[i]), x-50);
Dom.setY(Dom.get(selectedBlock[i]), y+50);
};
if( (Dom.get(selectedBlock[i]).type=='T-junction-r') &&
(Dom.get(selectedBlock[i]).ori == 180)){
var y = Dom.getY(Dom.get(selectedBlock[i]));
Dom.setY(Dom.get(selectedBlock[i]), y-50);
};

setBlockRot(Dom.get(selectedBlock[i]));
//選択されたものを縁取りする
block_selection(Dom.get(selectedBlock[i]));
}









};
var delkeyup_handler = function(e){

//YAHOO.util.Event.preventDefault(e);
```

```
//get selectedblock array and delete items
for (var i in selectedBlock)
{
Dom.setStyle(Dom.get(selectedBlock[i]), 'width', '0px');
Dom.setStyle(Dom.get(selectedBlock[i]), 'height', '0px');
var del_id = block_ids.indexOf(selectedBlock[i]);
//block_ids.splice(del_id,1);
delete block_ids[del_id];
}




};

//initial description (Click to start)
function fnDeleteDisplay(e) {
Dom.setStyle("initialDisplay", 'visibility', 'hidden');
Dom.setStyle("initialDescription", 'height', '0px');
Dom.setStyle("initialDescription", 'visibility', 'hidden');};
YAHOO.util.Event.addListener("initialDisplay", "click", fnDeleteDisplay);
YAHOO.util.Event.addListener("initialDescription", "click", fnDeleteDisplay);

    })();
</script>

</head>
```

```
<body>



<!--Frame/Canvas/Box -->


<div id="initialDisplay">
  <textarea name="loadForm" cols="70" rows="10" id="loadForm">
  # paste your data here</textarea>
  <input name="loadButton" id="loadButton" type="button" value="Load Data" />
  <input name="cancelButton" id="cancelButton" type="button" value="Cancel" />
</div>
<div id="initialDescription">
  <h2><strong>T-motif Designer (demo)</strong></h2>
  <p>Drag and drop blocks from the left toolbar to the grid.</p>
  <p><strong>Selection:</strong> Left Click</p>
  <p><strong>Move:</strong> Arrow key (Up/Down/Right/Left)</p>
  <p><strong>Rotation:</strong> <em>Shift</em>+Up/Down</p>
  <p><strong>Delete:</strong> Backspace/Delete</p>
  <p>If you are using Firefox, Safari or Opera,
  you can also use download/load functions (buttons at the left toolbar).</p>
  <p><em>Have Fun!</em></p>
  <p><strong>(Click to start)</strong></p>
</div>



<div id="toolBar"><div id="block_toolBar"></div>
<div id="block_T-junction-r_toolBar"></div>
<div id="block_T-junction-l_toolBar"></div>
```

```
<div id="load"></div><div id="save"></div></div>

<div id="canvas"></div><input name="" type="text" id = "evac"/>

<!--<div id="block_canvas"></div>-->
```

F.2 Simulations of self-assembly in free solution and on substrate (MATLAB)

Simulations of self-assembly in free solution and substrate-assisted self-assembly are using same codes, except excluding/including calculations of the phenomena on the surface and between surface/solution.

Nanoring kinetic simulation program

```
%%%%%%%%%%%%%%%%%%%%%%%%%%%%%%%%%%%%%%%%%%%%%%%%%%%%%%%%
%
%  Ring Kinetic simulation
%
%%%%%%%%%%%%%%%%%%%%%%%%%%%%%%%%%%%%%%%%%%%%%%%%%%%%%%%%

% x = conc. of m1-m12
% savet = temperature at each calculation
% formationrate = rate of formation (Tm is at 0.5)

%
% Parameters
%

%profile A
%stoptime = 12*60*60;%[sec]

%profile B
%stoptime = 2*60*60;%[sec]
%profile D
```

```
%stoptime = 2*60*60;%[sec]


%profile_Tf_capilary

%stoptime = 30*60;%70*60;[sec]

%stoptime = 30*60;

stoptime = 10*20*2*60;


%profile E2(71.9-20)

%stoptime = 7*60*60;%[sec]

%profile E2(51.9-20)

%stoptime = 4*60*60;%[sec]


% tick calc. per second


%profile A

%tick = 10;


%profile B,-B,D,E

tick = 100000;

%for best data, use 10^2 order

%tick = 200;

%tick = 100;


%initial conc.

Initconc = 0.1*10.^(-6);%0.66uM

%Initconc = 0.066*10.^(-6);%0.066uM


%anneal NOTE: x will be 3 dimension
```

```
%ring conc.
x = [Initconc 0;
    0 0;
    0 0;
    0 0;
    0 0;
    0 0;
    0 0;
    0 0;
    0 0;
    0 0;
    0 0;
    0 0;
    0 0;]
```

```
%Area of Mica Fragment
InitSurface = 2*5*10^(-3)*7*10^(-3);% 5mm x 7mm
```

```
%Exclusive area of DNA motif (per unit)
ExArea = 13.6^2*3.14/12 * 10^(-9)*10^(-9);
```

```
%Volume of Reaction Chamber
Volume = 200*10^(-6);%200[ul]
```

```
Rcal = 1.987;
```

```
%original formation rate
```

```
kf = 6*10.^5 ;


%formation rate on substrate

kfsub = 2.4*10.^11;


%DLVO binding energy parameter

DLVOEn = -0.0239;%[eV]


%length of each DNA monomer

Length = 52;%bp



%

% Calculation of average deltaH and deltaS of DNA Hybridizaiton

%


deltaH1 = (-8.6-7.4-6.7-7.7)*1000 ;

deltaS1 = -23.0-19.3-15.6-20.3-5.9 ;


deltaH2 = (-8.4-6.1-11.1-10.1)*1000 ;

deltaS2 = -1.02-16.1-28.4-25.5-5.9 ;


averageH = (deltaH1+deltaH2)./2 ;

averageS = (deltaS1+deltaS2)./2 ;



%

% Mica binding Energy [cal/bp/mol]
```

```
%

Na = 6.02*10^23;
eV = 1.602*10^(-19);
JtoCal = 0.239005736;

deltaGperbp = DLVOEn*Na*eV*JtoCal;



%initial and saved variables

savetemp = [tempAtSec(0)];
savetime = [0];
formationrate = [0];
leftsurface = [InitSurface];

newsavetemp = savetemp;
newsavetime = savetime;
newsaveformationrate = formationrate;
newsaveleftsurface = leftsurface;
newsavex = x;



%loop

for t=1:1:stoptime*tick
```

```
temp = tempAtSec(t./tick) ;




q1 = 6*10.^4;

q2 = 6*10.^4;

q3 = 6*10.^4;


%calculate deltaG at this temperature

deltaG = averageH-temp*averageS;



%

% set m as a current concentration of DNA nanorings

%


m = x;


%

% set spnow as a current concentration of DNA spirals

%


%return current size of x



%

% calculate reverse rate of kinetics

%
```

```
%solution
kr = kf.*(q1)*(exp(2*deltaG./(Rcal*temp)));
krcl = kf.*(exp(2*deltaG./(Rcal*temp)));%open/close
%substrate
krm = kfsub.*(q2)*(exp(2*deltaG./(Rcal*temp)));
krmcl = kfsub.*(exp(2*deltaG./(Rcal*temp)));%open/close



%
% set concleftover for current 'virtual concentration' for leftover
% mica->Initial area
%


%return current leftover area of mica
currentleftsurface = InitSurface;%leftsurface(:,t);

%convert area size to virtual concentration for each m_n
concleftover = [currentleftsurface/ExArea/Na/Volume;
                currentleftsurface/(ExArea*2)/Na/Volume;
                currentleftsurface/(ExArea*3)/Na/Volume;
                currentleftsurface/(ExArea*4)/Na/Volume;
                currentleftsurface/(ExArea*5)/Na/Volume;
                currentleftsurface/(ExArea*6)/Na/Volume;
                currentleftsurface/(ExArea*7)/Na/Volume;
                currentleftsurface/(ExArea*8)/Na/Volume;
                currentleftsurface/(ExArea*9)/Na/Volume;
```

```
                currentleftsurface/(ExArea*10)/Na/Volume;
                currentleftsurface/(ExArea*11)/Na/Volume;
                currentleftsurface/(ExArea*12)/Na/Volume;];


%
% calculate krmica(reverse rate) for mica adsorption
%

krmica = [kf.*(exp(deltaGperbp*Length*1./(Rcal*temp)));
          kf.*(exp(deltaGperbp*Length*2./(Rcal*temp)));
          kf.*(exp(deltaGperbp*Length*3./(Rcal*temp)));
          kf.*(exp(deltaGperbp*Length*4./(Rcal*temp)));
          kf.*(exp(deltaGperbp*Length*5./(Rcal*temp)));
          kf.*(exp(deltaGperbp*Length*6./(Rcal*temp)));
          kf.*(exp(deltaGperbp*Length*7./(Rcal*temp)));
          kf.*(exp(deltaGperbp*Length*8./(Rcal*temp)));
          kf.*(exp(deltaGperbp*Length*9./(Rcal*temp)));
          kf.*(exp(deltaGperbp*Length*10./(Rcal*temp)));
          kf.*(exp(deltaGperbp*Length*11./(Rcal*temp)));
          kf.*(exp(deltaGperbp*Length*12./(Rcal*temp)));
          ];


%
% calculate speed [M/sec]
%

%tempv = [inside sol,inside mica, bet. mica and sol.] of DNA
```

```
%m_1+m_n-1 = m_n


tempv = [-kf.*m(1,1)^2+kr.*m(2,1) -kfsub.*m(1,2)^2+krm.*m(2,2);
          -kf.*m(1,1).*m(2,1)+kr.*m(3,1) -kfsub.*m(1,2).*m(2,2)+krm.*m(3,2);
          -kf.*m(1,1).*m(3,1)+kr.*m(4,1) -kfsub.*m(1,2).*m(3,2)+krm.*m(4,2);
          -kf.*m(1,1).*m(4,1)+kr.*m(5,1) -kfsub.*m(1,2).*m(4,2)+krm.*m(5,2);
          -kf.*m(1,1).*m(5,1)+kr.*m(6,1) -kfsub.*m(1,2).*m(5,2)+krm.*m(6,2);
          -kf.*m(1,1).*m(6,1)+kr.*m(7,1) -kfsub.*m(1,2).*m(6,2)+krm.*m(7,2);
          -kf.*m(1,1).*m(7,1)+kr.*m(8,1) -kfsub.*m(1,2).*m(7,2)+krm.*m(8,2);
          -kf.*m(1,1).*m(8,1)+kr.*m(9,1) -kfsub.*m(1,2).*m(8,2)+krm.*m(9,2);
          -kf.*m(1,1).*m(9,1)+kr.*m(10,1) -kfsub.*m(1,2).*m(9,2)+krm.*m(10,2);
          -kf.*m(1,1).*m(10,1)+kr.*m(11,1) -kfsub.*m(1,2).*m(10,2)+krm.*m(11,2);
          -kf.*m(1,1).*m(11,1)+kr.*m(12,1) -kfsub.*m(1,2).*m(11,2)+krm.*m(12,2);
          -kf.*m(12,1)+krcl.*m(13,1) -kfsub.*m(12,2)+krmcl.*m(13,2);
     0 0;
         ];


tempvbindkf = [-kf.*m(1,1)*concleftover(1,1);
               -kf.*m(2,1)*concleftover(2,1);
               -kf.*m(3,1)*concleftover(3,1);
               -kf.*m(4,1)*concleftover(4,1);
               -kf.*m(5,1)*concleftover(5,1);
               -kf.*m(6,1)*concleftover(6,1);
               -kf.*m(7,1)*concleftover(7,1);
               -kf.*m(8,1)*concleftover(8,1);
               -kf.*m(9,1)*concleftover(9,1);
               -kf.*m(10,1)*concleftover(10,1);
               -kf.*m(11,1)*concleftover(11,1);
```

```
                -kf.*m(12,1)*concleftover(12,1);
                -kf.*m(13,1)*concleftover(12,1);
                %concleftover is same in m12 and 13
                ];

tempvbindkr = [krmica(1,1)*m(1,2);
                krmica(2,1)*m(2,2);
                krmica(3,1)*m(3,2);
                krmica(4,1)*m(4,2);
                krmica(5,1)*m(5,2);
                krmica(6,1)*m(6,2);
                krmica(7,1)*m(7,2);
                krmica(8,1)*m(8,2);
                krmica(9,1)*m(9,2);
                krmica(10,1)*m(10,2);
                krmica(11,1)*m(11,2);
                krmica(12,1)*m(12,2);
                krmica(12,1)*m(13,2);
                %krmica is same in m12 and 13
                ];

%tempvclose m_p + m_(12-p) = m_12
tempvcl = [-kf.*m(2,1).*m(10,1)+kr.*m(12,1)
 -kfsub.*m(2,2).*m(10,2)+krm.*m(12,2);
           -kf.*m(3,1).*m(9,1)+kr.*m(12,1)
            -kfsub.*m(3,2).*m(9,2)+krm.*m(12,2);
           -kf.*m(4,1).*m(8,1)+kr.*m(12,1)
            -kfsub.*m(4,2).*m(8,2)+krm.*m(12,2);
```

```
                -kf.*m(5,1).*m(7,1)+kr.*m(12,1)
                 -kfsub.*m(5,2).*m(7,2)+krm.*m(12,2);
                -kf.*m(6,1)^2+kr.*m(12,1)
                 -kfsub.*m(6,2)^2+krm.*m(12,2);
                ];




    %
    %conversion from M/sec to M/(1/tick)
    %

    tempv = tempv./tick;
    tempvcl = tempvcl./tick;
    tempvbindkf = tempvbindkf./tick;
    tempvbindkr = tempvbindkr./tick;

    %
    %final determination of update values
    %

    %v for rings

    v = [2*tempv(1,1)+tempv(2,1)+tempv(3,1)+tempv(4,1)+tempv(5,1)+tempv(6,1)
+tempv(7,1)+tempv(8,1)+tempv(9,1)+tempv(10,1)+tempv(11,1) 2*tempv(1,2)
+tempv(2,2)+tempv(3,2)+tempv(4,2)+tempv(5,2)+tempv(6,2)+tempv(7,2)
+tempv(8,2)+tempv(9,2)+tempv(10,2)+tempv(11,2);
```

```
    -tempv(1,1)+tempv(2,1) -tempv(1,2)+tempv(2,2);
    -tempv(2,1)+tempv(3,1) -tempv(2,2)+tempv(3,2);
    -tempv(3,1)+tempv(4,1) -tempv(3,2)+tempv(4,2);
    -tempv(4,1)+tempv(5,1) -tempv(4,2)+tempv(5,2);
    -tempv(5,1)+tempv(6,1) -tempv(5,2)+tempv(6,2);
    -tempv(6,1)+tempv(7,1) -tempv(6,2)+tempv(7,2);
    -tempv(7,1)+tempv(8,1) -tempv(7,2)+tempv(8,2);
    -tempv(8,1)+tempv(9,1) -tempv(8,2)+tempv(9,2);
    -tempv(9,1)+tempv(10,1) -tempv(9,2)+tempv(10,2);
    -tempv(10,1)+tempv(11,1) -tempv(10,2)+tempv(11,2);
    -tempv(11,1)+tempv(12,1) -tempv(11,2)+tempv(12,2);
    -tempv(12,1) -tempv(12,2);
    ];


vbindkf = [tempvbindkf(1,1) -tempvbindkf(1,1);
           tempvbindkf(2,1) -tempvbindkf(2,1);
           tempvbindkf(3,1) -tempvbindkf(3,1);
           tempvbindkf(4,1) -tempvbindkf(4,1);
           tempvbindkf(5,1) -tempvbindkf(5,1);
           tempvbindkf(6,1) -tempvbindkf(6,1);
           tempvbindkf(7,1) -tempvbindkf(7,1);
           tempvbindkf(8,1) -tempvbindkf(8,1);
           tempvbindkf(9,1) -tempvbindkf(9,1);
           tempvbindkf(10,1) -tempvbindkf(10,1);
           tempvbindkf(11,1) -tempvbindkf(11,1);
           tempvbindkf(12,1) -tempvbindkf(12,1);
           tempvbindkf(13,1) -tempvbindkf(13,1);
```

```
            ];
vbindkr = [tempvbindkr(1,1) -tempvbindkr(1,1);
            tempvbindkr(2,1) -tempvbindkr(2,1);
            tempvbindkr(3,1) -tempvbindkr(3,1);
            tempvbindkr(4,1) -tempvbindkr(4,1);
            tempvbindkr(5,1) -tempvbindkr(5,1);
            tempvbindkr(6,1) -tempvbindkr(6,1);
            tempvbindkr(7,1) -tempvbindkr(7,1);
            tempvbindkr(8,1) -tempvbindkr(8,1);
            tempvbindkr(9,1) -tempvbindkr(9,1);
            tempvbindkr(10,1) -tempvbindkr(10,1);
            tempvbindkr(11,1) -tempvbindkr(11,1);
            tempvbindkr(12,1) -tempvbindkr(12,1);
            tempvbindkr(13,1) -tempvbindkr(13,1);
            ];

vtempvcl = [0 0;
             tempvcl(1,1) tempvcl(1,2);
             tempvcl(2,1) tempvcl(2,2);
             tempvcl(3,1) tempvcl(3,2);
             tempvcl(4,1) tempvcl(4,2);
             tempvcl(5,1) tempvcl(5,2);
             tempvcl(4,1) tempvcl(4,2);
             tempvcl(3,1) tempvcl(3,2);
             tempvcl(2,1) tempvcl(2,2);
             tempvcl(1,1) tempvcl(1,2);
             0 0;
             -tempvcl(1,1)-tempvcl(2,1)-tempvcl(3,1)-tempvcl(4,1)-tempvcl(5,1)
```

```
                -tempvcl(1,2)-tempvcl(2,2)-tempvcl(3,2)-tempvcl(4,2)-tempvcl(5,2);
               0 0;
               ];

v = v + vtempvcl;




%update the conc.
newx = m + v;

%update the leftover area
tempconc = newx(1,2) + 2*newx(2,2) + 3*newx(3,2) + 4*newx(4,2)
+ 5*newx(5,2) + 6*newx(6,2) + 7*newx(7,2) + 8*newx(8,2) + 9*newx(9,2)
+ 10*newx(10,2) + 11*newx(11,2) + 12*newx(12,2) + 12*newx(13,2);

sumvbindkf = vbindkf(1,2) + 2*vbindkf(2,2) + 3*vbindkf(3,2) + 4*vbindkf(4,2)
+ 5*vbindkf(5,2) + 6*vbindkf(6,2) + 7*vbindkf(7,2) + 8*vbindkf(8,2)
+ 9*vbindkf(9,2) + 10*vbindkf(10,2) + 11*vbindkf(11,2)
+ 12*vbindkf(12,2) + 12*vbindkf(13,2);

sumvbindkr = vbindkr(1,2) + 2*vbindkr(2,2) + 3*vbindkr(3,2) + 4*vbindkr(4,2)
+ 5*vbindkr(5,2) + 6*vbindkr(6,2) + 7*vbindkr(7,2) + 8*vbindkr(8,2)
+ 9*vbindkr(9,2) + 10*vbindkr(10,2) + 11*vbindkr(11,2)
+ 12*vbindkr(12,2) + 12*vbindkr(13,2);
```

```
 v = v + (vbindkr);

%calc excess amount of mn on mica (with keeping balance between spiecies),
% then return to solution
for i=1:1:13
    temporaryconc = vbindkf(i,2);

    vbindkf(i,2) = temporaryconc * (InitSurface./(Na*ExArea*Volume)-tempconc)
    ./(sumvbindkf+sumvbindkr);

    vbindkf(i,1) = vbindkf(i,1) + (temporaryconc-vbindkf(i,2));


    temporaryconc2 = vbindkr(i,2);

    vbindkr(i,2) = temporaryconc2 * (InitSurface./(Na*ExArea*Volume)-tempconc)
    ./(sumvbindkf+sumvbindkr);

    vbindkr(i,1) = vbindkr(i,1) + (temporaryconc2-vbindkr(i,2));

end

newx = newx + vbindkf + vbindkr;


%minus error correction
for i=1:1:13
    for j=1:1:2
```

```
            if newx(i,j)<0
                if i==12
                    newx(13,j) = newx(13,j)+newx(12,j);
                end
                newx(i,j)=0;

            end
        end
    end

    %update the leftover area
    tempconc = newx(1,2) + 2*newx(2,2) + 3*newx(3,2) + 4*newx(4,2)
    + 5*newx(5,2) + 6*newx(6,2) + 7*newx(7,2) + 8*newx(8,2) + 9*newx(9,2)
    + 10*newx(10,2) + 11*newx(11,2) + 12*newx(12,2) + 12*newx(13,2);



    %calc excess amount of mn on mica (with keeping balance between spiecies),
    % then return to solution
    for i=1:1:13
        temporaryconc = newx(i,2);
        newx(i,2) = temporaryconc*(InitSurface/(tempconc*Volume*Na*ExArea));
        newx(i,1) = newx(i,1) + (temporaryconc-newx(i,2));
    end
```

```
%error correction
tempallconc = 0;
for j=2:-1:1
for i=1:1:13
    % correction by each types of molecules
    if newx(i,j)<0
        newx(i,j) = 0;
    end
    if newx(i,j)>Initconc
        newx(i,j) = Initconc;
    end
    %correction by whole number of molecules
    if i == 13
     tempallconc = tempallconc + newx(i,j)*12;
    else
        tempallconc = tempallconc + newx(i,j)*i;
    end

    if tempallconc > Initconc

        if i == 13
            newx(i,j) = newx(i,j)-(tempallconc-Initconc)./12;
        else
            newx(i,j) = newx(i,j)-(tempallconc-Initconc)./i;
        end
        tempallconc = Initconc;
    end
end
```

```
end



%new error correction
for i=1:1:13
    for j=1:1:2
        if newx(i,j)<0
            newx(i,j) = 0;
        end
    end
end



%update the leftover area
tempconc = newx(1,2) + 2*newx(2,2) + 3*newx(3,2) + 4*newx(4,2)
+ 5*newx(5,2) + 6*newx(6,2) + 7*newx(7,2) + 8*newx(8,2) + 9*newx(9,2)
+ 10*newx(10,2) + 11*newx(11,2) + 12*newx(12,2) + 12*newx(13,2);

newleftsurface = InitSurface - tempconc*Volume*Na*ExArea;

newleftsurfacerawdata = newleftsurface;

%error correction for mica surface
if newleftsurface<0
    newleftsurface=0;
end
if newleftsurface>InitSurface
    newleftsurface=InitSurface;
```

```
end

%modified places

%add new conc to x
x = newx;

%add new leftsurface to leftsurface
leftsurface = newleftsurface;

%sticky end formation rate (count only in solution)
seconc = (newx(2,1))*2 + (newx(3,1))*4 + (newx(4,1))*6 + (newx(5,1))*8
+ (newx(6,1))*10 + (newx(7,1))*12 + (newx(8,1))*14 + (newx(9,1))*16
+ (newx(10,1))*18 + (newx(11,1))*20 + (newx(12,1))*22 + (newx(13,1))*24;
allseconc = Initconc.*2;
formationrate = seconc./allseconc;

if mod(t,tick*60*0.1) == 0 %save per 0.1min

    % save temp
    newsavetemp = horzcat(newsavetemp,temp);

    %save time
    newsavetime = horzcat(newsavetime,t./tick);

    %add new conc to x
    newsavex = cat(3,newsavex,newx);
    %add new leftsurface to leftsurface
```

```
newsaveleftsurface = horzcat(newsaveleftsurface,newleftsurface);


newsaveformationrate = horzcat(newsaveformationrate,formationrate);


save('data.mat');
fprintf('%s %d \n','Now at...[min]: ',t/(tick*60));
fprintf('%s %d \n','%: ',t/(stoptime*tick)*100);
fprintf('%s %d \n','temp[K]: ',temp);


sumall = sum(newx(1,:) + 2*newx(2,:) + 3*newx(3,:) + 4*newx(4,:)
+ 5*newx(5,:) + 6*newx(6,:) + 7*newx(7,:) + 8*newx(8,:) + 9*newx(9,:)
+ 10*newx(10,:) + 11*newx(11,:) + 12*(newx(12,:)+newx(13,:)));


fprintf('%s %d \n','sum of all monomers: ',sumall);
fprintf('%s %d \n','m1(sol): ',newx(1,1));
fprintf('%s %d \n','m1(mica): ',newx(1,2));
fprintf('%s %d \n','m12open(sol): ',newx(12,1));
fprintf('%s %d \n','m12open(mica): ',newx(12,2));
fprintf('%s %d \n','m12close(sol): ',newx(13,1));
fprintf('%s %d \n','m12close(mica): ',newx(13,2));
fprintf('%s %d \n','leftsurface(%): ',newleftsurface/InitSurface*100);
fprintf('%s %d \n','leftsurface(Raw data): ',newleftsurfacerawdata);
disp(newx);
disp('--------------------');
fprintf('%s %d \n','vbindkf(m1): ',vbindkf(1,1));
fprintf('%s %d \n','vbindkr(m1): ',vbindkr(1,1));
disp('--------------------');
```

```
    end


end

disp('End of Calculation!!');
```

tempAtSec.m

```
%
% tempAtSec(Sec)
%
% Returns temperature[K] at input time[sec.]
% profileA (start c-> end c at about 24 hours based on exponetial annealing)
% profileB (start c-> inf at 0.5deg./min)


function temp = tempAtSec(Sec)

% Zuker 0.66uM, Na 14.6mM, Mg 12.5mM
% ?G = -43.1 ?H = -330.1 ?S = -925.5 Tm = 71.9?C

%starttemp = 40;
%starttemp = 71.9;
starttemp = 40;
endtemp = 20;

%profile A
%temp = (starttemp-endtemp)*exp(-Sec./(4*60*60)) + (273.15+endtemp);


%profile B
%temp = (starttemp+273.15) - (0.5./60)*Sec;

temp = (starttemp+273.15) - (0.05./60)*Sec;
```

```
%profile -B
%temp = (endtemp+273.15) + (0.5./60)*Sec;

%profile C
%temp = (44+273.15) - (0.2./60)*Sec;

%profile D
%temp = (starttemp+273.15) - (0.25./60)*Sec;

%profile E
%temp = (starttemp+273.15) - (0.5./60)*Sec;
%if temp < (endtemp+273.15)
%    temp = endtemp+273.15;
%end

%profile E2
%temp = (starttemp+273.15) - (0.125./60)*Sec;
%if temp < (endtemp+273.15)
%    temp = endtemp+273.15;
%end
```

Bibliography

[Adam 1968] G Adam and M Delbrück. *Reduction of dimensionality in biological diffusion processes.* Structural Chemistry and Molecular Biology, pages 198–215, 1968. (Cited on pages 46 and 70.)

[Axelrod 1994] D Axelrod and Michelle Dong Wang. *Reduction-of-dimensionality kinetics at reaction-limited cell surface receptors.* Biophysical Journal, vol. 66, no. 3, pages 588–600, 1994. (Cited on pages 46, 67 and 69.)

[Barish 2005] Robert D Barish, Paul W K Rothemund and Erik Winfree. *Two computational primitives for algorithmic self-assembly: copying and counting.* Nano Lett., vol. 5, no. 12, pages 2586–92, Dec 2005. (Cited on page 27.)

[Behrens 2001] Sven H Behrens and David G Grier. *The charge of glass and silica surfaces.* J. Chem. Phys., vol. 115, no. 14, page 6716, 2001. (Cited on page 63.)

[Berg 1977] H Berg and E Purcell. *Physics of chemoreception.* Biophysical Journal, vol. 20, no. 2, pages 193–219, Nov 1977. (Cited on page 70.)

[Bloomfield 1974] Victor A Bloomfield, Donald M Crothers and J Ignacio Tinoco. *Physical chemistry of nucleic acids.* Harper & Row, 1974. (Cited on page 66.)

[Brunauer 1938] S Brunauer, P H Emmett and E Teller. *Adsorption of gases in multimolecular layers.* Journal of American Chemical Society, vol. 60, pages 309–319, 1938. (Cited on page 63.)

[Carlsson 2004] Fredrik Carlsson, Elin Hyltner, Thomas Arnebrant, Martin Malmsten and Per Linse. *Lysozyme Adsorption to Charged Surfaces. A Monte Carlo Study.* J. Phys. Chem. B, vol. 108, no. 28, pages 9871–9881, 2004. (Cited on page 55.)

[Chan 1995] V Chan, DJ Graves and SE McKenzie. *The biophysics of DNA hybridization with immobilized oligonucleotide probes.* Biophys. J., vol. 69, no. 6, pages 2243–2255, 1995. (Cited on pages 46, 63, 66, 67 and 69.)

[Clegg 1994] R M Clegg, A I Murchie and D M Lilley. *The solution structure of the four-way DNA junction at low-salt conditions: a fluorescence resonance energy transfer analysis.* Biophysical Journal, vol. 66, no. 1, pages 99–109, Jan 1994. (Cited on page 8.)

[Deer 1966] W.A Deer, R A Howie and J Zussman. *An Introduction to the Rock Forming Minerals.* Longman, 1966. (Cited on page 55.)

[Derjaguin 1941] B Derjaguin and L Landau. *Theory of the stability of strongly charged lyophobic sols and of the adhesion of strongly charged particles in solutions of electrolytes.* Acta Physico Chemica URSS, vol. 14, page 633, 1941. (Cited on page 50.)

[Dietz 2009] Hendrik Dietz, Shawn Douglas and William Shih. *Folding DNA into Twisted and Curved Nanoscale Shapes.* Science, vol. 325, no. 5941, page 725, Aug 2009. (Cited on page 6.)

[Dill 2003] Ken A Dill and Sarina Bromberg. *Molecular Driving Forces.* Garland Science, 2003. (Cited on page 51.)

[Dong 1998] Ying Dong, , Sastry V. Pappu and Zhi Xu. *Detection of Local Density Distribution of Isolated Silanol Groups on Planar Silica Surfaces Using Nonlinear Optical Molecular Probes.* Anal. Chem., vol. 70, no. 22, pages 4730–4735, 1998. (Cited on page 56.)

[Douglas 2009] Shawn M Douglas, Hendrik Dietz, Tim Liedl, Björn Högberg, Franziska Graf and William M Shih. *Self-assembly of DNA into nanoscale three-dimensional shapes.* Nature, vol. 459, no. 7245, page 414, May 2009. (Cited on page 6.)

[Duckett 1988] D R Duckett, A I Murchie, S Diekmann, E von Kitzing, B Kemper and D M Lilley. *The structure of the Holliday junction, and its resolution.* Cell, vol. 55, no. 1, pages 79–89, Oct 1988. (Cited on page 8.)

[Erickson 2003] David Erickson, Dongqing Li and Ulrich J Krull. *Modeling of DNA hybridization kinetics for spatially resolved biochips.* Anal Biochem, vol. 317, no. 2, pages 186–200, Jun 2003. (Cited on pages 46, 67 and 70.)

[Fu 1993] T J Fu and N C Seeman. *DNA double-crossover molecules.* Biochemistry, vol. 32, no. 13, pages 3211–20, Apr 1993. (Cited on page 8.)

[Fujibayashi 2009] Kenichi Fujibayashi, David Yu Zhang, Erik Winfree and Satoshi Murata. *Error suppression mechanisms for DNA tile self-assembly and their simulation.* Nat Comput, vol. 8, no. 3, pages 589–612, Sep 2009. (Cited on page 36.)

[Hamada] Shogo Hamada and Satoshi Murata. *Algorithmic Self-assembly of Single-duplex DNA Nanostructures.* International Journal of Unconventional Computing, in press. (Cited on page 39.)

[Hamada 2009] Shogo Hamada and Satoshi Murata. *Substrate-Assisted Assembly of Interconnected Single-Duplex DNA Nanostructures.* Angewandte Chemie International Edition, vol. 48, no. 37, pages 6820–6823, Sep 2009. (Cited on page 19.)

[He 2005] Yu He, Yi Chen, Haipeng Liu, Alexander E Ribbe and Chengde Mao. *Self-assembly of hexagonal DNA two-dimensional (2D) arrays.* J. Am. Chem. Soc., vol. 127, no. 35, pages 12202–3, Sep 2005. (Cited on page 11.)

[He 2006] Yu He and Chengde Mao. *Balancing flexibility and stress in DNA nanostructures.* Chem Commun (Camb), no. 9, pages 968–9, Mar 2006. (Cited on page 23.)

[Hexemer 2005] Alexander Hexemer, Gila E Stein, Edward J Kramer and Sergei Magonov. *Block Copolymer Monolayer Structure Measured with Scanning Force Microscopy Moire Patterns.* Macromolecules, vol. 38, no. 16, pages 7083–7089, 2005. (Cited on page 92.)

[Israelachvili 1992] J.N Israelachvili. *Intermolecular and Surface Forces.* Academic Press, vol. Second Edition, 1992. (Cited on page 50.)

[Kallenbach 1983] Neville R Kallenbach, Rong-Ine Ma and Nadrian C Seeman. *An immobile nucleic acid junction constructed from oligonucleotides.* Nature, vol. 305, no. 5937, pages 829–831, Oct 1983. (Cited on page 7.)

[Keizer 1985] Joel Keizer. *Theory of rapid bimolecular reactions in solution and membranes.* Acc. Chem. Res., vol. 235-241, 1985. (Cited on page 70.)

[Koyfman 2009] Alexey Y. Koyfman, Sergei N. Magonov and Norbert O. Reich. *Self-Assembly of DNA Arrays into Multilayer Stacks.* Langmuir, vol. 25, no. 2, pages 1091–1096, 2009. (Cited on page 92.)

[LaBean 2000] T.H LaBean, Hao Yan, Jens Kopatsch, Furong Liu, Erik Winfree, John H. Reif and Nadrian C. Seeman. *Construction, Analysis, Ligation, and Self-Assembly of DNA Triple Crossover Complexes.* J. Am. Chem. Soc., vol. 122, no. 9, pages 1848–60, 2000. (Cited on page 11.)

[Liu 1994] Bing Liu, Neocles B Leonitis and Nadrian C Seeman. *Bulged three-arm DNA branched junctions as components for nanoconstruction.* Nanobiology, vol. 3, no. 3-4, pages 177–188, Jan 1994. (Cited on page 22.)

[Liu 2005] Haipeng Liu, Yu He, Alexander E Ribbe and Chengde Mao. *Two-dimensional (2D) DNA crystals assembled from two DNA strands.* Biomacromolecules, vol. 6, no. 6, pages 2943–5, Nov 2005. (Cited on page 22.)

[Nishimoto 2009] Satoshi Nishimoto, Shogo Hamada, Teruo Hayashinaka and Satoshi Murata. *DNA motifs for Substrate-Assisted Self-Assembly.* DNA15, 2009. (Cited on page 7.)

[Parkhurst 1995] Kay M Parkhurst and Lawrence J Parkhurst. *Kinetic Studies by Fluorescence Resonance Energy Transfer Employing a Double-Labeled Oligonucleotide: Hybridization to the Oligonucleotide Complement and to Single-Stranded DNA.* Biochemistry, vol. 34, no. 1, pages 285–292, 1995. (Cited on page 66.)

[Pastré 2003] David Pastré, Olivier Piétrement, Stéphane Fusil, Fabrice Landousy, Josette Jeusset, Marie-Odile David, Loïc Hamon, Eric Le Cam and Alain Zozime. *Adsorption of DNA to Mica Mediated by Divalent Counterions: A Theoretical and Experimental Study.* Biophysical Journal, vol. 85, no. 4, page 2507, Oct 2003. (Cited on page 50.)

[Pastré 2006] David Pastré, Loïc Hamon, Fabrice Landousy, Isabelle Sorel, Marie-Odile David, Alain Zozime, Eric Le Cam and Olivier Piétrement. *Anionic polyelectrolyte adsorption on mica mediated by multivalent cations: a solution to DNA imaging by atomic force microscopy under high ionic strengths.* Langmuir : the ACS journal of surfaces and colloids, vol. 22, no. 15, pages 6651–60, Jul 2006. (Cited on page 50.)

[Quartin 1989] Robin S Quartin and James G Wetmur. *Effect of ionic strength on the hybridization of oligodeoxynucleotides with reduced charge due to methylphosphonate linkages to unmodified oligodeoxynucleotides containing the complementary sequence.* Biochemistry, vol. 28, no. 3, pages 1040–1047, 1989. (Cited on page 66.)

[Reif 1965] F Reif. *Fundamentals of statistical and thermal physics.* McGraw-Hill, 1965. (Cited on page 67.)

[Richmond 1974] Peter Richmond. *Non-retarded van der Waals energies between a finite rod and a planar substrate.* J. Chem. Soc., Faraday Trans. 2, vol. 70, pages 229–239, Jan 1974. (Cited on page 52.)

[Rojas 2002] Orlando J Rojas, Marie Ernstsson, Ronald D Neuman and Per M Claesson. *Effect of Polyelectrolyte Charge Density on the Adsorption and Desorption Behavior on Mica.* Langmuir, vol. 18, no. 5, pages 1604–1612, 2002. (Cited on page 55.)

[Rothemund 2004a] Paul W K Rothemund, Axel Ekani-Nkodo, Nick Papadakis, Ashish Kumar, Deborah Kuchnir Fygenson and Erik Winfree. *Design and characterization of programmable DNA nanotubes.* J. Am. Chem. Soc., vol. 126, no. 50, pages 16344–52, Dec 2004. (Cited on page 22.)

[Rothemund 2004b] Paul W K Rothemund, Nick Papadakis and Erik Winfree. *Algorithmic self-assembly of DNA Sierpinski triangles.* PLoS Biol., vol. 2, no. 12, page e424, Dec 2004. (Cited on page 33.)

[Rothemund 2006] Paul W K Rothemund. *Folding DNA to create nanoscale shapes and patterns.* Nature, vol. 440, no. 7082, pages 297–302, Mar 2006. (Cited on page 6.)

[Sa-Ardyen 2003] Phiset Sa-Ardyen, Alexander V Vologodskii and Nadrian C Seeman. *The flexibility of DNA double crossover molecules.* Biophysical Journal, vol. 84, no. 6, pages 3829–37, Jun 2003. (Cited on page 23.)

[SantaLucia 1996] J SantaLucia, H T Allawi and P A Seneviratne. *Improved nearest-neighbor parameters for predicting DNA duplex stability.* Biochemistry, vol. 35, no. 11, pages 3555–62, Mar 1996. (Cited on page 49.)

[Schulman 2007] Rebecca Schulman and Erik Winfree. *Synthesis of crystals with a programmable kinetic barrier to nucleation.* Proc. Natl. Acad. Sci. U.S.A., vol. 104, no. 39, page 15236, Sep 2007. (Cited on page 27.)

[Seeman 1982] N C Seeman. *Nucleic acid junctions and lattices.* J Theor Biol, vol. 99, no. 2, pages 237–47, Nov 1982. (Cited on page 7.)

[Seeman 2007] N.C Seeman. *An overview of structural DNA nanotechnology.* Molecular biotechnology, vol. 37, no. 3, pages 246–257, 2007. (Cited on page 7.)

[Sushko 2006] M L Sushko and C Rivetti. *Simple Model for DNA Adsorption onto a Mica Surface in 1:1 and 2:1 Electrolyte Solutions.* Langmuir, vol. 22, pages 7678–7688, 2006. (Cited on page 50.)

[Sushko 2007] Maria L Sushko and AL Shluger. *DLVO theory for like-charged polyelectrolyte and surface interactions.* Materials Science and Engineering C, vol. 27, pages 1090–1095, 2007. (Cited on pages 50 and 53.)

[Sushko 2010] M L Sushko. *Personal communication.* 2010. (Cited on page 52.)

[Tuinier 2003] R Tuinier. *Approximate solutions to the Poisson–Boltzmann equation in spherical and cylindrical geometry.* Journal of Colloid and Interface Science, vol. 258, no. 1, pages 45–49, 2003. (Cited on page 56.)

[v Smoluchowski 1917] M v Smoluchowski. *Versuch einer mathematischen Theorie der Koagulationskinetik kolloider Lösungen.* Zeitschrift für physikalische Chemie (Phys. Chem. (Leipzig)), vol. 92, pages 129–168, 1917. (Cited on page 70.)

[Verwey 1948] E J W Verwey and J Th G Overbeek. *Theory of the stability of lyophobic colloids.* Elsevier (Amsterdam), 1948. (Cited on page 50.)

[Wang 1961] Hao Wang. *Proving theorems by pattern recognition – II.* Bell System Tech. journal, vol. 40, no. 1, pages 1–41, May 1961. (Cited on page 34.)

[Watson 1953] J. D. Watson and F. H. Crick. *Molecular Structure of Nucleic Acids.* Nature, vol. 171, pages 737–738, Jan 1953. (Cited on page 5.)

[Wetmur 1991] James G Wetmur and Jacques Fresco. *DNA Probes: Applications of the Principles of Nucleic Acid Hybridization.* Critical Reviews in Biochemistry and Molecular Biology, vol. 26, no. 3-4, pages 227–259, 1991. (Cited on page 60.)

[Winfree 1996] Erik Winfree. *On the computational power of DNA annealing and ligation.* DNA based computers, vol 27 of DIMACS. AMS Press, Providence, RI,, pages 199–221, Nov 1996. (Cited on page 36.)

[Winfree 1998a] E Winfree, F Liu, L A Wenzler and N C Seeman. *Design and self-assembly of two-dimensional DNA crystals.* Nature, vol. 394, no. 6693, pages 539–44, Aug 1998. (Cited on page 8.)

[Winfree 1998b] Erik Winfree. *Algorithmic Self-Assembly of DNA.* Thesis, California Institute of Technology, Aug 1998. (Cited on pages 60 and 66.)

[Yan 2003a] Hao Yan, Thomas H LaBean, Liping Feng and John H Reif. *Directed nucleation assembly of DNA tile complexes for barcode-patterned lattices.* Proceedings of the National Academy of Sciences, vol. 100, no. 14, pages 8103–8108, Jun 2003. (Cited on page 6.)

[Yan 2003b] Hao Yan, Sung Ha Park, Gleb Finkelstein, John H Reif and Thomas H LaBean. *DNA-templated self-assembly of protein arrays and highly conductive nanowires.* Science, vol. 301, no. 5641, pages 1882–4, Sep 2003. (Cited on pages 11 and 26.)

[Yang 1998] Xiaoping Yang, Lisa A. Wenzler, Jing Qi and Nadrian C Seeman. *Ligation of DNA Triangles Containing Double Crossover Molecules.* Journal of American Chemical Society, vol. 120, no. 38, pages 9779–9786, 1998. (Cited on page 22.)

[Yin 2008] Peng Yin, Rizal F Hariadi, Sudheer Sahu, Harry M T Choi, Sung Ha Park, Thomas H LaBean and John H Reif. *Programming DNA tube cir-*

cumferences. Science, vol. 321, no. 5890, pages 824–6, Aug 2008. (Cited on pages 11 and 27.)